INFORMATION TO USERS

This manuscript has been reproduced from the microfilm master. UMI films the text directly from the original or copy submitted. Thus, some thesis and dissertation copies are in typewriter face, while others may be from any type of computer printer.

The quality of this reproduction is dependent upon the quality of the copy submitted. Broken or indistinct print, colored or poor quality illustrations and photographs, print bleedthrough, substandard margins, and improper alignment can adversely affect reproduction.

In the unlikely event that the author did not send UMI a complete manuscript and there are missing pages, these will be noted. Also, if unauthorized copyright material had to be removed, a note will indicate the deletion.

Oversize materials (e.g., maps, drawings, charts) are reproduced by sectioning the original, beginning at the upper left-hand corner and continuing from left to right in equal sections with small overlaps. Each original is also photographed in one exposure and is included in reduced form at the back of the book.

Photographs included in the original manuscript have been reproduced xerographically in this copy. Higher quality 6" x 9" black and white photographic prints are available for any photographs or illustrations appearing in this copy for an additional charge. Contact UMI directly to order.

U·M·I

University Microfilms International
A Bell & Howell Information Company
300 North Zeeb Road, Ann Arbor, MI 48106-1346 USA
313/761-4700 800/521-0600

Order Number 9503312

Growth, fabrication, and measurement of superconducting $Ba_{1-x}K_xBiO_3$ thin films and devices

Schweinfurth, Ralph Alan, Ph.D.

University of Illinois at Urbana-Champaign, 1994

Copyright ©1994 by Schweinfurth, Ralph Alan. All rights reserved.

U·M·I
300 N. Zeeb Rd.
Ann Arbor, MI 48106

GROWTH, FABRICATION, AND MEASUREMENT OF SUPERCONDUCTING $Ba_{1-x}K_xBiO_3$ THIN FILMS AND DEVICES

BY

RALPH ALAN SCHWEINFURTH

B.S., Harvey Mudd College, 1987
M.S., University of Illinois, 1989

THESIS

Submitted in partial fulfillment of the requirements
for the degree of Doctor of Philosophy in Physics
in the Graduate College of the
University of Illinois at Urbana-Champaign, 1994

Urbana, Illinois

UNIVERSITY OF ILLINOIS AT URBANA-CHAMPAIGN

THE GRADUATE COLLEGE

APRIL 1994

WE HEREBY RECOMMEND THAT THE THESIS BY

RALPH ALAN SCHWEINFURTH

ENTITLED GROWTH, FABRICATION, AND MEASUREMENT OF

SUPERCONDUCTING $Ba_{1-x}K_xBiO_3$ THIN FILMS AND DEVICES

BE ACCEPTED IN PARTIAL FULFILLMENT OF THE REQUIREMENTS FOR

THE DEGREE OF DOCTOR OF PHILOSOPHY

Director of Thesis Research

Head of Department

Committee on Final Examination†

Chairperson

† Required for doctor's degree but not for master's.

O-517

© Copyright by Ralph Alan Schweinfurth, 1994

GROWTH, FABRICATION, AND MEASUREMENT OF SUPERCONDUCTING $Ba_{1-x}K_xBiO_3$ THIN FILMS AND DEVICES

Ralph Alan Schweinfurth, Ph.D.
Department of Physics
University of Illinois at Urbana-Champaign, 1994
Dale J. Van Harlingen, Advisor

This thesis discusses growth, fabrication and measurement of $Ba_{1-x}K_xBiO_3$ (BKBO) superconducting thin films and thin film devices. Interest in BKBO has been concerned with both fundamental questions concerning its mechanism of superconductivity and potential applications in superconductor devices. $Ba_{1-x}K_xBiO_3$ is a superconducting compound at a small range of potassium concentration, with the highest transition temperature being about 32 °K for $0.35 < x < 0.4$. The *in-situ* growth of high quality superconducting thin films is described, using pulsed laser deposition. Film quality was analyzed with RBS, XRD, and SEM as well as transport. Fabrication of transport, microwave, and tunneling structures and devices is described, including dry etching techniques (ion milling and RIBM) as well as annealing and processing effects. Transport measurements yield T_{c0} = 25-29 °K, $J_c \geq 1$ MA/cm^2 (4 °K), and $R_s \approx 1$ mΩ (at 4 °K and 10 GHz) for the best films. Dissipation in fields up to 5 Tesla suggests that the superconducting coherence length $\xi \approx 38$ Å and upper critical field $H_{c2}(0) \approx 22$ T. Tunneling studies were also made using a BKBO electrode, a native oxide barrier, and the following counterelectrodes: Ag, Pb, Nb, and BKBO. Results were consistent with classical tunneling of a weak to moderately coupled superconductor where Δ = 4.5 meV and $2\Delta/k_BT_c = 3.8$. Prospects for practical BKBO superconducting devices are discussed.

Acknowledgments

This work would not have been possible if not for the invaluable assistance of my advisor, Dale Van Harlingen. His generosity, patience, support, and enthusiasm have enabled me to pursue the breadth of my studies.

Many collaborators have contributed to this work. I am especially indebted to Chris Platt, Byung Moon, and Mark Teepe, who have been instumental in the growth, development, and microanalysis of the BKBO thin films. Ian Caiozzi was largely responsible for the room temperature annealing experiments as well as assisting in the assembly of the multitarget growth chamber. Tony Chou also assisted in the growth and characterization of BKBO.

Gratitude is also owed to Milton Feng's group and especially Jay Kruse in the Electrical and Computer Engineering department, where the design and measurement of our HTS microwave devices were done. I greatly appreciate their assistance and the manner in which they adopted me into their group.

Most of the MRL staff has contributed to this work at one point or another. I'd like to thank the staff in the Center for Microanalysis, especially Chris Loxton, Brad, Judy, Ernie and Irena. The shop has also contributed with advice or workmanship on innumerable projects, including Bud Dittman, Darrell, Spencer, Cliff, and Greg. Carroll Sarver and the storeroom has been an invaluable source of advice and information. Ray Strange helped greatly to keep the laser and the microfabrication facilities up and running.

I have enjoyed and appreciated the comraderie of the best research group around -- the DVH group. I wish to thank Gene Hilton and Fred Sharifi, in addition to Dale, for the core of my technical training in superconductive devices. Mark Wistrom and Joe Walko deserve credit for their many contributions the PLD deposition systems. Other members from whom I have benefited from friendship and discussions include Subashri Rao, Kevin Stawiasz, Lan Vu, Dave Wollman, and Stu Tessmer.

Social support was also needed to finish this task. In addition to those mentioned previously, I've been fortunate to have made good friends outside my studies. I especially refer to Karl, Steve, Toby, Greg, Katie, Owen, Ken, Mary, Dan, and Sara. I've enjoyed and been lightened by the many Sunday morning sporting events, Sunday 'ques, and general get-togethers. Another outlet was playing volleyball. I'd like to thank my many teammates over the years, including Greg Martin, Marcello, Claudio, Tom, Benno, Tony, Craig Jones, Mark Jones, Othello, Lem, and Mike Deterding.

Most important of all is the support and love shown me by Leyan, my parents, and my sister, Lynn. This thesis would have never been finished otherwise.

This work was funded in part by the Science and Technology Center for High Temperature Superconductivity under Grant STC-91-20000. Facilities and capabilities were also provided by the Materials Research Laboratory and the Microelectronics Laboratory at the University of Illinois.

Table of Contents

Chapter 1
INTRODUCTION

Since 1988, much research activity has been concerned with the bismuth oxide superconductor $Ba_{1-x}K_xBiO_3$ (BKBO).[1] There are two major sources of interest in these compounds. The first is a fundamental physics and materials interest in this new copperless perovskite superconductor with a relatively high transition temperature (T_c) near 30°K. The second is an applied approach towards making superconducting devices out of these compounds. I chose to work on both interests of this material by studying superconducting $Ba_{1-x}K_xBiO_3$ thin films. This project represents a first pass towards developing BKBO devices and building a BKBO thin film technology, as well as measuring fundamental superconducting constants of this material.

Superconductivity occurs in the barium bismuthate system from doping the insulating compound $BaBiO_3$ with K, Rb, or Pb. Although barium bismuthate has half-filled bands, typical of a metal, the material is an insulator without doping due to a charge density wave state that forms.[2] The superconducting compound $BaPb_xBi_{1-x}O_3$ was discovered in 1975[3] and had provided inspiration to the breakthrough of Bendorz and Muller's discovery of the cuprates.[4] For a Pb doping of $x \approx 0.75$, T_c is about 13°K, and was considered "high-T_c" in its time. Later, K or Rb doping on the Ba site ($Ba_{1-x}K_xBiO_3$ or $Ba_{1-x}Rb_xBiO_3$) was discovered where the maximum T_c

(a)

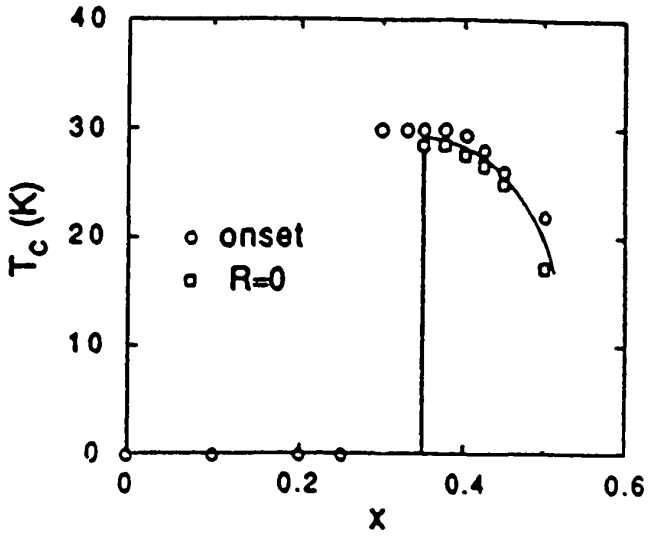

(b)

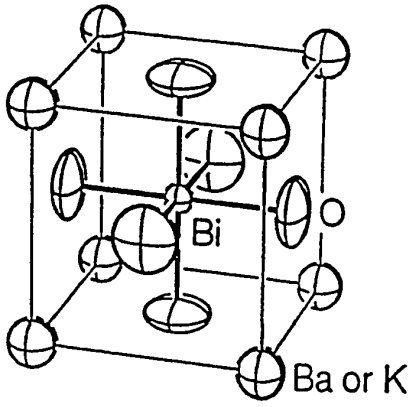

Figure 1.1 (a) Crystal structure of the superconducting cubic phase of $Ba_{1-x}K_xBiO_3$. (b) Superconducting transition temperatures T_c vs. x for $Ba_{1-x}K_xBiO_3$. Figures adapted from Pei.[4]

is 32°K for x = 0.35-0.4.[6,7] The crystal structure for BKBO is shown in Fig. 1.1 as is the T_c as a function of K doping (x). One should note that the highest transition temperature is obtained near the metal-insulator transition, and that the onset is sudden.

The scientific interest in the bismuthates comes from their relationship with the high-T_c cuprate superconductors, such as $La_{2-x}Sr_xCuO_4$, $YBa_2Cu_3O_7$, $Bi_2Sr_2CaCu_2O_8$, $Tl_2Ba_2Ca_2Cu_3O_{10}$, etc. The bismuthates have qualities of both the cuprate and classic BCS superconductors (Hg, Nb, Pb, In, Sn, etc.), and may act as a bridge between them.

First let us look at the similarities between the cuprates and bismuthates. Both LMCO and BMBO families are insulators in their parent forms, La_2CuO_4 and $BaBiO_3$, and will superconduct within a range of certain substitutional dopings for the La and Ba or Bi sites, respectively (e.g. $La_{2-x}Sr_xCuO_4$ and $Ba_{1-x}K_xBiO_3$).[8] Also, as with all cuprates, the bismuthates demonstrate a linear conductance (dI/dV vs. V) background at voltages just above the gap unlike classic superconductor tunneling, which is flat.[9] One study has found BKBO to show non-Drude behavior in the optical reflectivity and dielectric loss function, similar to the cuprates.[10] In addition, both the cuprates and bismuthates have low carrier concentrations in comparison with the classic BCS superconductors. Moreover, it has been shown that the bismuthates and cuprates share a similar correlation between T_c and the superconductor carrier density per effective mass, again different from the classic superconductors.[11]

In contrast, a fundamental difference between the bismuthate and cuprate systems is that the cuprates have two dimensional conducting sheets of CuO while the bismuthates have a three dimensional BiO conduction network.[12] The barium bismuthate family shows no antiferromagnetism, contrary to the cuprate family.[13] Another difference is that conduction in the bismuthates is via electron carriers (negative Hall coefficient) rather than hole carriers (positive Hall coefficient) seen in the cuprates, with the exception of $Nd_{2-x}Ce_xCuO_{4-\delta}$. Our magnetic field dissipation data in Chapter 5 shows BKBO to lack the severe flux flow seen in the cuprates.[14] Also, contrary to the data of Bozovic,[15] different measurements of BKBO optical spectra show the bismuthates and cuprates to have many differences.[16,17,18] The importance of classic BCS electron-phonon coupling in BKBO is shown with the strong oxygen isotope effect and the phonon effects in tunneling.spectra.[19] Strong BCS similarity is also indicated with tunneling that has exhibited a BCS-like tunneling gap. Tunneling measurements have measured $2\Delta/k_BT_c$ to be 3.5-4 (weak to moderately coupled) with low subgap currents compared to the much stronger coupling and significant subgap currents seen in the cuprates.

In addition to being a fundamental probe, the tunneling properties of the bismuthates make them very attractive for superconducting electronics. As already shown, $Ba_{1-x}K_xBiO_3$ has a T_c of 30°K for $x \approx 0.4$, and has a superconductive tunneling gap of roughly 4.5 meV. This is higher than NbN, a current device material,

and almost 3 times the transition temperature and gap of Nb. In contrast to the cuprates, BKBO is an isotropic superconductor, which greatly facilitates film growth and device fabrication. Also, BKBO has a coherence length of $\xi \approx 50\text{-}75$Å, which is considerably longer than the cuprates where ξ is anisotropic and ranges from 2-20Å. This also facilitates device fabrication. The key feature of this material is the ability to make a hysteretic Josephson tunnel junction,[20] which has proved difficult in the cuprates.[21,22] These BKBO properties show promise in making practical superconducting devices that would work in modern cryocoolers.

There are many varied kinds of potentially useful devices. Some of the possibilities include mixers, oscillators, digital switches, microwave components, three terminal devices, and practical SQUIDs.[23]

A well defined application is a quasiparticle SIS mixer for use in astronomical observation.[24] These devices have superior sensitivity in sub-millimeter wavelength astronomy. Currently there is a large effort to make mixers above 500 GHz using Nb, NbN and other materials. The intrinsic frequency limit of such a device is roughly limited by the gap of the tunnel junction. With BKBO's gap, a BKBO SIS mixer would be able to function easily at these frequencies, and may work up to a few THz. For the mixer, the active device would require a low capacitance SIS Josephson tunnel junction. The local oscillator for the mixer could also be made from a BKBO Josephson junction (JJ).[25]

BKBO digital latching logic is another possibility. It would work at cryocooler temperatures, would have less dissipation than an equivalent HTSC circuit due to its smaller gap, and would offer dc capability lacking in RFSQ logic.

BKBO microwave components have potentially superior microwave performance than both conventional superconductors and HTSC superconductors. It's gap is larger than standard BCS superconductors, resulting in higher frequency operation and theoretically less surface impedance.[26] BKBO also doesn't have states in the gap as been observed in the cuprates, which produce microwave loss.

Concerning three terminal devices, there has been an effort to make superconducting base transistors.[27] Efforts with BKBO have produced Au/I/BKBO/$SrTiO_3$(Nb doped) and In/I/BRBO/$SrTiO_3$(Nb doped) devices where the metal (Au or In) layer is the emitter, "I" is a natural insulating barrier, the superconductor (BKBO or BRBO) is the base, and the Nb doped $SrTiO_3$ is the semiconducting collector. So far these devices have shown limited gain.[28,29]

Last, but definitely not least, is the possibility of practical BKBO SQUIDs capable of working at cryocooler temperatures. SQUIDs are the dominant superconducting electronic device currently used. With BKBO hysteretic tunnel junctions, one can fabricate a SQUID with optimized parameters, yielding superior performance.[30] With HTSC SQUIDs, one usually has a limited parameter variance due to the nature of the junctions.

In order to achieve both the applied and fundamental goals, one needs a good understanding of the materials and physical properties of BKBO. We have started development of a BKBO technology while characterizing physical properties of our BKBO thin films. First and foremost is the ability to grow quality thin films. Described in Chapter 2 is the laser ablation process we have used to make superior BKBO thin films. Chapter 3 describes the characterization of as-grown films with both microanalysis and electrical measurements. Also, the fabrication methods that were developed for these films are described in Chapter 4. Chapters 5, 6 and 7 describe measurements that were performed on patterned film structures and devices, yielding physical constants for our BKBO films. Lastly, in Chapter 8, progress and future directions are discussed and summarized.

References

[1] L.F. Mattheiss, E.M. Gyorgy, and D.W. Johnson, Jr., "Superconductivity above 20°K in the Ba-K-Bi-O system," Phys. Rev. B., vol. 37(7), pp. 3745-6, Mar. 1988.

[2] D.E. Cox and A.W. Sleight, Solid State Commun, vol. 19, p. 969, 1976.

[3] A.W. Sleight, J.L. Gillson, and P.E. Bierstedt, "High-temperature superconductivity in the $BaPb_{1-x}Bi_xO_3$ system," Solid St. Commun., vol. 17(1), pp. 27-28, Jul. 1975.

[4] J.G. Bednorz and K.A. Muller, "Possible high T_c superconductivity in the Ba-La-Cu-0 system," Z. Phys., vol. B64(2), pp. 189-193, Sept. 1986.

[5] S. Pei, J.D. Jorgensen, B. Dabrowski, D.G. Hinks, D.R. Richards, A.W. Mitchell, J.M. Newsam, S.K. Sinha, D. Vaknin, and A.J. Jacobson, "Structural phase diagram of the $Ba_{1-x}K_xBiO_3$ system," Phys. Rev. B, vol. 41(7), pp. 4126-4141, Mar. 1990.

[6] R.J. Cava, B. Batlogg, J.J. Krajewski, R. Farrow, L.W. Rupp Jr., A.E. White, K. Short, W.F. Peck, and T. Kometani, "Superconductivity near 30 K without copper: the $Ba_{0.6}K_{0.4}BiO_3$ perovskite," Nature, vol. 332(6167), pp. 814-6, Apr. 1988.

[7] D.G. Hinks, B. Dabrowski, J.D. Jorgensen, A.W. Mitchell, D.R. Richards, S. Pei, and D. Shi, "Synthesis, structure, and superconductivity in the $Ba_{1-x}K_xBiO_{3-y}$ system," Nature, vol. 333(6176), p. 836-8, 1988.

[8] J. T. Markert, Y. Dalichaouch, and M. D. Maple, Physical Properties of High Temperature Superconductors, vol I, edited by D. M. Ginsberg, World Scientific Press, New Jersey, 1989, p. 320.

[9] F. Sharifi, A. Pargellis, and R. C. Dynes, "Tunneling density of states in the lead-bismuth-oxide superconductors," Phys. Rev. Lett., vol. 67(4), pp. 509-511, July 1991.

[10] I. Bozovic, J. H. Kim, J. S. Harris, Jr., E. Hellman, E. H. Hartford, and P. K. Chan, "Free-charge-carrier plasmons in $Ba_{1-x}K_xBiO_3$: A close relation to cuprate superconductors," Phys. Rev. B, vol. 46(2), pp. 1182-1187, July 1992.

[11] Y.J. Uemura, L.P. Le, G.M. Lake, B.J. Sternlieb, W.D. Wu, J.H. Brewer, T.M. Riseman, C.L. Seaman, M.B. Maple, M. Ishikawa, D.G. Hinks, J.D. Jorgensen, G. Saito, and H. Yamochi, Phys. Rev. Lett., vol. 66(20), pp. 2665-7, May 1991.

[12] J.T. Markert, et. al., ibid

[13] Y.J. Uemura, "Muon spin relaxation studies on high-Tc superconductors and related antiferromagnets," J. Appl. Phys., vol. 64(10), pp. 6087-6091, Nov. 1988.

[14] R.A. Schweinfurth, C.E. Platt, M.R. Teepe, and D.J. Van Harlingen, "Electrical and magnetic transport properties of laser-deposited $Ba_{1-x}K_xBiO_3$ thin films," Appl. Phys. Lett., vol. 61(4), pp. 480-482, July 1992.

[15] I. Bozovic, ibid.

[16] M.A. Karlow, S.L. Cooper, A.L. Kotz, M.V. Klein, P.D. Han, and D.A. Payne, "Optical conductivity of $Ba_{1-x}K_xBiO_3$ through the metal-semiconductor transition," Phys. Rev. B, vol. 48(9), pp. 6499-6505, Sept. 1993.

[17] H. Sato, S. Tajima, H. Takagi, and S. Uchida, Nature, vol. 338, p. 241, 1989.

[18] S.H. Blanton, R.T. Collins, K.H., Kelleher, L.D. Rotter, Z. Schlesinger, D.G. Hinks, and Y. Zheng, Phys. Rev. B., vol. 47, p. 996, 1993.

[19] D.G. Hinks, B. Dabrowski, D.R. Richards, J.D. Jorgensen, S. Pei, and J.F. Zasadzinski, "Tunneling spectroscopy in $Ba_{1-x}K_xBiO_3$," Physica C, vol. 162-164, pp. 1405-1408, 1989.

[20] A.N. Pargellis, F. Sharifi, R.C. Dynes, B. Miller, E.S. Hellman, J.M. Rosamilia, and E.H. Hartford, Jr., "All-high T_c Josephson tunnel junction: $Ba_{1-x}K_xBiO_3$/ $Ba_{1-x}K_xBiO_3$ junctions," Appl. Phys. Lett., vol. 58(1), pp. 95-97, Jan. 1991.

[21] M.E. Klausmeier-Brown, G.F. Virshup, I. Bozovich, J.N. Eckstein, K.S. Ralls, "Engineering of ultrathin barriers in high Tc, trilayer Josephson junctions," Appl. Phys. Lett., vol. 60(22), pp. 2806-9, Jun. 1992.

[22] P.A. Rosenthal, E.N. Grossman, R.H. Ono, and L.R. Vale, "High temperature superconductor-normal metal-superconductor Josephson junctions with high characteristic voltages," Appl. Phys. Lett., vol. 63(14), pp. 1984-1986, Oct. 1993.

[23] A. Barone and G. Paterno, Physics and Applications of the Josephson Effect, John Wiley and Sons, New York, 1982.
M.Y. Kupriyanov and K. Likharev, Sov. Phys. Uspekhi **33**, 340 (1990)

[24]J.R. Tucker and M. J. Feldman, "Quantum detection at millimeter wavelengths," Rev. Mod. Phys., vol. 57, pp. 1055-1113, Oct. 1985.
J.R. Tucker, IEEE Quantum Electronics, **QE15**, 1234 (1979).

[25]A. Barone and G. Paterno, Physics and Applications of the Josephson Effect, John Wiley and Sons, New York, 1982, pp. 309-318.
R.P. Robertazzi and R.A. Buhrman, "NbN Josephson tunnel junctions for terahertz local oscillators," Appl. Phys. Lett., vol. 53(24), pp. 2441-3, Dec. 1988.

[26]T. Van Duzer and C.W. Turner, Principles of Superconductive Devices and Circuits, Elsevier North Holland, Inc., New York, 1981, pp. 128-138.

[27]D.J. Frank, M.J. Brady, and A. Davidson, IEEE Trans. Magn., p 721 (1985)

[28]H. Suzuki, M. Iyori, T. Yamamoto, S. Suzuki, K. Takahashi, T. Usuki, and Y. Yoshisato, "Junction characteristics of an Au/$Ba_{1-x}K_xBiO_3$/niobium-doped $SrTiO_3$ structure," Jpn. J. Appl. Phys., vol. 31(9A), pp. 2716-2720, Sept. 1992.

[29]H. Abe, F, Toda, and M. Ogihara, IEEE Electron Device Lett., vol. 14, p 100, 1993.

[30]J. Clarke, W. M. Goubau, and M. B. Ketchen, "Tunnel Junction dc SQUID: Fabrication, operation, and performance," J. Low Temp. Phys., vol. 25(1/2), pp. 99-144, Oct. 1976.

Chapter 2
GROWTH

2.1 Introduction

The foundation for studying thin film BKBO is the ability to grow quality material. Many different methods have been employed to make films in the bismuthate family which includes the materials $Ba_{1-x}K_xBiO_3$, $Ba_{1-x}Rb_xBiO_3$ and $BaPb_xBi_{1-x}O_3$. These methods are pulsed laser deposition (PLD),[1,2,3,4,5] off-axis sputtering,[6,7,8,9,10] ECR assisted coevaporation,[11] and MBE.[12,13] We have successfully used PLD for growing $Ba_{1-x}K_xBiO_3$ superconducting thin films.[14] Pulsed laser deposition, also referred to as laser ablation, laser evaporation, and laser sputtering, has been used to grow a variety of materials for the past two decades, including dielectrics, piezoelectrics, ferroelectric, semiconductors, superlattices, and superconductors. Since 1987, the technique has had renewed interest due to its success in growing thin films of high temperature superconductors, especially $YBa_2Cu_3O_{7-\delta}$. Simply described, the process consists of vaporizing a target with a laser, and collecting the vapor onto a substrate. In this chapter, I will describe the advantages, disadvantages, kinetics, and our specific BKBO growth techniques and hardware.

It is much more difficult to grow medium and high temperature superconductors vs. single element superconductors. One must obtain the correct multielement phase with good

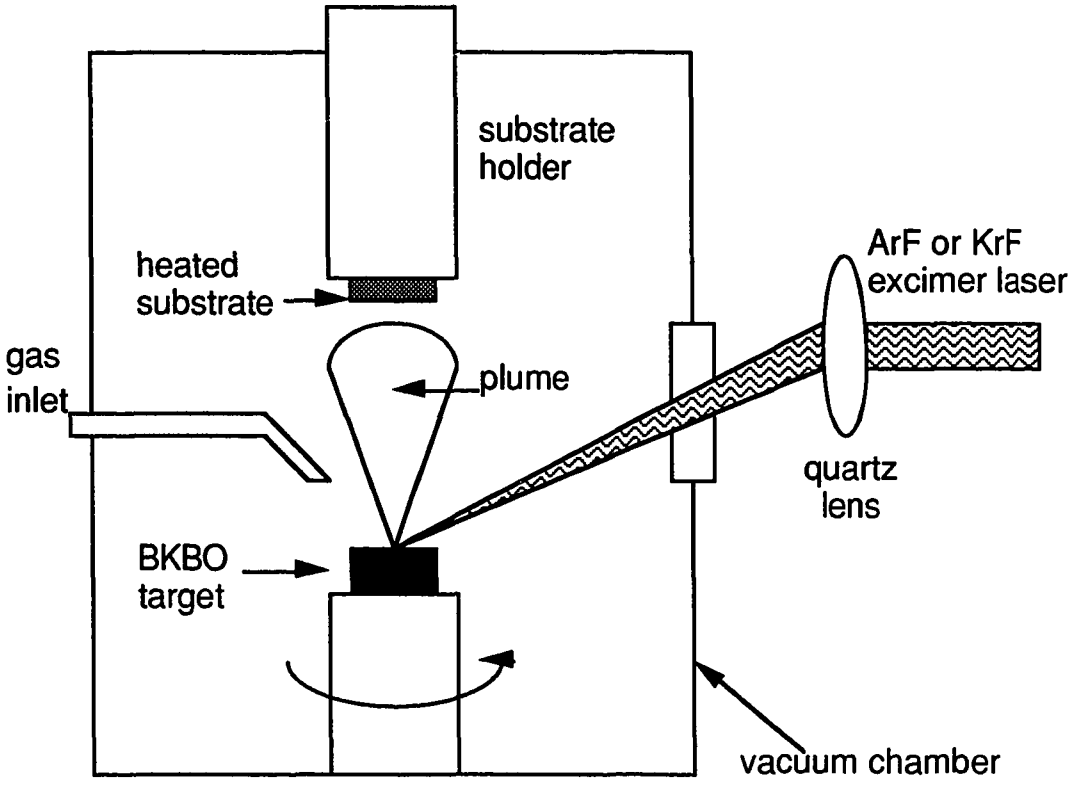

Figure 2.1 Diagram of the single source laser ablation chamber.

microstructure and little contamination. The superconducting phase is metastable at room temperature and may only be stabilized in certain areas of the pressure-temperature phase diagram. *In-situ* films are deposited stoichiometrically onto a heated substrate and a specific gas environment in order to get the superconducting HTS phase upon removal. It is also possible to deposit the material cold and subsequently anneal the film to make it superconducting. This is called *ex-situ* processing. *In-situ* films tend to be superior to *ex-situ* as the former involves a condensation growth rather than a solid state reaction. Recent progress in YBCO though shows that *ex-situ* methods are closing the gap.[15]

There are many advantages to using Pulsed Laser Deposition. Probably the most important is that under proper conditions the pellet material is stoichiometrically evaporated onto the substrate. This makes deposition of multielement compounds relatively simple. It eliminates the complications of matching rates and sticking coefficients of multiple sources during coevaporation and doesn't involve the time consuming optimization of target composition needed for on-axis sputtering. Also, the PLD process can grow films at a much quicker rate (greater than 250Å/min @ 4Hz) than off-axis sputtering or MBE. This makes for quick turn around for film growth and thus quicker optimization. Another advantage of PLD is that high energy species (atoms, molecules, ions, and clusters) are created which can aid in epitaxial growth (e.g. allow for films to be grown at

lower temperatures). Lastly, PLD uniquely works for a wide array of materials in a wide range of ambient gas pressures.

There are also disadvantages with using PLD. The plume coats only a small area uniformly, thus making it difficult to scale up to larger substrates. Also, the deposition plume contains debris which collects on the surface of the film, which can detrimentally impact multilayers and electronic devices.

2.2 Kinetics

The laser ablation process occurs in roughly three steps. First, there is absorption of photons from a focused laser beam (for us a pulsed UV excimer laser) and ejection of material from the target surface. Second, there is transport across the space between the pellet and substrate while target material in the gas phase interacts with the ambient gas. Lastly, there is condensation and film growth on the substrate. I will provide a qualitative description of the laser ablation process. Although this thesis is concerned with BKBO ablation, I will often refer to YBCO ablation for quantitative reference as most HTSC PLD work has been done on the latter compound. Presently, ablation optimization has been determined empirically, as the ablation process is currently a research topic.[16]

2.2.1 Laser-Solid-Plasma Interaction

Let us first look at the laser-target interaction. When the laser pulse hits the pellet, the surface layers are heated by photo-absorption. If the energy density is high enough, laser fluence > 0.11 J/cm^2 for YBCO material removal,[17] the near surface layers will melt

and congruently evaporate. It is this rapid localized surface heating which produces the stoichiometric evaporation, although stoichiometric deposition also requires the proper vapor transport. For efficient material removal and congruent evaporation, shorter wavelengths and pulse widths are superior (e.g. UV excimer lasers).

While the laser-solid interaction provides for congruent evaporation of multicomponent targets, it also produces the debris or "boulders" seen on PLD film surfaces. These particles typically are 0.5-5μm in size and number 10-100000/mm^2.[18] According to one model, when the molten surface material starts to evaporate, it cools the underlying material by the latent heat of vaporization. This produces subsurface superheating, which in turn gives rise to microexplosions that produce particulates.[19] Many factors affect particulate production, including the target properties, target history, and method of ablation. Practical aspects of particulate generation are discussed in section 2.3.6.

Throughout the duration of the laser pulse, a sophisticated laser-solid-plasma interaction occurs. There are many types of species desorbed from the heated target surface including ions, electrons, atoms, molecules, and clusters. The laser pulse continues to interact with these evaporants by dissociating molecules and aggregates as well as photoionizing neutrals. Photoionization creates an expanding plasma above the target surface. The plasma then absorbs incoming laser radiation, further heating the plasma and self-regulating further laser-target interaction. Shorter wavelength

lasers have higher ionizing efficiency which produce hotter and more highly ionized plasmas which is advantageous to stoichiometric deposition; this is another reason for using excimers. As discussed below, the plasma properties have a large impact on the vapor transport to the substrate.

2.2.2 Plume-Gas Interaction

After the laser pulse, the plasma expands across the space to the substrate. The initial energy of the species is roughly 10-400 eV.[20] The hallmark of PLD is the unique plume generated during the deposition, indicative of the forward and peaked nature of the deposition. Thickness measurements indicate two components of deposition that vary as a function of the angle θ of the radial vector from the normal of the target.[21] The first is the stoichiometric component that has a forward peaked distribution of $\cos^n(\theta)$, with $3 < n < 14$,[22] although it is typically about 10 for 1-2-3 compounds.[23] The second component, like evaporation, has a $\cos(\theta)$ thickness variation and is not stoichiometric. Therefore, one is usually careful to aim the center of the plume at the substrate. The magnitude of the peaked component increases relative to the evaporative component with increasing energy density, forcing a minimum bound for the laser fluence used. For stoichiometric deposition, YBCO has a fluence threshold between 1.5-2.0 J/cm^2.[24] Also, the $\cos^n(\theta)$ distribution widens ($n \downarrow$) with increasing gas pressure and reduction of the beam spot size, keeping the same energy density.[25] For further details, the reader is referred to Singh and Narayan's

adiabatic expansion model of deposition into a vacuum. This model describes many features of the vapor transport and the resulting thickness and stoichiometric variations in the deposited film.[26]

Indeed, much of the PLD research is involved with characterizing the plasma expansion and its interaction with the ambient gas. The problem is complex due to the multicomponent plasma and the (reactive) medium in which it is expanding. Light and mass spectroscopies, time of flight (TOF) measurements, and fast photographic techniques have been used to study the expansion. An important observation these techniques have shown has been that for YBCO, the production of monoatomic oxides (e.g. CuO, BaO, and YO) is maximized in one (CuO) to a few hundred (YO) millitorr of oxygen; the same as the empirically determined optimal PLD growth pressure. This indicates the importance of plume oxides in the deposition process and undoubtedly impacts PLD BKBO growth as well.

The collisions that occur while the plume is expanding through the gas also have a large effect on deposition. The extent of collisions depends on how large the pressure-distance product is. At low pressures, the plume sprays the substrate fairly directionally and at high growth rates. At high pressures and distance, the material is evaporated diffusively. As the species travel and collide with gas molecules, they become thermalized while the ions are additionally neutralized. Also, the gas species can attenuate as they scatter, diminishing their flux at the substrate. In order to gain the benefit

of the excited deposition species for epitaxy, one should have less than 10 collisions before hitting the substrate.[27]

2.2.3 Condensation and Growth

When the material reaches the substrate, the energy of the ions and neutrals have typically been reduced to ≤ 10 eV.[28,29] This kinetic energy adds to the surface mobility of the condensate, enabling crystalline growth at lower temperatures than would otherwise occur. Similarly, particle mobility has also been increased by introducing a plasma into the chamber or biasing the substrate. These allow for the HTS phase to be formed at very low temperatures,[30] but the crystallinity suffers until the temperature is increased.

Sometimes with *in-situ* PLD, the stoichiometry isn't reproduced on the surface as expected. There are a number of possible reasons for this. First, if the compound has volatile components in it, like K and Bi in BKBO, they evaporate away if not quickly incorporated into a stable crystal phase. Oxygen helps to incorporate volatile components, and has been shown to be important to incorporate K into BKBO during sputtering.[31] Thus, it is important to be in the correct process regime in order to preserve the correct stoichiometry at high growth temperatures. Also, it is possible that some precipitates may form, leeching material from the desired compound. Examples are the Cu-rich precipitates in YBCO[32], and K or Bi precipitates in BKBO thin films.

2.3 BKBO Growth Technique

There are many important aspects to successfully grow BKBO thin films. I will describe the PLD techniques used to grow films as well as our interpretation of the chemical process. I will also describe the hardware and materials needed to grow films.

2.3.1 Standard Procedure and Apparatus

Let us first look at the generic BKBO laser ablation procedure. Symbolic diagrams of the two ablation chambers are shown in Fig. 2.1 and Fig. 2.2. First, a cleaned substrate is mounted on the substrate holder with Ag paste or paint[33] and heated to drive off the casting solvent. The substrate surface may additionally be treated with an ion mill or an oxygen glow discharge inside the vacuum system. We use a Questek 2820 excimer laser for the deposition, using either ArF (193 nm) or KrF (248 nm) laser gas mixtures at pulse rates of 1-4 Hz and FWHM $\approx$ 20 ns. The sample holder is held at 600°C inside the vacuum system with feedback from a K-type thermocouple imbedded into the holder. The laser beam pulse is sent through an aperture and focused by a fused silica optic (focal length=75cm) through a fused silica chamber window, hitting the laser target. The aperture is used to improve the energy density (fluence) uniformity over the beam spot. The fluence is determined by the laser pulse energy and the distance of the optic from the pellet/ target surface. The target is either scanned or rotated for even wear while the gas nozzle is pointed towards the target to help cool it. For BKBO, the ablation is done in 1-2 Torr of Ar, whereas

YBCO is done in roughly 200mT of oxygen. Thus our BKBO ablations are done more towards the diffusive limit and in a reducing atmosphere. After the ablation is finished, the sample is quickly ramped down to an *in-situ* anneal temperature (350-400°C) and the chamber is then vented with oxygen. The sample soaks for 10-15 minutes at the anneal temperature, then the heater is turned off. The sample is removed when the substrate stage has cooled. Our current growth parameters are summarized below:

Ablation Parameters	
Substrate	MgO
Substrate Prep	O_2 glow discharge and 800°C *in-situ* anneal
Growth Temperature	600°C
Fluence	1.0 J/cm^2 (KrF) @ 4Hz
Pressure	2 torr Ar (200 sccm)
Pellet	Phase pure $Ba_{0.6}K_{0.4}BiO_3$
Anneal Temperature	15 min at 350°C in 1atm O_2

Table 2.1 Typical BKBO thin film ablation parameters.

2.3.2 Off-center BKBO Ablation

Alternatively, we sometimes employ a different procedure to obtain films. This uses what I will call off-center laser ablation. As discussed in section 2.2.2, the plume is usually aimed directly at the substrate. Under certain conditions, we have found that high quality BKBO can be grown by intentionally aiming away from the substrate. The conditions for this type of growth are slightly different than standard ablation. The temperature is roughly the same or slightly

lower than for on-axis ablation. The most significant difference is that the Ar pressure is half of our normal ablation pressure. This again begs the question as to the role of the Ar gas during the ablation. I speculate that away from the plume, especially with lower laser fluences, the film has a higher concentration of the more volatile elements-- K and Bi.

As previously mentioned, the superconducting properties are superb, and may even have slightly higher superconducting transitions. However, this form of ablation has the drawback of cracking. While on-axis films have had little cracking at up to 2000Å, off-center films must be kept to less than 1000Å to eliminate cracks. Off-center films also have the drawback of non-uniform thickness over the substrate, an important quality for fabrication purposes.

2.3.3 Chemical Description of Growth Process

Presently, a detailed understanding of the growth process is lacking. It is currently hypothesized that during the ablation at 600°C in Ar, an oxygen deficient phase is formed which is relatively stable at the growth conditions. Evidence for oxygen deficient behavior has been seen in BKBO, and the films may perhaps be more accurately written as $Ba_{1-x}K_xBiO_{3-\delta}$.[34,35,36] At the anneal temperature, these oxygen vacancies are filled. The films are superconducting upon removal from the chamber. Strangely, the films can not be recycled through the deposition process because

they decompose. Apparently, the fully oxygenated compound is not stable at the deposition conditions.

In fact, this variable oxygen content is very problematic for film growth. The lattice constant shrinks with increasing oxygen content, causing film cracking and degrading transport characteristics. We avoid this problem by growing thin strained films ($t < 1500Å$). The thicker the films, the more likely they crack.

2.3.4 Deposition Systems

The original chamber is represented in Fig. 2.1. The sample heater was inserted through a KF flange on top of the chamber to point down onto the ablation target. The heater was made of a coiled heater wire where the heating element was surrounded with MgO insulation and encased in an Inconel sheath.[37] This enabled us to repeatably heat up substrates past 800°C in 100mT of oxygen.[38] The temperature was measured with an encased Inconel K-type thermocouple,[39] inserted into a hole far inside the heater block. The pellet was mounted on a copper holder of roughly the same diameter as the target pellet. The small cross-section viewed by the heater and the gas jet directed onto the pellet kept the target from melting during the ablation. There was a magnetic rotational feedthrough driven by an electric motor on which the target holder sat. Rotating the target during the ablation decreased wear of the target. A shutter was used to pre-clean the target before the ablation, and to allow aligning the substrate with the ablation plume without depositing on the substrate.

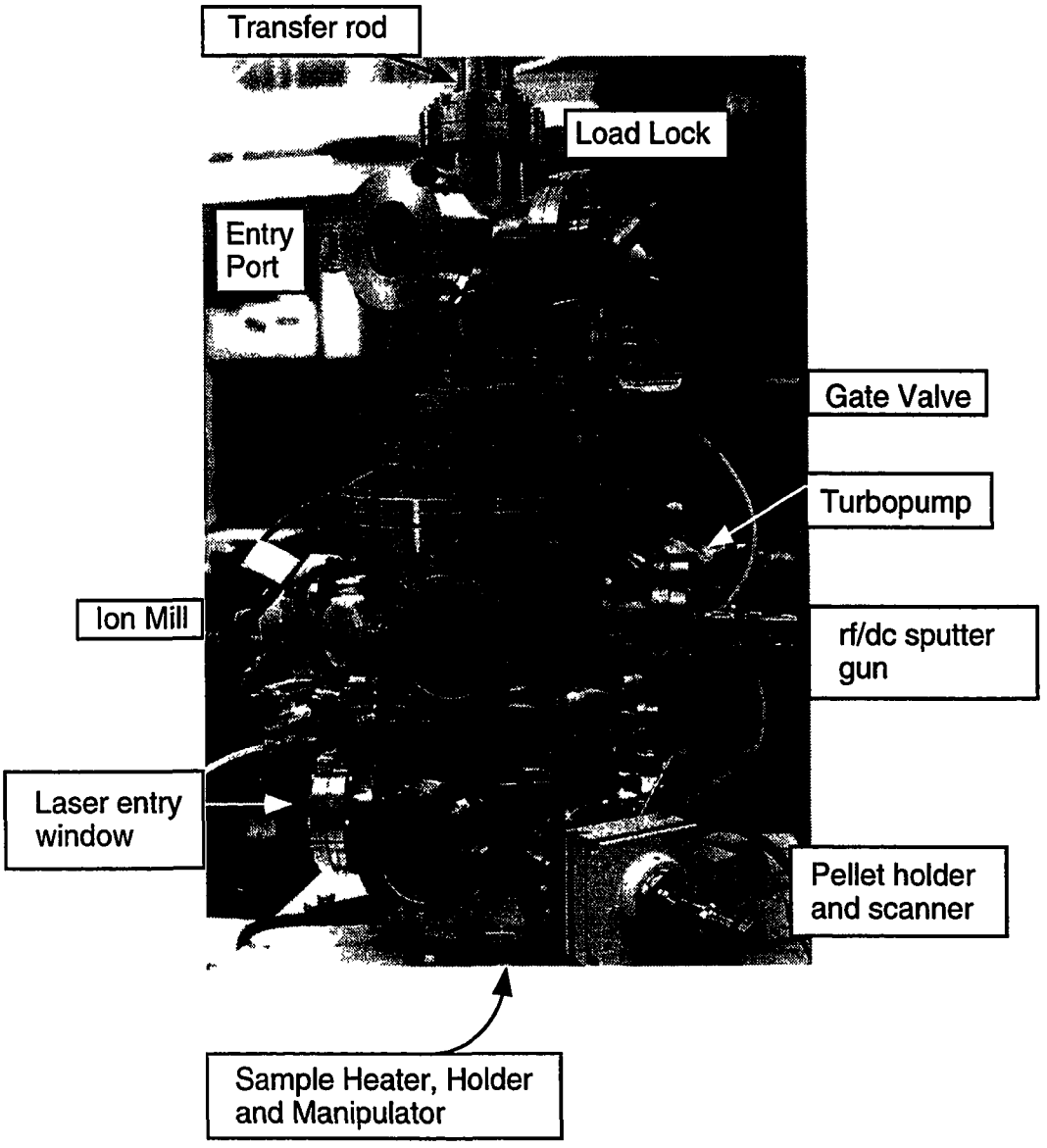

Figure 2.2 Diagram of multitarget ablation chamber

The next generation of our ablation growth systems is shown in Fig. 2.2 and was commissioned the Axl chamber in June 1992. The first benefit this chamber offers is a load lock to introduce samples into the chamber. This allows the growth chamber to be kept at high vacuum at all times, providing throughput and reproducibility. Probably the most important feature is the *in-situ* multilayer growth capability. This chamber has a 6 target carousel for PLD, a dc sputter gun, and a rf sputter gun. *In-situ* multilayers are important in order to get abrupt, clean and reproducible Josephson junction interfaces and also to obtain low contact resistances between metal and HTS.[40] In addition, the system has an ion mill to help provide clean interfaces and etching. Both the load lock and chamber have insulated electrical feedthroughs, allowing for dc (oxygen) glow discharges for precleaning the substrate before deposition and cleaning the chamber interior. The substrate holder is a radiative heater surrounded by a water cooled heat shield that uses a 1000W quartz halogen lamp.[41] This holder can be scanned as it is mounted on a 3 dimensional UHV manipulator, enabling uniform PLD coating of larger substrates.

2.3.5 Substrates and Substrate Preparation

An important aspect to HTS growth is the choice and preparation of substrates. The two dimensional nature of cuprate conduction requires oriented, textured films to get superconducting films. Although BKBO has a three dimensional conduction network, we have found that crystalline films are necessary for good

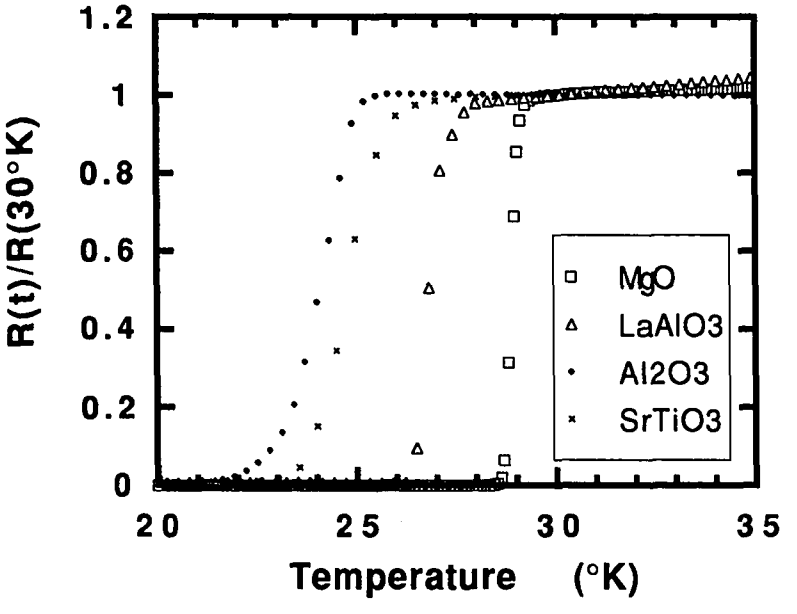

Figure 2.3 Normalized resistance [R(t)/R(30°K)] vs. temperature for PLD grown films on several crystalline substrates: (100) MgO, (110) $SrTiO_3$, (100) $LaAlO_3$, and (1$\underline{1}$02) Al_2O_3. As the growth conditions have not been optimized for the different substrates, this graph is only meant to show the diversity of substrates on which BKBO can grow.

superconducting properties. To achieve crystallinity, one must start with a single crystal substrate. Lattice match, thermal match, chemical compatibility, microwave loss, and phase stability up to growth temperature are important substrate attributes. Some important crystalline substrates for HTS are $LaAlO_3$, $SrTiO_3$, MgO, Al_2O_3, $NdGaO_3$,[42] YSZ, GaAs, and Si. We have successfully grown films on $LaAlO_3$,[43] MgO, Al_2O_3, and $SrTiO_3$, as shown in Fig. 2.3. We currently use MgO. It has the best lattice match, good thermal match, good chemical compatibility, decent microwave losses, and no structural phase transformations under growth conditions.

Substrate preparation is also important to grow quality films. A dirty and/ or amorphous surface won't produce superconducting films. The MgO substrates we use are either new or are reused by mechanically polishing with Buehler Mastermet (basic pH solution with 0.06μ SiO_2 abrasive grit). The standard substrate cleaning procedure involves sequentially scrubbing with Alconox detergent, rinsing with deionized (DI) water, acetone, isopropanol alcohol, rinsing again with DI water, and finally blowning dry with clean nitrogen gas. One should note that MgO is hygroscopic and reacts with the atmosphere. Thus, one should use prepared substrates quickly, as the surface degrades within a day if left out in the air. We keep our substrates in a dessicator for longevity. Annealing can be used to reorder the surface of the substrate, usually at temperatures of 1000-1200°C in air or flowing oxygen.[44,45] We usually do not externally anneal, but rather *in-situ* anneal the

substrate at 800°C in 100mT of oxygen prior to the ablation. The *in-situ* anneal complements both the ion mill and the oxygen plasma cleaning treatments, as it may repair resulting minor surface damage. Another possible, but for us unexplored, method of preparing the MgO substrate is to deposit buffer layers. One possibility is a thin MgO layer just prior to superconductor growth, assuring a fresh, crystalline surface. Other buffer layers that have aided in low temperature BKBO growth include $SrTiO_3$,[46] $BaZrO_3$, $BaBi_2O_y$, and $Ba_{2-x}Pb_xO_{4-x}$.[47]

A critical aspect to film reproducibility is the consistent mounting of the substrate to the heater, as this determines the thermal connection to the heater block. If the mounting technique is reproducible, then the temperature of the thermocouple can then be correlated to the substrate's surface temperature. We prefer thinner Ag paint over paste. The less material between the substrate and the block, the less thickening of the Ag solution will affect the thermal contact. A good way to mount the substrate is to press down on the middle of the substrate with some utensil and a fragment of the same type of substrate between the utensil and substrate. This prevents contamination of the substrate and uniformly presses the substrate into the Ag paint/paste, avoiding gaps and air bubbles that can occur when pressing down by the corners.

2.3.6 Particulate Generation

As previously discussed, an important consideration of PLD is the generation of particulates during the process. The target

material properties play a large role in determining the type and amount of particulates produced. A target produces less particulates with increased thermal conductivity, cohesiveness, and optical absorption coefficient.[48] Thus, higher density pellets work better. In the case of MgO which doesn't absorb UV well, very dense pressed targets work even better than single crystals as the solid defects will absorb light, enhancing ablation.

An important practical concern is keeping the ablation target cool during deposition. Heating results from the growth stage radiating onto the target while the laser is pulsing. This can change the stoichiometry of deposited material, especially for high volatility elements in the pellet. Also, the surface can "melt," resulting in large droplets being deposited.[49] Heating effects occur more often in loosely pressed ablation targets, which have lower heat conductivity. This effects can be avoided by using water cooled heat shields for the laser target.

Target history also affects particulate formation. It has been observed that the surface of the pellet changes both physically and chemically with continued exposure to laser pulses. Columnar structures form on the target surface, and are suspected of contributing to the film particulates. Also, the deposition rate decreases asymptotically with laser exposure. For example, YBCO decreases to 10-25% of the "fresh" rate. Surprisingly enough, the film stoichiometry isn't affected by the surface modification. By scraping, sanding, or repolishing the target surface, the surface is

renewed, the original growth rate restored, and particulates are reduced.[50,51]

Factors external to the pellet also effect debris. Particulate density is minimized by using the following: low laser fluence (but high enough for ablation), short laser wavelengths and pulse widths[52] (e.g. UV excimer lasers), rastering the beam over the target during ablation, and pointing the gas source away from the ablation target.

A novel new method employed to both coat large substrates and avoid particulates is to use off-axis laser ablation. This is the ablation of material onto a rotating substrate which is lying in the center of the plume where the substrate normal is perpendicular to the plume direction. This lessens the amount of particulates because the lighter elements are scattered by the gas onto the substrate whereas large, heavy particles are not. This has been used successfully with YBCO.[53]

2.4 Process Development

Of course, development of a laser ablation system is not to be taken lightly. A good hardware setup is the first step. Desirable qualities are a leak free vacuum and pure gases (UHP or better), as these will limit the purity of the deposited film, especially the latter. A good leak detector is necessary, and a RGA (Residual Gas Analyzer) is useful. Also critical to the success of ablation is the uniformity and quality of the output laser beam. It is striking how much better the films are after cleaning and carefully aligning the laser optics. Since

the properties of the film are critically dependent on the temperature of the substrate, one needs a stable PID controlled heater stage and reproducible routine to mount the substrate on the holder. I found with MgO especially, it is also necessary to have a good substrate preparation treatment-- dc oxygen plasma-- for reproducibility.

The target quality is also critical for quality as well as reproducibility, as the film is only as good as the target that made it. Desirable qualities in the pellet include high density, high purity (especially low Na contamination, which can degrade the T_c), and single phase. We have achieved excellent results using high purity melt-quenched targets.[54] Also, since a loss of K and Bi can occur during the ablation, sometimes a K rich target is used. This can offer wider process latitude. We have had good success with a $Ba_{0.55}K_{0.45}BiO_3$ target. Although less desirable, multi-phase targets have been used successfully[55] and offer a wide composition variation.

Yield is always an important question when growing these films. Our yield of superconducting films for the past 500 films has been about 40%. The yield for films of good quality (T_c > 25 °K and ΔT < 2°K) is much lower at 10-15%. The region in phase space for good film growth is rather small. This is likely to be improved in the future as understanding improves. In order to debug a new PLD system, it can be useful to first grow YBCO; which is easier to grow than BKBO.

Finally, the most important aspect of the growth is throughput. Much trial and error will inevitably need to be done in order to get the system running as well as optimizing the system. Optimization can best be done with the statistical design of experiments (DOE).[56]

2.5 Future Directions

There are many different area of film growth that are unknown or not well understood. Presently, an understanding of the kinetics (section 2.2) and chemistry of the PLD BKBO growth process is lacking. Especially interesting is the role of both oxygen and argon in the ablation process. Use of a high pressure of Argon gas has been necessary for us to grow superconducting films. Ar gas pressure's effect on-axis and off-center ablation is remarkable. Since we are in the diffusive limit, the Ar gas serves to thermalize the components of the plume, possibly increasing the sticking coefficients of the deposited elements. Also, the argon attenuates the oxygen by scattering, thus realizing a lower partial pressure at the film. Another possibility is that the diffusive expansion may allow for the oxygen to form metal oxides within the plume before reaching the substrate, enhancing growth. Like the cuprates, oxygen plays a critical role in growth of the bismuthates. Some progress has been achieved towards development of a phase diagram of temperature and oxygen pressure, although further study is needed.[57,58,59]

There are also practical questions that need to be answered concerning the ablation process. A useful development would be a way to accurately correlate the superconducting properties with

microanalytical results. Currently, a film's good microanalytic measures are necessary, but not sufficient for good superconductivity. This will be discussed more fully in Chapter 4. Also, the reproducibility and quality of the films need to be improved for applications purposes. Critical to applications is finding a method to reduce the stress in films seen in all current deposition schemes. Stress degrades superconductive film and junction properties as well as making multilayers difficult.

One possible future direction that may help reproducibility is the use of N_2O during the laser ablation of BKBO. This has already achieved some results at lower growth temperatures.[60] N_2O may provide a stabilizing component for superconducting thin film BKBO growth. During the deposition phase, the BKBO thin film is very sensitive (i.e. can decompose) to small amounts of oxygen introduced into the process gas. However, some oxygen is needed to form the precursor film before the oxygen cooldown. We have been able to reduce a film's resistance by orders of magnitude with annealing the pellet in oxygen prior to the ablation. Apparently, the interstitial oxygen annealed into the pellet is extracted during the ablation, benefiting film growth. Thus there may exist a very small amount of oxygen that could be introduced during growth to make the process more reproducible. However, this amount must be less than 1 mbar of O_2, as we have found this level of gas will degrade the film. This level of flow is difficult to manage simultaneously with a 1 Torr argon flow without a variable leak valve. N_2O is relatively

unreactive but is strongly oxidizing when photodissociated.[61] This oxidant has been used successfully to grow *in-situ* PLD $Nd_{1.85}Ce_{0.15}CuO_{4-\delta}$ without the vacuum anneal step used to eliminate extra oxygen incorporated during the film growth.[62,63] Thus, N_2O may allow for a larger flow and partial pressure of gas to be used to stabilize the growth process.

References

[1] R.C. Lacoe, J.P. Wendt, and P.M. Adams, "Deposition of barium potassium bismuth oxide (BKBO) thin films by laser ablation," IEEE Trans. Appl. Superconductivity, vol. 3(1), pp. 1563-66, Mar. 1993.

[2] J. Geerk, supplementary presentation in section C15, American Physical Society meeting, Seattle, Wash., March 1993.

[3] W.T. Lin, S.M. Pan, Y.F. Chen, "Parametric study of the *in situ* growth of BaKBiO thin films by laser ablation," J. Appl. Phys., vol. 75(2), pp. 1179-1184, Jan. 1994.

[4] H.T. Kim, A. Sumi, H. Uwe, J. Fujita, and K. Ohshima, "Synthesis of superconducting epitaxial films of $Ba_{1-x}K_xBiO_3$ by laser ablation," Jpn. J. Appl. Phys., vol. 32(10), pp. 4529-34, Oct. 1993.

[5] D.P. Norton, J.D. Budai, B.C. Chakoumakos, and R. Feenstra, "Epitaxial growth of $Ba_{1-x}K_xBiO_3$ thin films by pulsed laser deposition," Appl. Phys. Lett., vol. 62(4), pp. 414-6, Jan. 1993.

[6] C.J. Hou, H. Steinfink, L. Rabenberg, C. Hilbert, and H. Kroger, "Superconducting $Ba_{0.6}K_{0.4}BiO_3$: Thin film preparation by RF magnetron sputtering," J. Mater. Res., vol. 8(8), pp. 1798-1804, Aug. 1993.

[7] B.A. Baumert and J. Talvacchio, "Artificial barriers for Ba-K-Bi-O tunnel junctions," IEEE Trans. Appl. Superconductivity, vol. 3(1), pp. 1567-70, Mar. 1993.

[8] H. Sato, S. Tajima, H. Takagi, and S. Uchida, "Optical study of the metal-insulator transition on $Ba_{1-x}K_xBiO_3$," Nature, vol. 338, pp. 241-3, Mar. 1989.

[9] J. Amano, H. Ko, M. Narbutovskih, J. Sheats, and K. Tibbs, "Superconducting $Ba_{1-x}K_xBiO_3$ thin films and junctions," J. Appl. Phys., vol. 74(7), pp. 4620-4626, Oct. 1993.

[10] R. Hu, A.E. Lee, H.W. Chan, and C.L. Pettiette-Hall, "Superconducting $Ba_{1-x}K_xBiO_3$ thin film by in-situ sputtering," IEEE Trans. Appl. Superconductivity, vol. 3(1), pp. 1556-58, Mar. 1993.

[11] Y. Enomoto, T. Murakami and K. Moriwaki, "$Ba_{1-x}K_xBiO_3$ thin film preparation by ECR ion-beam oxidation and film properties," Jpn. J. Appl. Phys., vol. 28, pp. L1355-7, 1989.

[12]E.S. Hellman, E.H. Hartford, and R.M. Fleming, "Molecular beam epitaxy of superconducting (Rb,Ba)BiO_3," Appl. Phys. Lett., vol. 55(20), pp. 2120-2, Nov. 1989.

[13]M. Ogihara, T. Makita, and H. Abe, "Ultrathin film deposition of $Ba_{1-x}Rb_xBiO_3$ by molecular beam epitaxy using distilled ozone," Appl. Phys. Lett., vol. 63(19), pp. 2694-6, Nov. 1993.

[14]B.M. Moon, C.E. Platt, R.A. Schweinfurth, and D.J. Van Harlingen, "In situ pulsed laser deposition of superconducting $Ba_{1-x}K_xBiO_3$ thin films," Appl. Phys. Lett., vol. 59(15), pp. 1905-7, Oct. 1991.

[15]M.P. Siegal, S.Y. Hou, J.M. Phillips, T.H. Tiefel, and J.H. Marshall, "Growth and characterization of $Ba_2YCu_3O_{7-\delta}$ films in reduced oxygen partial pressures using the BaF2 post annealing process," J. Mater. Res., vol. 7(10), pp. 2658-66, Oct. 1992.

[16]Pre-HTSC: C.L. Chan and J. Mazumder, J. Appl. Phys. vol. 62, p. 4579
Post-HTSC: J. Cheung and J. Horwitz, "Pulsed laser deposition history and laser-target interactions," vol. 17, p30-36, Feb. 1992.

[17]A. Inam, X. D. Wu, T. Venkatesan, S. B. Ogale, C. C. Chang, D. Dijkkamp, Appl. Phys. Lett., vol. 51, p. 1112 (1987)

[18]R.K. Singh and J. Narayan, "The pulsed-laser deposition of superconducting thin films," JOM, vol. 43, pp. 13-20, (March 1991)

[19]R.K. Singh, and J. Narayan, JOM, ibid.
R.K. Singh, D. Bhattacharya, and J. Narayan, "Subsurface heating effects during pulsed laser evaporation of materials," Appl. Phys. Lett., vol. 57(19), pp. 2022-4, Nov. 1990.

[20]R.K. Singh and J. Narayan, JOM, ibid.

[21]T. Venkatesan, X. D. Wu, A. Inam, and J. B. Wachtman, "Observation of two distinct components during pulsed laser deposition of high Tc superconducting films," Appl. Phys. Lett., vol. 52(14), p 1193-5, April 1988.

[22]R.K. Singh and J. Narayan, JOM, ibid.

[23]R.A. Neifeld, S. Gunapala, C. Liang, S.A. Shaheen, M. Croft, J. Price, D. Simons, and W.T. Hill, "Systematics of thin films formed by excimer laser ablation: Results on $SmBa_2Cu_3O_7$," Appl. Phys. Lett., vol. 53, p703-704, August 1988.

[24]A. Gupta, "Gas-phase oxidation chemistry during pulsed laser deposition of $YBa_2Cu_3O_{7-\delta}$ films," J. Appl. Phys., vol. 73, p7877-7886, June 1993.

[25]R.E. Muenchausen, K.M. Hubbard, S. Foltyn, R.C. Estler, and N.S. Nogar, and C. Jenkins, "Effects of beam parameters on excimer laser deposition of $YBa_2Cu_3O_{7-\delta}$," Appl. Phys. Lett., vol. 56(6), pp. 578-80, Feb. 1990.
R.C. Dye, T. Brainard, S.R. Foltyn, R.E. Muenchausen, X.D. Wu, and N.S. Nogar "Evolution and dynamics of excimer laser vaporized $YBa_2Cu_3O_{7-\delta}$ plumes," Laser Ablation in Materials Processing: Fundamentals and Applications, Ed. B. Braren, J.J. Dubowski, D.P. Norton, Materials Research Society Symposium Proceedings (Boston, Dec. 1992), published by Materials Research Society, Pittsburgh, Pennsylvania, vol. 285, p. 15-26, 1993

[26]R.K. Singh and J. Narayan, Phys. Rev. B, ibid.

[27]R.C. Tolman, The Principles of Statistical Mechanics, Dover, New York, 1979, Chapter VI.

[28]R.C. Dye, ibid.

[29]R.K. Singh and J. Narayan, Phys. Rev. B, ibid.

[30]H.S. Kwok, H.S. Kim, S. Witanachchi, E. Petrou, J.P. Zheng, S. Patel, E. Narumi, and D.T. Shaw, "Plasma-assisted laser deposition of $YBa_2Cu_3O_{7-\delta}$," Appl. Phys. Lett., vol. 59(27), pp. 3643-5, Dec. 1991.

[31]C.J. Hou, H. Steinfink, L. Rabenberg, C. Hilbert, and H. Kroger, "Superconducting $Ba_{0.6}K_{0.4}BiO_3$: Thin film preparation by RF magnetron sputtering," J. Mater. Res., vol. 8(8), pp. 1798-1804, Aug. 1993.

[32]See for example, J.P. Locquet, A. Catana, E. Machler, C. Gerber, and J.G. Bednorz, "Block-by-block deposition: A new growthy method for complex oxide thin films," Appl. Phys. Lett., vol. 64(3), pp. 372-4, Jan. 1994.

[33]High purity silver paste, part # 5061, SPI Supplies, Westchester, PA. Silver ink, part # 16, Englehard, East Newark, NJ.

[34]E.S. Hellman, E.H. Hartford, and E.M. Gyorgy, "Epitaxial $Ba_{1-x}K_xBiO_3$ films on MgO: Nucleation, cracking, and critical currents," Appl. Phys. Lett., vol. 58(12), pp. 1335-7, Mar. 1991.

[35]K. Ueki, A. Tokiwa, M. Kikuchi, T. Suzuki, M. Nagoshi, R. Suzuki, N. Kobayashi, and Y. Syono, in Advances in Superconductivity II: Proceedings of the 2nd International Symposium on Superconductivity (ISS '89), November 14-17, 1989, Tsukuba, edited by T. Ishiguro and K. Kajimura (Springer, Tokyo, 1990), p. 489.

[36]Y. Idemoto, Y. Iwata, and K. Fueki, "Oxygen content and T_c of $Ba_{0.6}K_{0.4}BiO_{3-\delta}$," Physica C, vol. 201, pp. 43-49, 1992.

[37]Thermocoax, part # 1NCI15, Philips Electronic Instruments Company, Industrial Automation Division, Norcross, GA.

[38]Two other oxygen heaters are quartz halogen lamps and Kanthal wire. A Kanthal wire heater is described in B.D. Oh and R.P. Robertazzi, Rev. Sci. Instrum., vol. 62, p. 3104, 1991.

[39]K type thermocouple probe, part # CAIN-116U-24, Omega Engineering, Inc., Stamford, CT.

[40]R.P. Robertazzi, A.W. Kleinsasser, R.B. Laibowitz, R.H. Koch, and K.G. Stawiasz, "*In-situ* $Ag/YBa_2Cu_3O_7$ contacts for superconductor-normal metal-superconductor devices," Phys. Rev. B, vol. 46(16), p8469, Oct. 1992.

[41]ANSI code for halogen lamp was FEL. The lamp was manufactured by either General Electric or Ushio Inc. In order to use the bulb in a vacuum, the mount and insulation of the bulb is removed leaving the bare wires emerging from the quartz tube. This is possible for GE or USHIO bulbs, but not Sylvania.

[42]G. Koren, A. Gupta, E.A. Giess, A. Segmuller, and R.B. Laibowitz, "Epitaxial films of $YBa_2Cu_3O_{7-\delta}$ on $NdGaO_3$, $LaGaO_3$, and $SrTiO_3$ substrates deposited by laser ablation," Appl. Phys. Lett., vol. 54(11), pp. 1054-6, Mar. 1989.

[43]R.W. Simon, C.E. Platt, A.E. Lee, G.S. Lee, K.P. Daly, M.S. Wire, J.A. Luine, M. Urbanik, "Low-loss substrate for epitaxial growth of high-temperature superconducting thin films," Appl. Phys. Lett., vol. 53(26), pp. 2677-9, 1988.

[44]B.H. Moeckly, S.E. Russek, D.K. Lathrop, R.A. Buhrman, J. Li, and J.W. Mayer, "Growth of $YBa_2Cu_3O_7$ thin films on MgO: The effect of substrate preparation," Appl. Phys. Lett., vol. 57(16), pp. 1687-9.

[45]M.G. Norton and C.B. Carter, "Growth of $YBa_2Cu_3O_{7-\delta}$ thin films--nucleation, heteroepitaxy and interfaces," Scanning Microscopy, vol. 6(2), pp. 385-98, 1992.

[46]B.A. Baumert, J. Talvacchio, and M.G. Forrester, "SrTiO3 buffer layer and tunnel barriers for Ba-K-Bi-O junctions," Appl. Phys. Lett., vol. 62(17), pp. 2137-9, Apr. 1993.

[47]E.S. Hellman and E.H. Hartford Jr., "Normal-state resistivity and Hall effect in $Ba_{1-x}K_xBiO_3$ epitaxial films," Phys. Rev. B, vol. 47 (17), pp. 11346-11352, May 1993.

[48]R.K. Singh, D. Bhattacharya, and J. Narayan, "Control of surface particle density in pulsed laser deposition of superconducting $YBa_2Cu_3O_7$ and diamondlike carbon thin films," vol. 61, p. 483-485, July 1992

[49]F.C. Wellstood, J.J. Kingston, and John Clarke, "Thin-film multilayer interconnect technology for $YBa_2Cu_3O_{7-\delta}$," J. Appl. Phys., vol. 75(2), pp. 683-702, Jan. 1994.

[50]S. R. Foltyn, R. C. Dye, K. C. Ott, E. Peterson, K. M. Hubbard, W. Hutchinson, R. E. Muenchausen, R. C. Estler, and X. D. Wu, "Target modification in the excimer laser deposition of $YBa_2Cu_3O_{7-x}$ thin films," vol. 59, p594-596, July 1991.

[51]J.J. Kingston, F.C. Wellstood, Ph. Lerch, A.H. Miklich, and J. Clarke, Appl. Phys. Lett., vol. 56, p 189, 1990.

[52]G. Koren, A. Gupta, R. J. Baseman, M. I. Lutwyche, and R. B. Laibowitz, "Laser wavelength dependent properties of $YBa_2Cu_3O_{7-\delta}$ thin films deposited by laser ablation," Appl. Phys. Lett., vol. 55, p2450-2452 (December 1989)

[53]B. Holzapfel, B. Roas, L. Schultz, P. Bauer and G. Saemann-Ischenko, "Off-axis laser deposition of $YBa_2Cu_3O_{7-\delta}$ thin films," vol. 61(26), pp. 3178-80, Dec. 1992.

[54]D.G. Hinks, A.W. Mitchell, Y. Zheng, D.R. Richards, and B. Dabrowski, "Synthesis of high-density $Ba_{1-x}K_xBiO_3$ superconducting samples," Appl. Phys. Lett., vol. 54(16), pp. 1585-7, Apr. 1989.

[55]R.C. Lacoe, J.P. Wendt, and P.M. Adams, "Deposition of barium potassium bismuth oxide (BKBO) thin films by laser ablation," IEEE Trans. Appl. Superconductivity, vol. 3(1), pp. 1563-66, Mar. 1993.

[56]G.E.P. Box, W.G. Hunter, and J.S. Hunter, Statistics for Experimenters: An introduction to design, data analysis, and model building, John Wiley and Sons, New York, 1978.

[57]E.S. Hellman and E.H. Hartford Jr., "Synthesis of new oxide materials by molecular beam epitaxy: the Dy-Ba-Cu-O and Ba-K-Bi-O systems," Physica C, vol. 190(1), pp. 31-34, Dec. 1991.

[58]J. Geerk, ibid.

[59] W.T. Lin, S.M. Pan, Y.F. Chen, "Parametric study of the *in situ* growth of BaKBiO thin films by laser ablation," J. Appl Phys., vol. 75(2), pp. 1179-1184, Jan. 1994.

[60]W.T. Lin, S.M. Pan, and Y.F. Chen, J. Appl. Phys., ibid.

[61]A. Gupta, B.W. Hussey, and M.Y. Chern, "Effect of different oxidizing gases on the in-situ growth of $YBa_2Cu_3O_{7-\delta}$ films by pulsed laser deposition," Physica C, vol. 200, pp. 263-70, 1992.

[62]A. Kussmaul, P.M. Tedrow, and A. Gupta, "Comparison of laser ablated films of $Nd_{1.85}Ce_{.15}CuO_{4-\delta}$ made in O2 and in N2O," Bull. Amer. Phys. Soc., vol. 37(1), Mar. 1992.

[63]S.N. Mao, X.X. Xi, S. Bhattacharya, Q. Li, T. Venkatesan, J.L Peng, R.L. Greene, J. Mao, D.H. Wu, and S.M. Anlage, "Deposition and reduction of $Nd_{1.85}Ce_{.15}CuO_{4-\delta}$ superconducting thin films," vol. 61(19), pp. 2356-8, Nov. 1992.

Chapter 3
FILM CHARACTERIZATION

A critical part of making films and devices is feedback from various characterization methods. This includes both microanalytical and electrical characterization. I will discuss various microanalytical measures of our BKBO thin films, including Rutherford backscattering (RBS), X-ray diffraction (XRD), Scanning electron microscopy (SEM). Electrical characterization is also critical with superconductors. Our unpatterned films are usually tested using a mutual inductance technique, allowing us to screen films before fabricating devices and structures. Some film and device issues to be characterized include film stress (cracking), transport (T_c, J_c, R_s), uniformity, smoothness, interfaces, and multilayers.

3.1 Microanalysis

Although microanalysis has been used for quite some time, its importance to superconductivity has been largely realized with the discovery of the perovskite superconductor compounds. In a nutshell, it is much more difficult to make a single phase, crystalline, multielement superconductor than an elemental superconductor. Like most characterizations, each microanalytical method tells only a partial story, and a combination of techniques are needed to be conclusive. Along these lines, immediate returns from microanalysis are often small, or at least smaller than one would like. Much of its usefulness comes from helping to understand the process, in this case

growing BKBO thin films, which requires a long term commitment establishing correlations and baselines. If a process goes astray, as it eventually will, good process understanding will expedite problem correction, which otherwise may take months to determine by trial and error.

In this section, I will discuss some of the microanalytical tools used to study our PLD thin films. RBS, XRD, SEM, have aided in determining our film's composition, crystallinity, phase purity, and surface quality. For information on TEM and Moiré fringes of our films, the reader is referred to elsewhere.[1]

3.1.1 XRD

X-ray diffraction is ubiquitous in its use of determining crystallinity and phase composition in HTS superconductors. XRD uses a beam of x-rays, in our case the Cu Kα line at $\lambda = 1.541 Å$, interfering off the crystalline lattice of the sample. The interference has maximums at the following angles:

$$n\lambda = 2d\sin\theta, \qquad \text{(Eq. 3.1)}$$

where n is an integer, d is the lattice spacing, and 2θ is the angle between the incident and reflected light. The power of this technique comes from the fact that different compound phases have different lattice constants. This allows one to identify the crystalline phases in a sample. Mostly, one needs epitaxial growth off the substrate in order to get strong interference peaks from a thin film. An amorphous film will give, if any, weak diffraction peaks. Shown in Fig. 3.1 is a BKBO film grown on a (100)-MgO substrate. We see

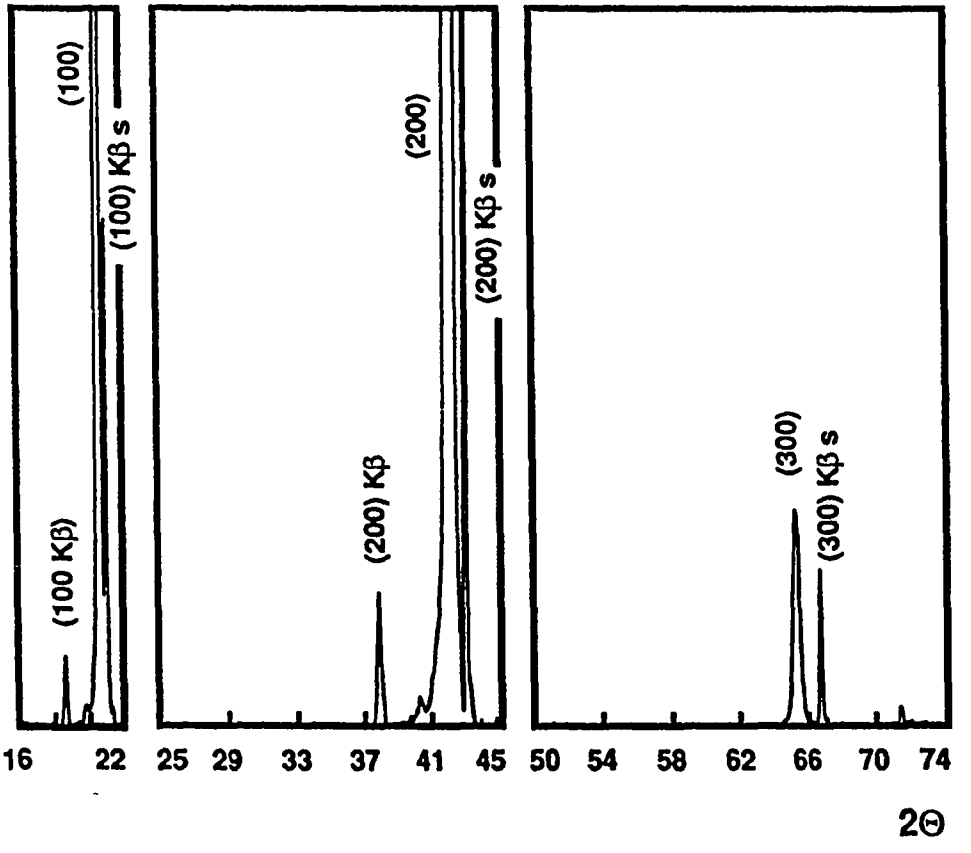

Figure 3.1 X-ray diffraction 2θ scan of PLD BKBO thin film on (100)-MgO substrate. XRD shows BKBO is oriented in the (100) direction and is single phase.

that the BKBO film exhibits a single phase (100)-orientation. The lattice constants of our films are 4.28-4.30 Å. In bulk, the lattice constant of BKBO is sensitive to the K content and can be used to determine doping;[2] however, substrate mismatch and resulting film stress make this inconsistent and unreliable in films. A measure of the crystallinity is the width of the diffraction peaks, often referred to as a rocking curve, which our films have measured less than 1°.

3.1.2 RBS

Rutherford Backscattering (RBS) is a powerful microanalytic tool. Its advantages include the relative speed, its ability to characterize composition as a function of depth, and its quantitative results. RBS can also measure the crystallinity of a single crystal sample. We have mainly used RBS to determine the relative composition of our films. RBS is more quantitative than SIMS, AES, XPS and EDAX and for us, more reproducible than ICP.

Disadvantages of RBS include its insensitivity to the lighter elements, difficulty in separating elements of similar mass, and its lack of chemical information. We have also found RBS to be destructive in its testing in our films, although this technique can be non-destructive with certain materials. Also, like all surface analysis methods, RBS interpretation can be affected by surface morphology.

The sensitivity of RBS is about 1% for the light elements and 0.01% for the heavy elements. In order to determine the film composition from the spectra, we model the film and substrate with

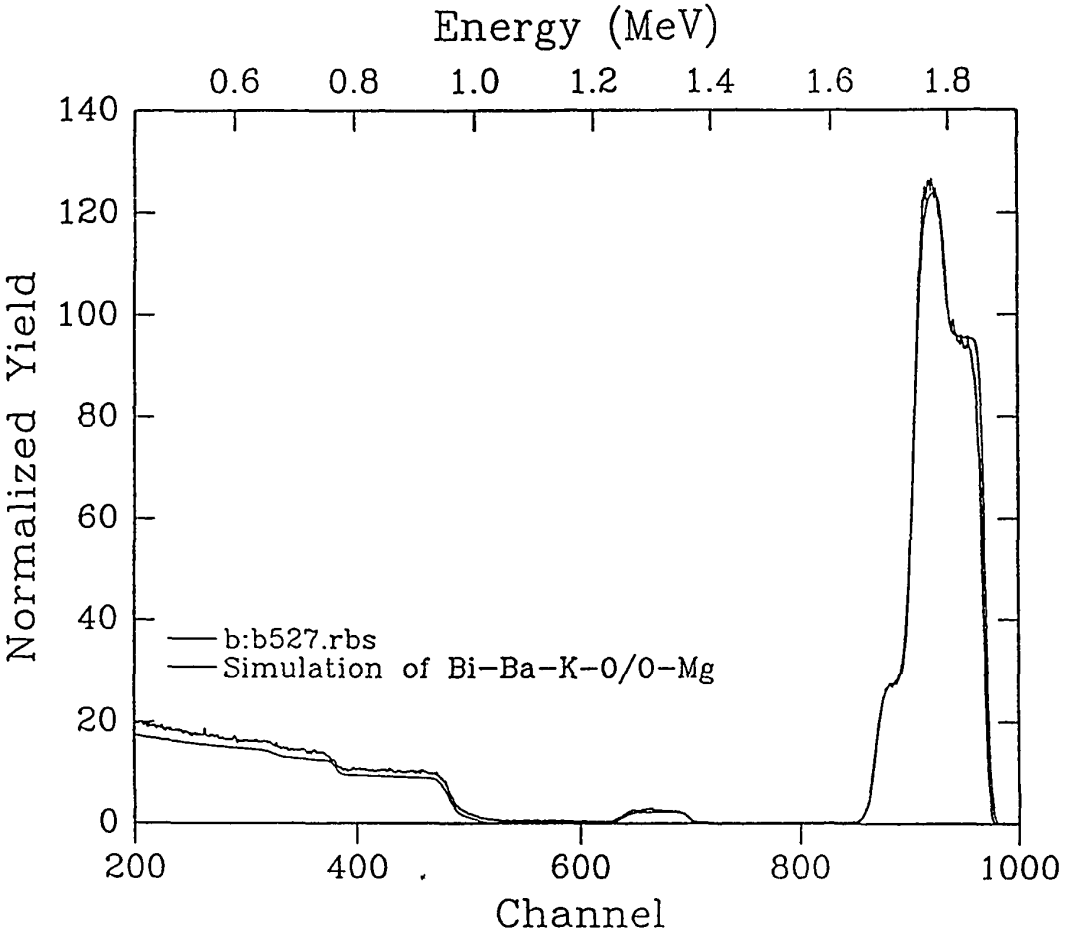

Figure 3.2 RBS spectra from a PLD BKBO thin film grown on MgO from a target with composition $Ba_{0.55}K_{0.45}BiO_3$. Also shown is the RUMP modeling of the film, which yields a thickness of 2585Å and a composition of $Ba_{0.62}K_{0.42}BiO_3$.

RUMP; a shareware program from Cornell. We are able to model our films with the precision of a few percent, with the K content being the most difficult to model. Modeling can also determine the film thickness with reference to BKBO density. Thickness was calibrated with reference to an etched film measured with a Dektak profilometer.

RBS, as the name implies, works by detecting alpha particles scattered at high angles. Our accelerator uses alpha particles with energy 2 MeV accelerated by a Van de Graaff accelerator. The alpha particles scatter off the sample into a solid state detector located at a large fixed scattering angle near 180°. The detector output is binned and sorted with a multichannel analyzer (MCA) to count the number and energy of the scattered particles.

The ratio of the scattered energy, E_1, to the incident energy, E_o, is given by the kinematic factor, K. The variation of K with scattering angle, θ, is given by,

$$K_{M_2} \equiv \frac{E_1}{E_o} = \left[\frac{\left(M_2^2 - M_1^2 \sin^2\theta\right)^2 + M_1 \cos\theta}{M_2 + M_1} \right]^2, \qquad \text{(Eq. 3.2)}$$

where M_1 and M_2 are the incident projectile mass (alpha particle) and scattering sample mass, respectively. This relation comes from simple elastic scattering and shows how the different elements are identified in a sample.

Also important to the spectroscopy is how often a given scattering event occurs. This can be understood by the differential cross section for a collision, represented by $d\sigma/d\Omega$ in CGS units below:

$$\frac{d\sigma}{d\Omega} = \left(\frac{Z_1 Z_2 e^2}{4E_o}\right)^2 \frac{4}{\sin^4\theta} \frac{\left\{\left[1 - \left((M_1/M_2)\sin\theta\right)^2\right]^{1/2} + \cos\theta\right\}^2}{\left[1 - \left((M_1/M_2)\sin\theta\right)^2\right]^{1/2}}, \quad \text{(Eq. 3.3)}$$

where Z_1 and Z_2 are the atomic number of the incident particle and target particle, respectively. In most cases, $M_1 \ll M_2$, as the incident particle is an alpha particle. Eq. 3.3 can then be simplified with a power expansion,

$$\frac{d\sigma}{d\Omega} \approx \left(\frac{Z_1 Z_2 e^2}{4E_o}\right)^2 \left[\sin^{-4}\left(\frac{\theta}{2}\right) - 2\left(\frac{M_1}{M_2}\right)^2 + \ldots\right]. \quad \text{(Eq. 3.4)}$$

The increased sensitivity of RBS of heavier elements is explained in Eq. 3.4, as they have a higher cross section to scatter incident alpha particles into the detector. Further information on RBS can be found in Chu, Mayer, and Nicolet.[3]

In Fig. 3.2 is shown a RBS spectra illustrating good compositional control over our films. RUMP modeling yields a composition of $Ba_{0.62}K_{0.42}BiO_3$ and a thickness of 2585Å.

Like others,[4] we see a strong correlation with film color and RBS spectra, especially potassium content. A film with potassium content of $x \approx 0.4$ will appear have a purple surface. As the potassium content drops, the film will appear blue, green, gold and

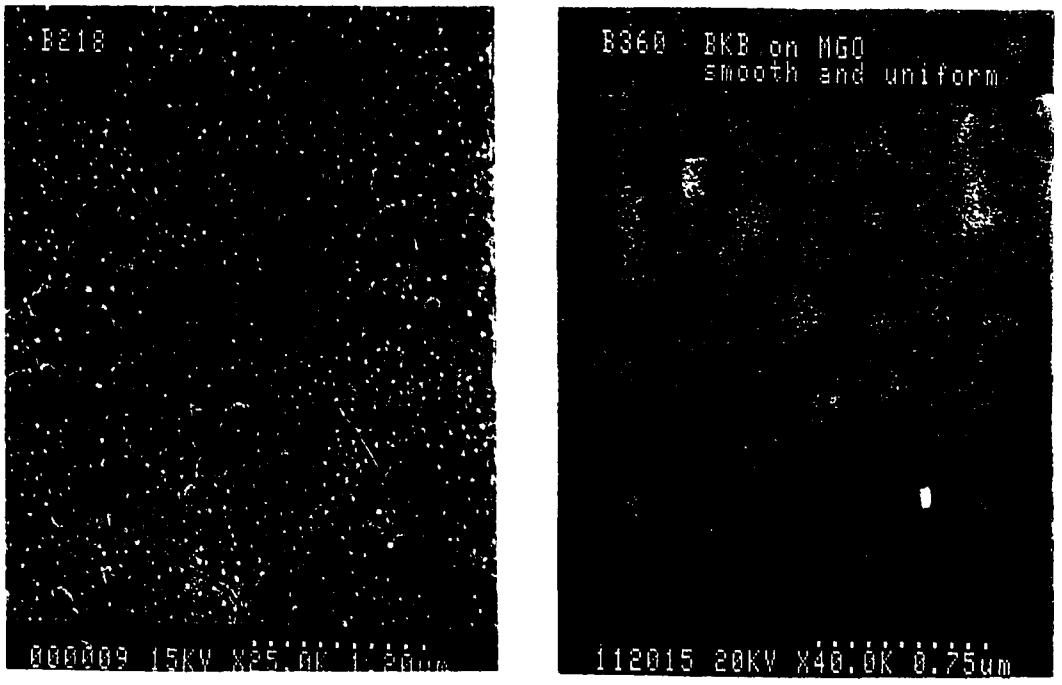

Figure 3.3 (a) SEM micrograph of a PLD BKBO thin film showing a smooth surface. (b) SEM micrograph of a PLD BKBO thin film showing microcracking.

sometimes reddish. If a film appears gold or red, it has very little potassium. This is a quick simple test for a film after deposition.

3.1.3 SEM

An important and basic microanalytical tool is the Scanning Electron Microscope (SEM). It acts as a high magnification microscope, usually used between 50X to 100,000X, which allows one to look at both fabricated and unfabricated samples. It works by rastering a focusing electron beam, usually < 40KeV, on a sample and detecting the emitted electrons from the surface. There are both backscattered and secondary electrons emitted from the sample. Backscattered electrons (BSE) are the result of elastic collisions with the sample whose energies are comparable to the incident energy. BSE electrons offer contrast between different atomic elements as shown by Eq. 3.4. Secondary electrons (SE) are low energy (< 50eV) and are emitted within a few nm from the surface. We usually use the SEM in the SE electron mode to look at surfaces.

Shown in Fig. 3.3 are two different BKBO films grown with PLD. The first film (Fig. 3.3a) shows a smooth surface, while the second (Fig. 3.3b) exhibits microcracking. We find that lower temperature growth, like YBCO, aids in smooth surfaces. Microcracking in BKBO has been documented using a number of different techniques.[5] We find that on-axis ablation prevents much microcracking and allows the growth of thicker films. Microcracking in BKBO thin films is thought to originate during the common oxygen anneal step in BKBO growth. Studies have shown that the lattice constant of oxygen

deficient $Ba_{1-x}K_xBiO_{3-\delta}$ will shrink as the oxygen vacancies are filled ($\delta \downarrow$). For this reason, all BKBO thin films grown with different methods have stress. Stress is a critical issue for BKBO thin film development, as this makes thick films and multilayers difficult, and can impact Josephson junction behavior.[6,7]

3.2 Electrical

While microanalysis helps improve film quality and assists moving towards superconducting growth parameters when the process is off, it cannot currently predict superconducting film properties. When growth parameters produce superconducting films, electrical characterization is crucial for film application and development. While there are many ways to do this using both patterned and unpatterned films, I will focus on unpatterned measurements in this chapter and patterned measurements in Chapters 5,6, and 7.

Methods of characterizing an unpatterned superconducting thin film include microwave surface impedance, SQUID magnetic susceptibility, resistivity, mutual inductance techniques, and room temperature resistance. All these techniques measure the aforementioned quantity while varying the temperature through the transition, except for the room temperature resistance measurement. We have mainly used the latter two methods.

3.2.1 Room Temperature Resistance

The first characterization of any PLD film is a two-probe measure of the film resistance. This is done with a common

ohmmeter from one corner of the sample to the other. For superconducting YBCO, this resistance should nominally be $\leq 300\Omega$, while for BKBO it is $\leq 3K\Omega$. Of course, this value will vary with thickness and other parameters. The purpose of this test is to determine if the film is somewhat metallic; a requirement for superconductivity. If the film passes this test, we cool it down measuring the mutual inductance to determine, hopefully, the T_c and ΔT_c.

3.2.2 Mutual Inductance Technique

The two-coil mutual inductance technique was first developed by Fiory and Hebard for studying the kinetic inductance and dissipation of thin superconducting films.[8] We used the technique to non-destructively test the T_c of a superconducting film, and also infer qualitative information concerning the superconducting uniformity and the J_c of the film from the transition width (ΔT_c). This method can also yield quantitative information concerning the film's critical current density (J_c) and penetration depth (λ), if calibration and care for film thickness, film size effects, film temperature, and coil position are performed. A similar technique uses a single coil simultaneously for both drive and pickup.[9]

We measure the mutual inductance with a two coil configuration shown below in Fig. 3.4a. The drive coil is oscillated at 20KHz at an amplitude of 0.1V. The coils are wound with 20 turns of 36 gauge copper wire and a diameter of a few mm. It is important that the leads to the pickup and drive coil are isolated with coaxial

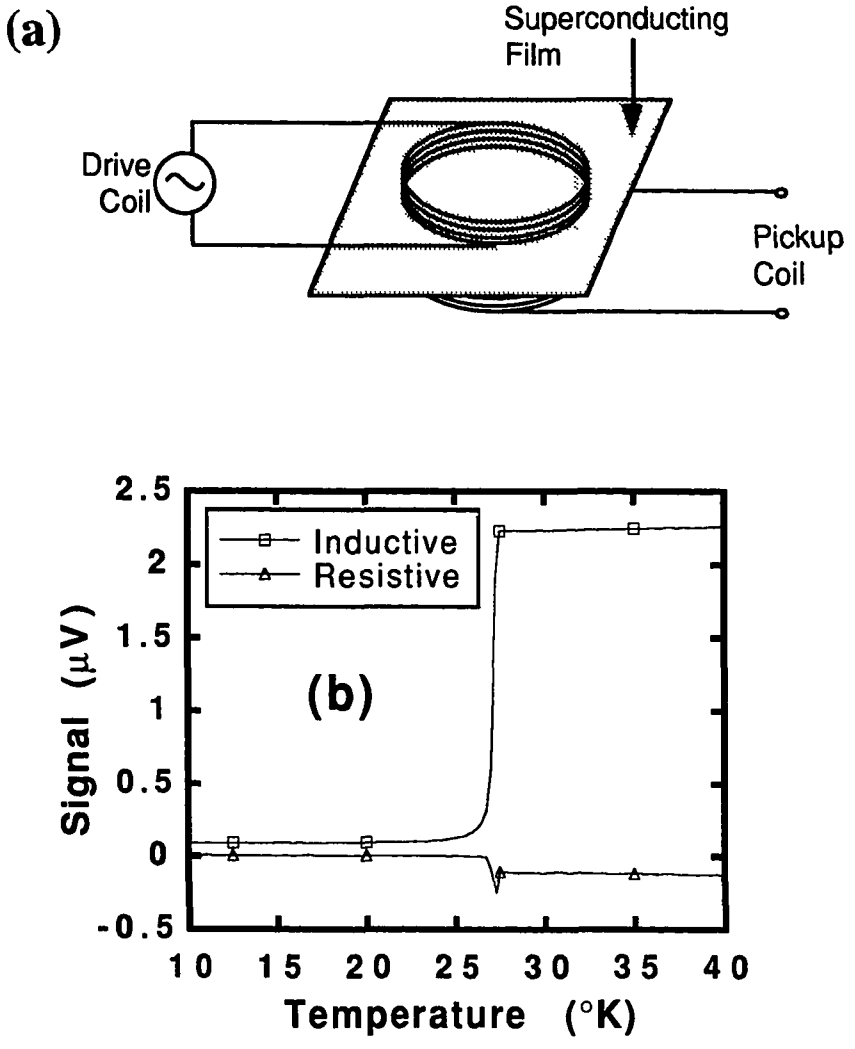

Figure 3.4 (a) Schematic sketch of the two-coil mutual inductance technique. (b) Two-coil mutual inductance measurement of a PLD BKBO thin film.

line or separate twisted pairs to prevent crosstalk. The nominal pickup signal is about 5 μV when not superconducting. In order for the test to be non-destructive, we are also careful to keep any water from condensing on the film after testing.

The measurement works by inductively coupling the top drive coil to the bottom pickup coil through the superconducting film. While superconducting, the film's Meissner effect screens the magnetic field from the pickup coil. This creates the inductive (in-phase) signal transition and also the dissipation peak in the resistive (quadrature) signal as shown in Fig. 3.4c. This can be modeled by a resistor in parallel with an inductor, where the resistance are the film losses and the inductance is due to screening currents. The impedance of the film modeled as, $Z = R + j\omega L$. The in-phase pickup signal is about $\pi/2$ out of phase with the drive signal before the transition, due to the inductive coupling. Above T_c, the film resistive impedance is much larger than the reactive impedance in the film. As the temperature sweeps through the transition, the resistive component drops first, then the film inductance starts to increase. The film inductance where thickness $<< \lambda$ is mostly due to kinetic inductance. As the inductance increases to expel the field, the inductive signal drops. The largest dissipation occurs when $R \approx L$, which produces the dip in the resistive signal.

The width of the transition also provides information. Broadening can come from both the resistive and inductive components of the film. The inductance of the film is strongly

dependent, in the thin-film limit, on both the penetration depth and the critical current. Near the transition, the critical current is low, which inhibits the screening ability of the superconductor. The resistive component, however, can also broaden the transition if the T_c of various superconducting grains making up the film have different transition temperatures. If the transition is sharp, we can infer film homogeneity and high J_c, as exhibited by the film in Fig. 3.4b.

3.3 Summary

We have characterized our films both microanalytically and electrically. We have achieved smooth, epitaxial, stoichiometric films with excellent superconducting properties, which will be further elaborated on in later chapters. The two-coil mutual inductance technique has been especially useful for non-destructive superconducting characterization, determining information about T_c, ΔT_c, J_c, and homogeneity.

References

[1] C. Ciofi, C.E. Platt, J.A. Eades, J. Amano, and R. Hu, "Structural comparison of $Ba_{1-x}K_xBiO_3$ superconducting thin films," J. Mater. Res., vol. 9(2), pp. 305-313, Feb. 1994.

[2] S. Pei, J.D. Jorgensen, B. Dabrowski, D.G. Hinks, D.R. Richards, A.W. Mitchell, J.M. Newsam, S.K. Sinha, D. Vaknin, and A.J. Jacobson, "Structural phase diagram of the $Ba_{1-x}K_xBiO_3$ system," Phys. Rev. B, vol. 41(7), pp. 4126-41, Mar. 1990.

[3] W.K. Chu, J.W. Mayer, M.A. Nicolet, Backscattering Spectrometry, Academic Press, Inc., San Diego, CA, 1978.

[4] E.S. Hellman, E.H. Hartford Jr., and R.M. Fleming, "Molecular beam epitaxy of superconducting (Rb,Ba)BiO_3," Appl. Phys. Lett., vol. 55(20), pp. 2120-2, Nov. 1989.

[5] See for example: E.S. Hellman, E.H. Hartford, and E.M. Gyorgy, "Epitaxial $Ba_{1-x}K_xBiO_3$ films on MgO: Nucleation, cracking, and critical currents," Appl. Phys. Lett., vol. 58(12), pp. 1335-7, Mar. 1991.

[6] K. Kuroda and M. Yuda, J. Appl. Phys., vol. 63, p. 2352, 1988.

[7] K. Char, L. Antognazza, T.H. Geballe, "Study of interface resistances in epitaxial $YBa_2Cu_3O_{7-x}$/barrier/$YBa_2Cu_3O_{7-x}$ junctions," Appl. Phys. Lett., vol. 63(17), pp. 2420-2, Oct. 1993.

[8] A.F. Hebard and A.T. Fiory, "Evidence for the Kosterlitz-Thouless transition in thin superconducting aluminum films," Phys. Rev. Lett., vol. 44(4), pp. 291-4, Jan. 1980.
A.T. Fiory and A.F. Hebard, AIP Conf. Proc., vol. 58, p. 293, 1980.
A.T. Fiory, A.F. Hebard, P.M. Mankiewich, and R.E. Howard, "Penetration depths of high T_c films measured by two-coil mutual inductances," Appl. Phys. Lett., vol. 52(25), pp. 2165-7, Jun. 1988.

[9] J.H. Claassen, M.E. Reeves, and R.J. Soulen Jr., "A contactless method for measurement of the critical current density and critical temperature of superconducting films," Rev. Sci. Instrum, vol. 62(4), pp. 996-1004, Apr. 1991.

Chapter 4
FABRICATION

The fabrication of tunneling, microwave and transport structures was necessary in order to make the measurements described later in this thesis. In this chapter, I will describe how these structures were fabricated, and the tools used in the fabrication. Also, I will discuss the effects of annealing these films ex-situ; an important consideration in device fabrication.

4.1 Single Layer Fabrication

Many of the structures fabricated involve patterning single layer BKBO thin films. Fig. 4.1 and Table 4.1 describe this process. First, we must start with a quality BKBO thin film (high T_c, small ΔT_c) deposited on a smoothly polished substrate. Then an etch mask is spun, baked, exposed, and then developed over the film protecting the transport pattern while exposing the film area to be removed. The sample is then etched in a Ar ion mill. The mask is removed, and a new one applied to the sample. The exposed BKBO contact areas are cleaned with a brief exposure to a low energy ion mill. Metal is then evaporated through this stencil, and the excess metal floated off when the stencil is dissolved. In good films, we find no evidence that the film properties are degraded by the lithography process. Films are stable when stored in a dry environment at room temperature; films stored for six months have shown no appreciable change in their superconducting properties.

Step1	Grow quality BKBO thin film with PLD (Chapter 2)
Define basic structure	
Step 2	Photolithographically pattern a photoresist etch mask (AZ 1350J), baking resist at 50°C and using KOH based developer (AZ 400K)
Step 3	Etch exposed film in ion mill (Ar gas, 500V beam voltage) Sample milled on a LN_2 cooled substrate holder
Step 4	Strip photoresist in acetone
Add low resistance contact pads	
Step 5	Photolithographically pattern a liftoff photoresist mask, baking resist at 50°C and using KOH based developer (AZ 400K)
Step 6	Preclean exposed BKBO with reactive, low energy ion mill (gas mixture is 80% Ar + 20% O_2, Beam Voltage at 350V, then 60V)
Step 7	Deposit Ag or Au film
Step 8	Liftoff excess metal by dissolving photoresist in acetone

Table 4.1. Fabrication of Single Layer BKBO Thin Film Structure

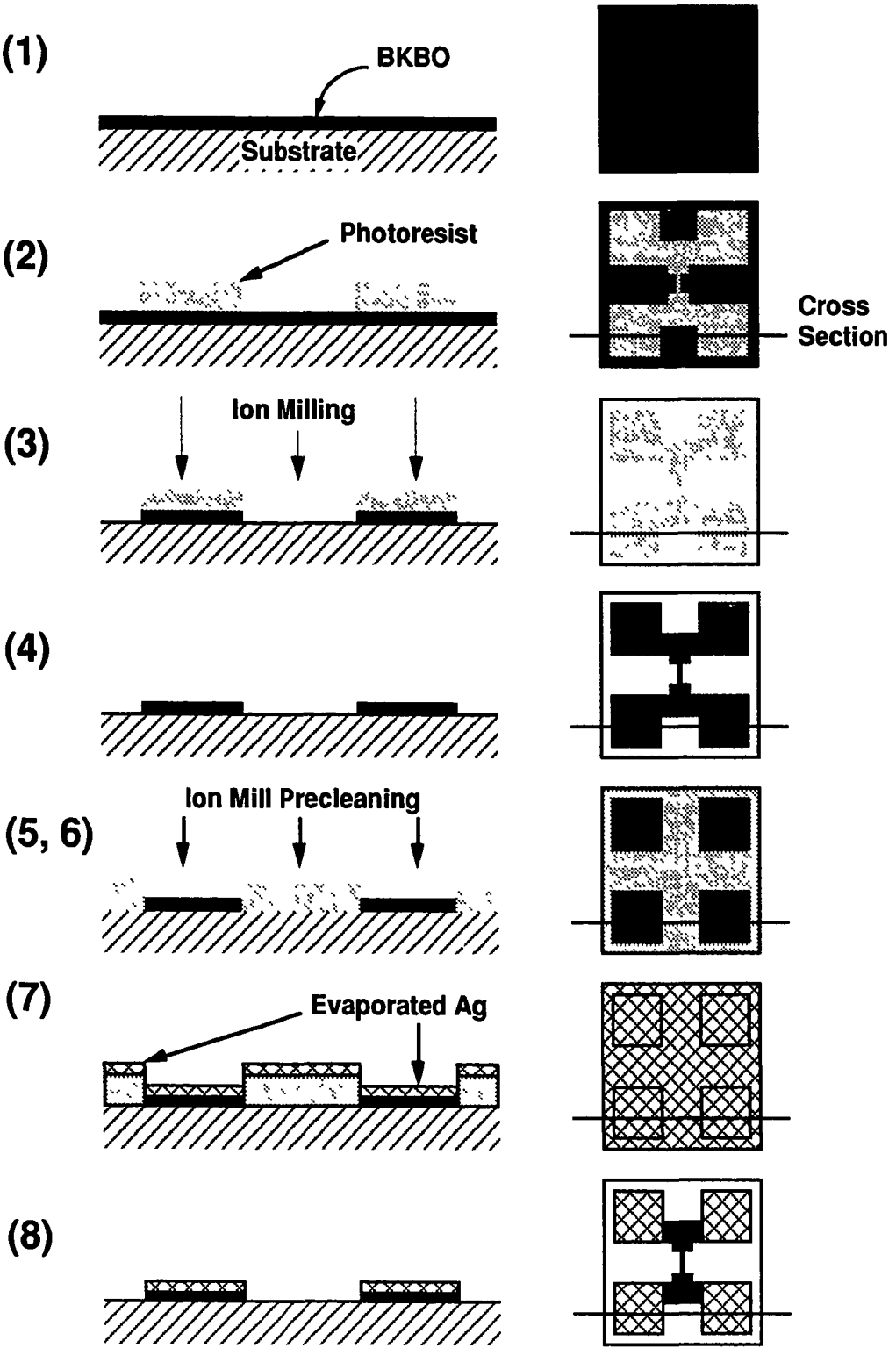

Figure 4.1. Fabrication sequence of a four lead transport structure. Steps 1-8 correspond to Table 4.1.

4.2 Photolithography

Each fabrication step requires photolithography which allows for pattern dimensions to be accurately reduced to ~1μm while also providing reproducibility. Photolithography is based upon light sensitive polymers called photoresist (PR). When exposed to light, these polymers change, either becoming either soluble (positive resist) or insoluble (negative resist) in a developer relative to the unexposed resist. Making a stencil in this way allows for selective exposure of the thin film during each step of the processing. We use AZ 1350J for positive resist and AZ 5214 for either positive or negative resist, depending on processing conditions.

All photoresist processing was done in a microfabrication clean room with filtered yellow lighting. The clean room and flow benches are HEPA filtered to provide a clean, dust-free enviroment (Class 100 in the flow benches) essential for successful microcircuits and microstructures. The filtered light prevents inadvertant exposure of the photoresist during processing.

We use an eyedropper to apply photoresist to the substrate, then spin the substrate with a vacuum chuck at 4000-5000 RPM for 30 seconds. The sample is then baked at 50-90°C for 5 minutes on a hot plate, which drives the casting solvent out of the resist. I use 50°C for BKBO films in order to minimize degradation of the superconducting properties described in section 4.5. This leaves a 1-2μm resist layer now ready for UV exposure. The thickness of the resist layer can be varied in order of decreasing effect by the

dilution of the PR, the spinning speed, or the spinning time. We use a Karl Suss MJB3 contact mask aligner with 300nm optics to expose our resist. An aligner is a device integrating a microscope, mask holder, moveable sample stage, and UV light source. Our aligner allows us to precisely align a mask over the sample, press the sample and mask into intimate contact, and then expose with UV light the resist visible through the mask. The mask is composed of a UV opaque pattern of Cr/CrO_x or FeO on soda lime glass or quartz. Typical exposure times are 10-30 seconds. If using AZ 5214 in the positive mode or AZ 1350J, the substrate is immersed in a dilute developer solution (AZ 400K [KOH] or Shipley 351 [NaOH]) which dissolves away the exposed resist. We use KOH based developers for our BKBO thin films as NaOH based developers degrade the films as seen by discoloration and resistance. One explanation is that Na doped $BaBiO_3$ isn't very conductive[1]. If using AZ 5214 in the negative mode, the sample is given a post-exposure bake at 130°C for 30 seconds, followed by a blanket exposure in the aligner for 1 minute. Then the sample is developed in full strength AZ 421K developer. After development, the sample is quickly rinsed in deionized water, blown dry with nitrogen gas and inspected with a high quality microscope to ensure that development is complete.

Crucial to successful lithography is the edge profile of the photoresist. There are different requirements for etching and liftoff processes, as shown in Fig. 4.1, and must often be modified for each specific application. For etching, the resist wall should ideally be

vertical; but for proper lift-off of films, the resist profile must be slightly undercut. The undercut separates the film deposited on the substrate surface from the material deposited on top of the resist. Vertical edges are obtained through careful optimization of the photolithographic process, including factors like humidity, room temperature, resist thickness, resist baking temperature, dilution of developer, development time, and exposure time. To produce an undercut, we have either soaked the baked resist, AZ 1350J, in chlorobenzene held in a temperature controlled bath or have used the negative mode of AZ 5214 resist, which can undercut with proper processing. Generally, good film lift-off is synonymous with good undercut. For BKBO transport structures, we have been able to get reasonable liftoff using only AZ 1350J due to wide tolerances and also because the deposited film is much thinner than the resist layer.

4.3 Etching

The first resist layer is used to etch the BKBO. Three ways to achieve etching include plasma etching, chemical etching, and ion milling. A plasma or RIE etching procedure for BKBO has not yet been developed, and it may prove to be difficult as one must generate volatile compounds of all elements, especially barium. BKBO can be chemically etched with a weak HCl solution; however, chemical etching has three drawbacks. First, it is difficult to control the linewidth due to photoresist undercutting, second, a residue remains from the etch, and third, the use of an aqueous solution can

degrade the film's superconducting properties. Therefore, we have used ion milling which is "dry" and allows for good linewidth control.

Ion milling has many unique attributes from other types of etching. Ion milling is the use of monoenergetic ions to sputter away material, figuratively described as sandblasting on an atomic scale. An important feature of ion milling is the ability to etch anisotropically a material under a mask layer. As mentioned previously, chemical etches tend to etch isotropically, including under the photoresist. On the negative side, the selectivity of Ar ion etching is poor as the variability of the etch rate of different materials is only somewhat larger than an order of magnitude. This difference pales in comparison with chemical and plasma etching, and makes multilevel processing difficult. The selectivity of the ion mill can improved by adding a reactive gas to the process, either in the gun (Reactive Ion Beam Etching: RIBE) or at the substrate (Chemical Assisted Ion Beam Etching: CAIBE). However, lack of selectivity has the benefits of broad applicability and simplicity, as a simple Ar ion mill can etch anything. Ion milling can also damage the crystallinity of exposed surfaces. The depth of the damage layer increases with ion energy (Beam Voltage) and decreases as the milling angle increases, relative to the surface normal. Lastly, the milling process heats the sample, especially those using a hot wire neutralizer.

The type of ion mill we use is an 8 cm diameter Kaufman source from Commonwealth (1000V, 250mA) which gives a

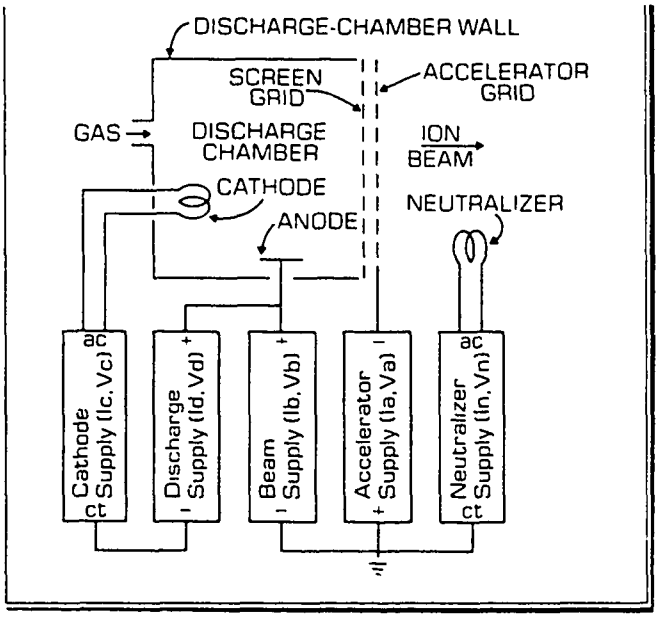

Figure 4.2 Schematic of Kaufman ion source. Adapted from Commonwealth.[2]

broadbeam source at both small to large voltages (50V - 1000V). An illustration of the mill is shown in Fig. 4.2. The ion mill generates a plasma within the mill (discharge region) from collisions between the process gas and energetic electrons generated from a hot filament cathode and accelerating discharge voltage. An internal magnet increases the electron-gas-ion interaction allowing the plasma to be sustained at operating pressures of 10^{-4} torr. The ion mill body floats electrically and is biased with respect to the chamber and the sample, which are both grounded. The plasma-target potential is referred to as the Beam Voltage and is the source of kinetic energy of the bombarding ions. Two precisely aligned grids control the ions leaving the discharge region. The screen grid is attached directly to the discharge chamber and helps confine the discharge. The acceleration grid is negatively biased with respect to ground in order to extract ions coming through the screen grid. The acceleration voltage increases beam uniformity over a given area. The rate of milling is proportional to the ion beam current coming through the grids, appropriately called the Beam Current. The beam is neutralized by generating a matched electron current equal to the beam current with a resistively heated filament located in the beam path. The neutralization of beam current is especially necessary when etching insulators.

There are many practical considerations to using an ion mill. Primarily, the sample must be cooled to prevent heating the sample and/ or burning the photoresist. This is especially important for HTS

superconductors as heating can degrade the superconducting properties. This is usually accomplished by attaching the sample with vacuum grease or Ag paste to a water or liquid nitrogen cooled stage. We have also seen improvement by directing processing gas at the sample during milling. Another useful procedure is rotating the sample at a slight angle away from the mill during etching. This helps increase the uniformity of the step and also prevents redeposition is especially evident when etching thick samples (>3000 Å). The typical ion mill parameters we use to etch BKBO are shown in Table 4.2.

Three factors control the etch rate. The etch rate increases with both Beam Voltage and Beam Current. Also, the milling rate increases up to an optimum angle from the ion mill-sample vector, usually near 45°, and then decreases. Film density, defects, and growth technique can have a large effect on milling rate.

After ion milling, we usually strip the resist by ultrasounding the sample in acetone. Since we don't post-anneal our samples, this

Beam Voltage	500 V
Beam Current	50 mA
Acceleration Voltage	100 V
Gas	Ar
Gas Pressure	2.5×10^{-4} torr
Stage Cooling	LN_2
Etch rate (BKBO)	250 Å/min

Table 4.2 Ion mill parameters for etching BKBO

is okay. However, if post-annealing is desired, one should strip all traces of resist by using an RF oxygen plasma.

4.4 Contacts

After etching the main pattern into the film, the next step is to deposit the contacts. Good ohmic contacts are necessary in order to make the electrical connection to the superconductor. As well as being ohmic, it is important to have low contact resistivity. Contact resistivity is usually represented by the R_nA values, where R is the contact resistance and A is the contact area. Low contact resistances produce less heating (I^2R) and correspondingly allow smaller linewidth microcircuits. What will follow is a description of the various methods and how we achieved ohmic contacts.

There are many methods used in order to achieving low resistance contacts in a superconductor. Common to all methods is the use of a compatible metal electrode. HTS superconductors have surface degradation at most metal interfaces. The two (elemental) exceptions are Ag and Au, due to their low oxygen affinity[3] and bonding to the superconductor without intermediate phase formation.[4] YBCO/Au junctions have achieved R_nA values of 10^{-8}-10^{-10} Ω-cm^2.[5] The lowest BKBO/Au junctions have achieved resistivities of 10^{-5} Ω-cm^2 with heated deposition. We have achieved a resistivity of 4×10^{-3} Ω-cm^2 without heating as described in Table 4.1.

An important step (Step 6) is the precleaning of the superconductor before deposition. Often this is done using ions to

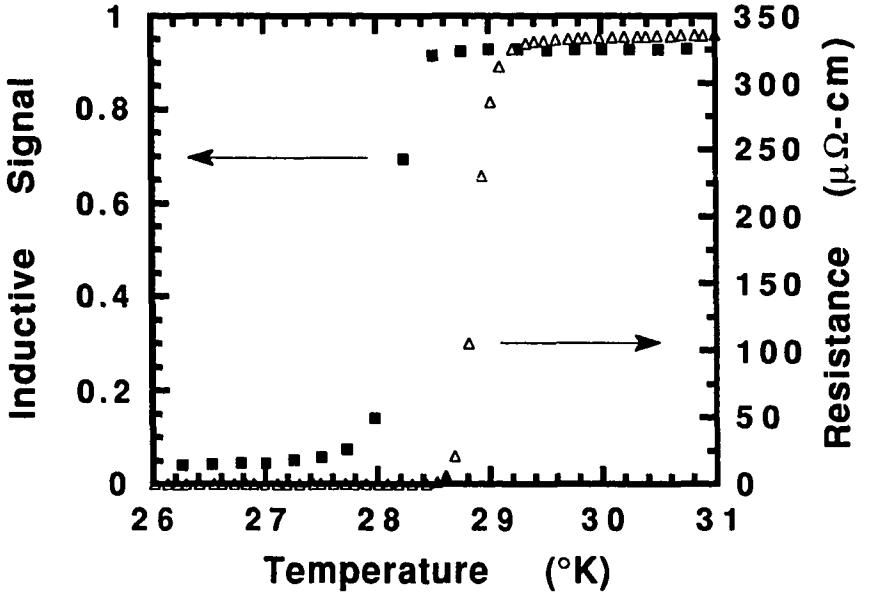

Figure 4.3 A plot of the inductive transition before fabrication (squares) and the resistive transition after fabrication (triangles). As the inductive transition characteristically starts near the end of a resistive transition, we do not see evidence of film degradation from patterning.

sputter away surface contaminants in either a plasma (RF/ DC), an ECR, or an ion mill. We used the latter. We found that using the same energy as for etching (500 eV) resulted in tunnel junctions, as shown later in Chaper 6. Thus, we used a two step process. We used an initial energy of 350 eV for the initial cleaning. A 20% O_2 mixture was used in the ion mill[6] as we had found that it produced lower resistances than pure Ar at the same energy. The second step in the process was milling the surface at a low energy of 60 eV with the 20% oxygen mixture. This gave ohmic contacts with resistivity as low as 4 x 10^{-3} Ω-cm^2 at 4°K. A benefit is that it is a simple and compatible process with our standard lithography, and doesn't involve the extra step of annealing. The disadvantage to this method is that the contact resistivity is inferior to YBCO, and needs to be lower for a feasible BKBO technology. Our process works without resolvable degradation of T_c, as shown in Fig. 4.3.

With or without precleaning, a standard approach with both YBCO and BKBO is the annealing of contacts into the superconductor. However with BKBO, often a degradation is observed for film properties. Another procedure is to evaporate the metal contact *in-situ*, so as not to contaminate the surface. This has the benefit of higher reproducibility and low resistivities as demonstated with YBCO,[7,8,9,10] where R_nA products of 10^{-8} to 10^{-10} Ω-cm^2. This has yet to be done with BKBO.

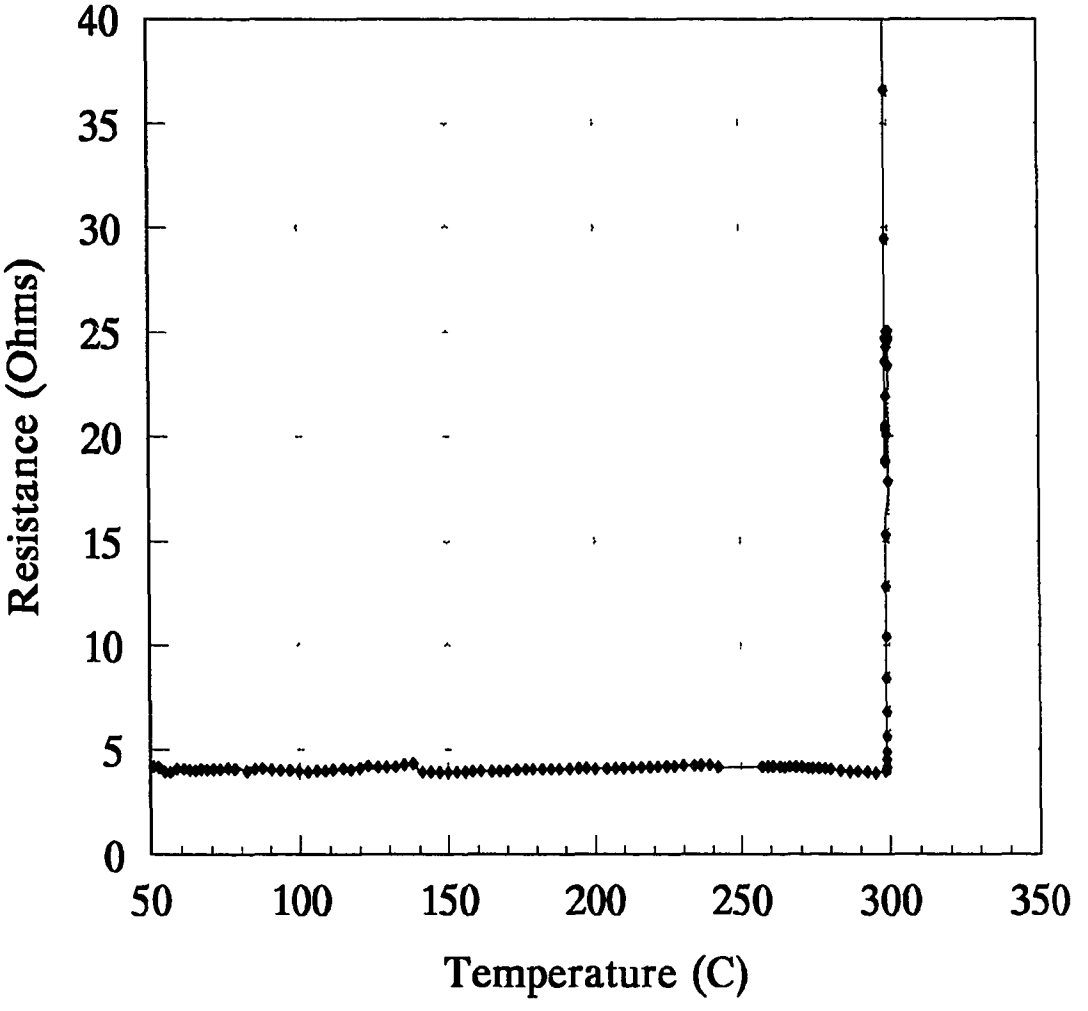

Figure 4.4 *In-situ* resistance vs. temperature taken while heating a BKBO thin film at 20°C/min. in an argon atmosphere.

4.5 Annealing Studies

As mentioned previously, annealing and heating can be used extensively in processing. Thus we did a number of studies aimed at determining the sensitivity of superconducting properties to annealing. One of the main points of this was to determine how hot we could anneal our samples without degradation.

Both patterned and unpatterned films were used in this study. For the unpatterned (etched) films, we simply evaporated through a shadow mask Ag metal contacts onto the four corners of film. For the patterned film, a narrow neck (100 μm) was etched between the two halves of the superconductor in order to test the critical current of the superconductor. Also, contacts were made by evaporating through a shadow mask.

4.5.1 Argon Anneals

In order to determine the breakdown temperature of BKBO, we measured the *in-situ* resistance of the film in the annealing furnace as we ramped up the temperature in a flowing Ar atmosphere. The furnace used was a Rapid Thermal Anneal (RTA) furnace that was capable of rapid temperature changes. The sample was mounted on a quartz slide with four gold pins and attached wires which were pressed into the evaporated contacts. The pins were held in place by springs coiled from piano wire that where also mounted on the quartz slide. The current used was $\leq$ 1 mA which corresponds to $\leq$ 1 KA/cm^2 current density. The results of one such measurement are shown in Fig. 4.4, where we can see that the breakdown temperature

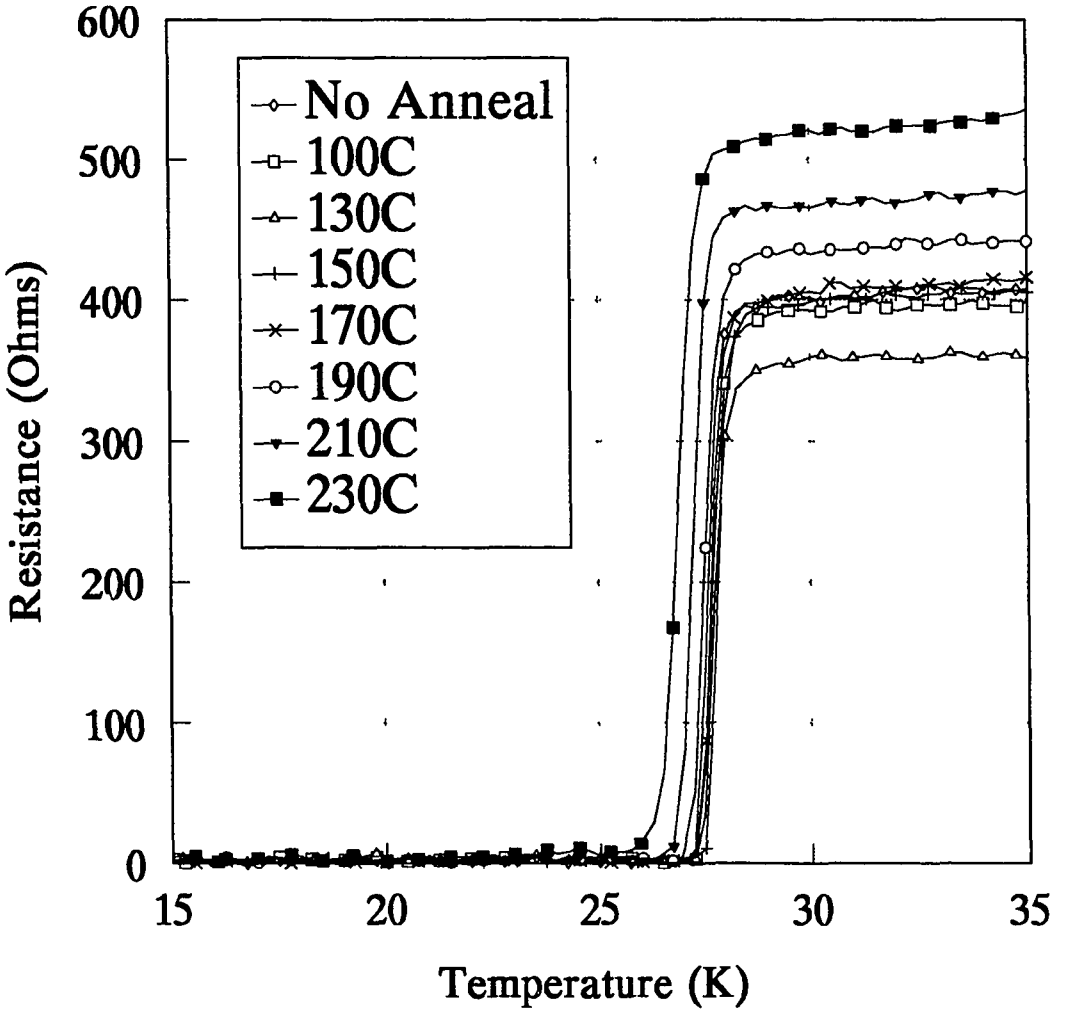

Figure 4.5 Resistive superconducting transitions for a 100μm wide BKBO patterned line for successive 10 min. anneals in an argon atmosphere as grown, at 100°C, 130°C, 150°C, 170°C, 190°C, 210°C, and 230°C.

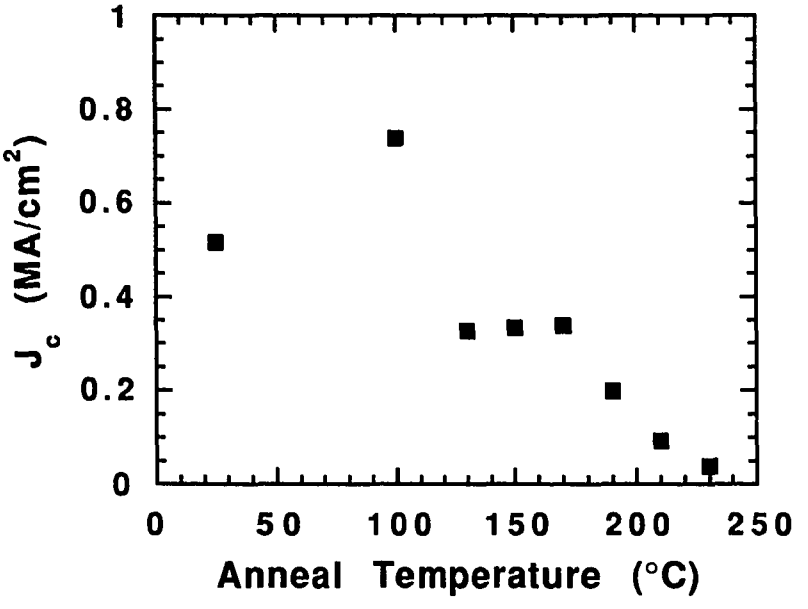

Figure 4.6 Critical current of a 100μm line fabricated from a BKBO thin film after successive 10 min. anneals in argon as grown, at 100°C, 130°C, 150°C, 170°C, 190°C, 210°C, and 230°C.

was about 300°C. The resulting film was colorless and clear in contrast to the initial bluish color. We observed that the better films (high and sharp T_c) decomposed near 300°C, whereas worst could show effects as low as 200°C.

Interpretation of this result is unclear. Electromigration (EM) effects are apparently very significant in both BKBO[11] and YBCO[12] films and could be the cause of this effect. Elevated temperature EM studies of YBCO sintered rods have observed oxygen electromigration at low currents and 200°C and 350°C[13]. Further study needs to be done concerning the effect of the electromigration as a function of current density, temperature, and gas atmosphere. Also, determination of the mobility of the various ions needs to be determined. However, as we will see below, degradation has also been observed near these temperatures without applying a current during heating. This suggests that material breakdown is important at these temperatures.

Another interesting effect we have observed with argon annealed BKBO films is the existence of a room temperature photoelectric effect. A photoelectric effect has also been observed in oxygen deficient YBCO[14]. We observed a significantly lower resistance with application of light (a flashlight) than without to an Ar annealed BKBO thin film. Unfortunately, we have not been able to pursue this further.

The next step was to determine the effect that annealing had on the film's observed transport properties, without the current

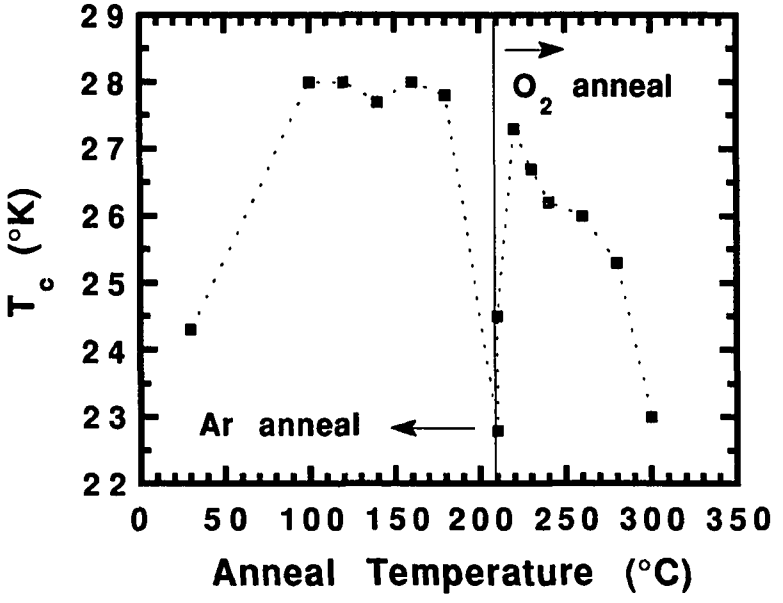

Figure 4.7 Resistive transition temperature (T_c) as a function of successive 10 minute anneals in argon and oxygen atmospheres.

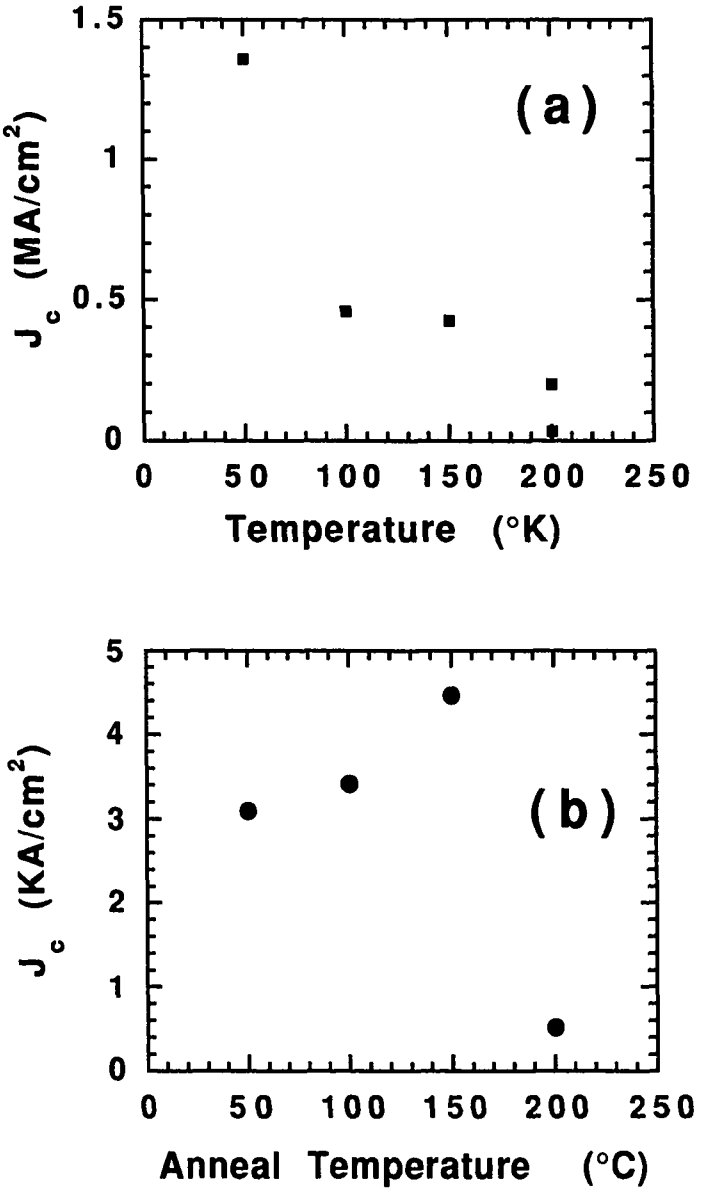

Figure 4.8 Critical current as a function of oxygen anneal temperature for successive 10 minute anneals for a (a) high J_c film and a (b) low J_c film.

applied during heating. Shown in Fig. 4.5 is a graph of the change in resistive transition vs. temperature for various short anneals in argon. A significant feature of this plot is how little the resistance changes with the anneals. However, we see that in Fig. 4.6 that the critical current of the same film significantly decreases with higher anneal temperatures.

4.5.2 Oxygen Anneals

A natural question to ask is how the behavior of BKBO thin films is affected by oxygen, as the transport properties of YBCO are critically dependent on oxygen concentration. Decrease in the oxygen content may therefore account for the decrease in T_c and J_c in Fig. 4.5 and 4.6. There have been reports that there may be variable oxygen in thin film bismuthates, including $Bi_{1-x}Pb_xBaO_3$ [15] and $Ba_{1-x}K_xBiO_3$ [16]. For BKBO single crystals; however, the oxygen content is stable from sensitive electrochemical cell studies[17]. We have seen signs that the oxygen content is variable as shown in Fig. 4.7 and 4.8. The T_c of the film in Fig. 4.5 was recovered with annealing in oxygen. In Fig. 4.8, we see two different behaviors of critical current with annealing. For films of high critical current, a quick decrease in critical current is observed as the film is annealed. For a low J_c film, the critical current was increased with annealing in oxygen.

From these anneal studies we notice a number of things. First, our laser ablated BKBO films are rather sensitive to annealing. Thus we have endeavored to keep our process temperatures as low as

possible, resulting in fabrication without degradation. Also, our films are sensitive to the oxygen content of the films. There are also interesting questions about electromigration and photoelectric effects in these films.

References

[1] D. Tseng and E. Ruckenstein, "Structure and superconductivity of $BaBiO_3$ doped with alkali ions," J. Mater. Res.,vol. 5, pp. 742-745, Apr. 1990.

[2] Commonwealth brochure, 1993.

[3] For example, see K. Oka and T. Ira, "Contact resistance of several metals on $YBa_2Cu_3O_{7-\delta}$," Jap. J. Appl. Phys., vol. 31(9A), pp. 2689-2691, Sept. 1992.

[4] M.E. Tidjani and R. Gronsky, "Structural characterization of the Ag-$YBa_2Cu_3O_{7-x}$ interface," Physica C, vol. 191(1-2), pp. 260-270, Feb. 1992.

[5] R.P. Robertazzi, A.W. Kleinsasser, R.B. Laibowitz, R.H. Koch, and K.G. Stawiasz, "*In-situ* Ag/$YBa_2Cu_3O_7$ contacts for superconductor-normal metal-superconductor devices," Phys. Rev. B, vol. 46, p8469, Oct. 1992.

[6] A.N. Pargellis, F. Sharifi, R.C. Dynes, B. Miller, E.S. Hellman, J.M Rosamilia, and E.H. Hartford Jr., "All-high T_c Josephson tunnel junction: $Ba_{1-x}K_xBiO_3$/ $Ba_{1-x}K_xBiO_3$ junctions," Appl. Phys. Lett., vol. 58(1), pp. 95-7, Jan. 1991.

[7] R.P. Robertazzi, ibid.

[8] M. Lee, D. Lew, C.B. Eom, T.H. Geballe, and M.R. Beasley, "Anisotropic proximity coupling in small $YBa_2Cu_3O_7$-normal-Pb junctions," Appl. Phys. Lett., vol. 57(11), pp. 1152-4, Sept. 1990.

[9] J.W. Ekin, S.E. Russek, C.C. Clickner, and B. Jeanneret, "In situ noble metal $YBa_2Cu_3O_7$ thin-film contacts," Appl. Phys. Lett., vol. 62(4), pp. 369-71, Jan. 1993.

[10] P.A. Rosenthal, E.N. Grossman, R.H. Ono, and L.R. Vale, "High temperature superconductor-normal metal-superconductor Josephson junctions with high characteristic voltages," Phys. Rev. Lett., vol. 63(14), pp. 1984-6, Oct. 1993.

[11] R. Geerk, private communication.

[12] B.H. Moeckly, D.K. Lathrop, and R.A. Buhrman, "Electromigration study of oxygen disorder and grain-boundary effects in $YBa_2Cu_3O_{7-\delta}$ thin films," Phys. Rev. B., vol. 47, pp. 400-416, Jan. 1993.

[13] K.G. Rajan, P. Parameswaran, J. Janaki, and T.S. Radakrishnan, "Electromigration of oxygen in YBa2Cu3O7-d," J. Phys. D.: Appl. Phys., vol. 23, pp. 694-697, 1990.

[14] D. Lederman, J. Hasen, I. Schuller, E. Osquiguil, and Y. Bruynseraede, "Photoinduced superconductivity and structural changes in high temperature superconducting films," Appl. Phys. Lett., vol. 64, pp. 652-654, Jan. 1994.

[15]A.W. Sleight, J.L. Gillson, and P.E. Bierstedt, "High-temperature superconductivity in the $BaPb_{1-x}Bi_xO_3$ system," Solid St. Commun., vol. 17(1), pp. 27-28, Jul. 1975.

[16]Y. Idemoto, Y. Iwata, and K. Fueki, "Oxygen content and T_c of $Ba_{0.6}K_{0.4}BiO_{3-\delta}$," Physica C, vol. 201, pp. 43-49, 1992.

[17]P. Han, private communication

Chapter 5

TRANSPORT

In this chapter, we report measurements of the electronic and magnetic transport properties of BKBO films. This data provides information for applications and fundamental issues concerning the superconducting coupling, scattering, upper critical field, and the coherence length of BKBO. In zero-field, the BKBO films exhibit low metallic normal state resistivities and excellent superconducting state properties, with the sharp transitions and high current densities required for electronic device applications. In an applied magnetic field, the resistive transition shifts in accordance with BCS theory, and there is substantial broadening of the magnetoresistance indicating that flux flow may be important in the BKBO films. The critical current density is also BCS-like in its temperature and magnetic field dependence, showing no evidence for weak link coupling. Parts of this chapter are adapted from Schweinfurth, et. al.[1]

5.1 Sample Preparation

Transport measurements were made from patterned PLD grown films as described in Chapter 2 using a stoichiometric $Ba_{0.6}K_{0.4}BiO_3$ target with an ArF excimer laser. The films were grown on (100)-MgO substrates with a nominal thickness of 1500Å and good microstructure. Four probe structures were patterned with 25μm or 100μm wide bridges as described in Chapter 3.

The films used for these high field measurements demonstrate excellent quality with sharp magnetic and resistive transitions. In Figure 5.1(a), the magnetic and inductive transitions of one are shown; unpatterned and patterned, respectively. The film exhibits an inductive onset at about 28°K and a width (10%-90%) of less than 0.5°K. The patterned resistive transition occurs at a higher temperature. The film exhibits zero resistivity at about 28°K (corresponding to the onset of the magnetic screening) and a transition width of 0.3°K, demonstrating our ability to fabricate without degradation.

5.2 Experimental Methods

The transport measurements performed include inductive, resistive, and critical current determination. Since the inductive transition method was described in Chapter 4, I will discuss how the resistive transitions and the critical current are measured, and subsequently the procedures involved using high fields.

The measurement procedures share many common features. They are all four-probe measurements, performed on a cryogenic insert inside a dewar and cooled with either He^4 vapor or liquid. The temperature without field was monitored with a Lakeshore DT-470 Si diode thermometer, while a Lakeshore CGR carbon glass thermometer was used for high fields. Any contacts were made with Ag paint, as this was easy to remove and redo without increasing contact resistance. All leads were heat sunk to a copper block which held the sample and were strung to the top of the insert in twisted

pairs. The sample was enclosed in a copper shield to provide temperature stability.

Resistance was measured on-the-fly using a computer. The current was set to 10μA ($65A/cm^2$) with a dc current source and both the temperature and sample voltage, proportional to the resistance, was read into the computer. The temperature was measured from a IEEE bus from the Lakeshore DRC-91C temperature controller and the preamplified sample voltage through a ADC input. While the sample was slowly cooled, data was taken continuously. Each R-T pair was averaged from data inside a given temperature window, say ±0.05°K, around a predetermined data temperature. This allows for improved signal-to-noise as well as the variation of cooling rates so as not to overfill the data array.

Critical current was also measured using computer data acquisition, but in a different way. The sample temperature was set to specific setpoints using the DRC-91C PID temperature controller. Through a DAC and a voltage-controlled current source, the current was increased until the voltage across the sample reached 5μV as monitored with a preamp and a computer ADC, at which time the current value was recorded. At the higher currents, heating could be produced in the contacts, so the current was pulsed on and off as the current was stepped upwards.

Field measurements were done inside a Janis flow-through cryostat and a 8 Tesla Oxford superconducting magnet. The field was monitored with a Hall Probe, and adjusted by changing the current

flowing through the magnet. Magnet field changes were done slowly in order to avoid flux creep, which induces heating and can even quench the magnet. The sample was located inside the sample tube in the middle of the magnet solenoid, immersed in He^4 vapor. The magnet is submersed in liquid He^4, separate from the sample. The sample was cooled with He vapor leaked into the chamber with a needle valve at the bottom of the cryostat.

5.3 Zero-field Measurements

In the normal state, the best films are metallic rather than semiconducting. A nearly linear resistivity above T_c extends to well above room temperature in Figure 1(b). Just above the transition, the resistivity flattens out. This could be as a result of simultaneous semiconducting and superconducting transport channels, as suggested by Hall Effect data.[2] All films exhibit a large residual resistivity; the resistivity at the transition for the sample shown is 250$\mu\Omega$-cm and is increased by only a factor of two at room temperature.

We have measured the superconducting critical current density both magnetically and by transport. Magnetic hysteresis measurements indicate current densities approaching $10^6 A/cm^2$ at 4.2°K in our films; measurements on single crystals give current densities about one order of magnitude lower.[3,4] By transport, we have achieved current densities higher than $3x10^6$ A/cm^2. In Figure 5.2(a), we plot the transport current density vs. temperature for the BKBO film in Figure 5.1. Near T_c, J_c exhibits a region of upward

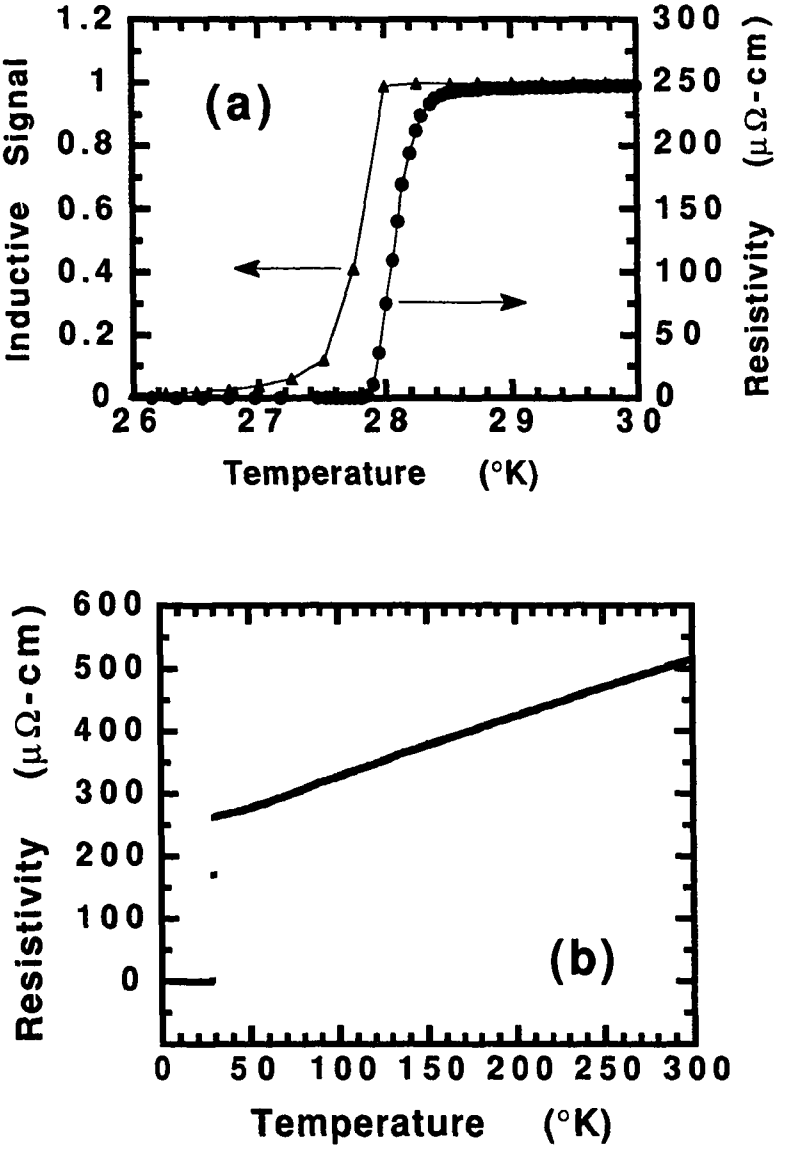

Figure 5.1 (a) Comparison of the magnetic screening and resistivity transitions for a BKBO thin film. The onset of the magnetic transition and the zero resistance temperature each occur at 28°K, with transition widths less than 0.5°K. (b) Resistivity vs. temperature for a patterned BKBO line. The resistivity is nearly linear from the transition to above room temperature, with residual resistance ratio $\rho(300)/\rho(T_c) \sim 2.5$

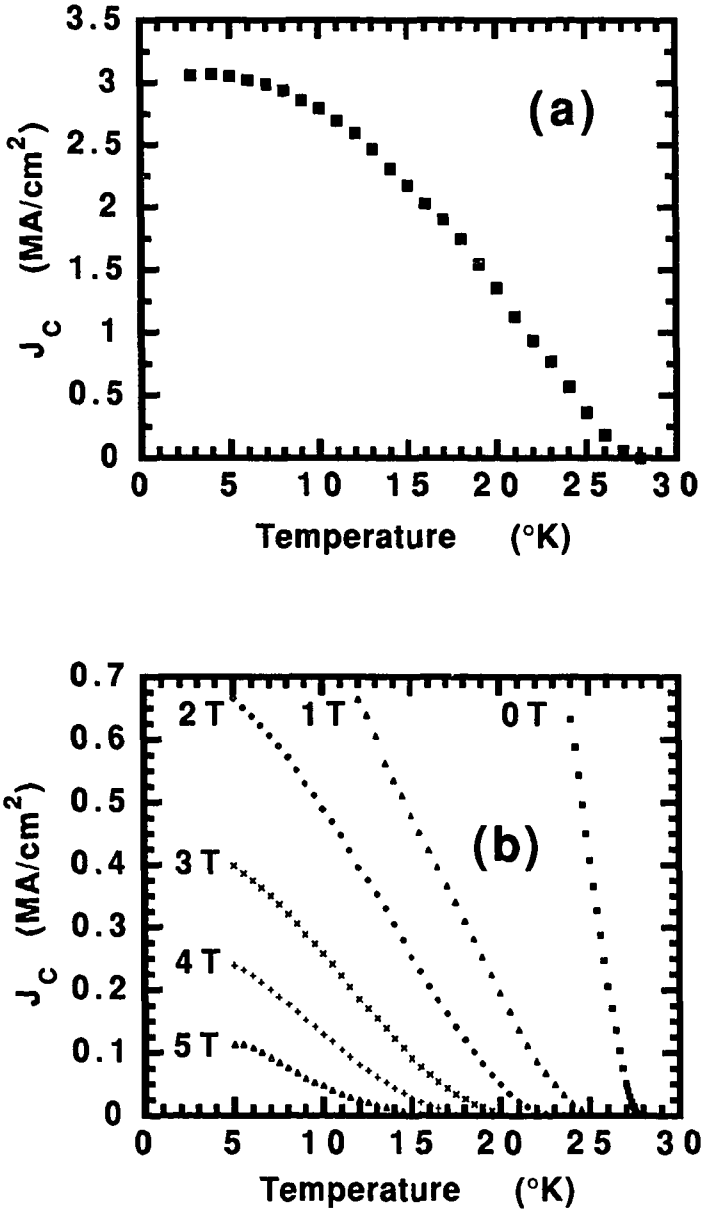

Figure 5.2 (a) Superconducting critical current density vs. temperature at zero magnetic field measured by transport in a 25μm-wide line patterned from the same BKBO film as in Figure 5.1, attaining $3x10^6 A/cm^2$ at low temperature. (b) Critical current density vs. temperature in transverse magnetic fields up to 5T applied normal to the film surface.[6]

curvature followed by a regime in which Jc varies as $(1-T/T_c)$; this is most clearly seen in the zero field curve of Figure 5.2(b). At lower temperature, J_c is BCS-like, saturating at $3.1x10^6 A/cm^2$.

5.4 Field Transport

In Figure 5.2(b), we plot the critical current vs. temperature in magnetic fields up to 5T applied perpendicular to the film surface. Application of a magnetic field suppresses J_c significantly; at a field of 5T, the critical current density at T=5°K is reduced by a factor of 30 to $1x10^5$ A/cm^2. Although this suppression is somewhat more rapid than expected for a conventional BCS superconductor, it is much less severe than would occur for a granular system coupled by weak links. This indicates good uniformity of our BKBO films.

Measurements of the transverse magnetoresistance as a function of field and temperature are plotted in Figure 5.3(a) for a perpendicular field. We see only a small variation in the resistance (<20%) as the film plane is rotated relative to the field. Since BKBO is cubic, we attribute this anisotropy to the film geometry. The magnetoresistance transition shows characteristics intermediate between classical (low T_c) and the cuprate (high T_c) superconductor. The shift in the onset temperature is characteristic of a classic BCS superconductor, but there is also substantial broadening of the transition with increasing field. From the field dependence of the onset temperature, determined by extrapolating the magneto-resistance to the normal state value (at T_c), we determine dH_{c2}/dT from Figure 5.3(b). The critical field slope (-0.78T/°K) and

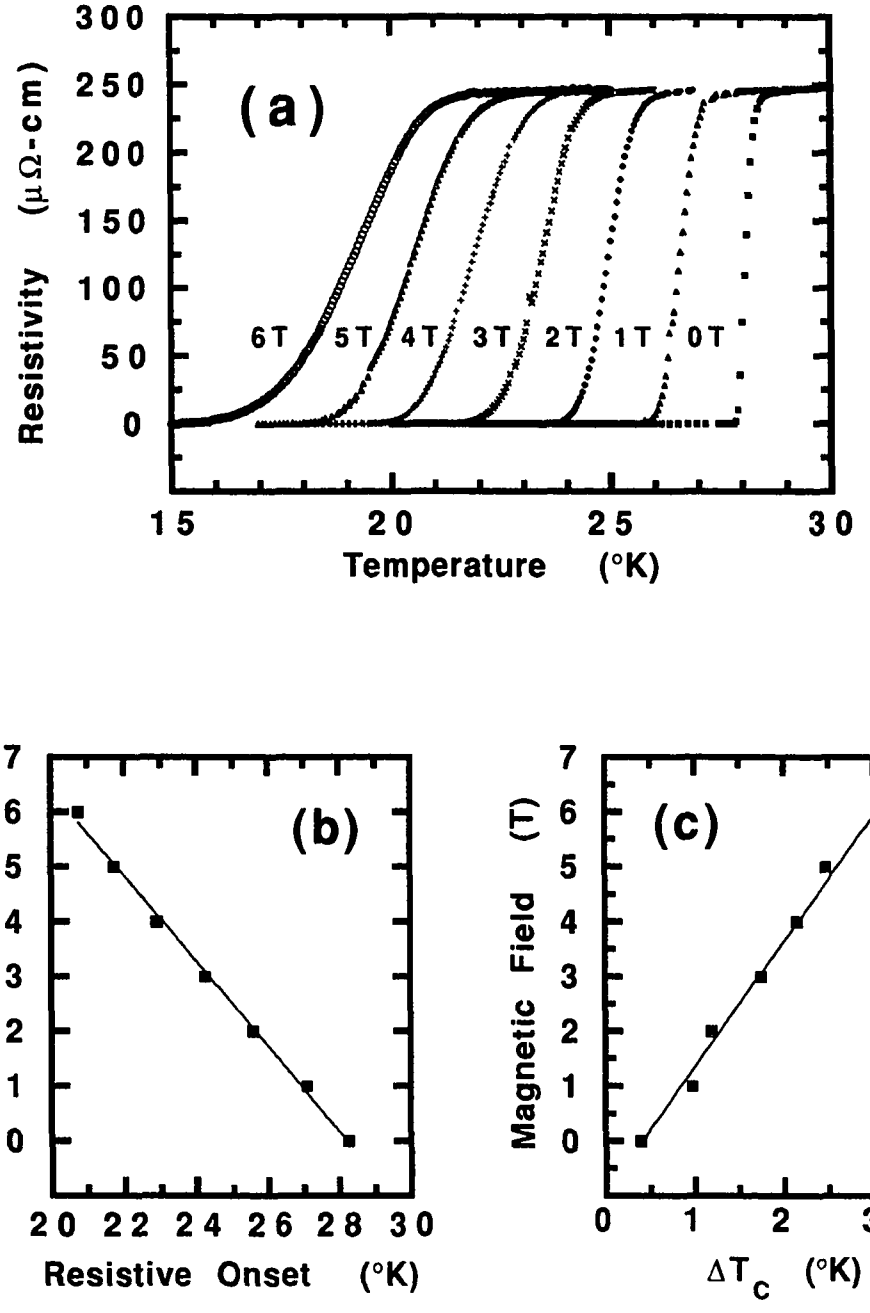

Figure 5.3 (a) Resistivity vs. temperature in magnetic fields up to 6T for the patterned film in Figure 5.2. (b) Upper critical magnetic field vs. the onset transition temperature. The critical field slope is -0.78T/°K. (c) Broadening of the resistive transition vs. field.[7]

zero field transition temperature (28.5°K) implies an upper critical field $H_{c2}(0)$ of 15.2T, assuming the Werthamer-Helfand-Hohenberg formula[8]

$$H_{c2}(0) = -0.69T_c(dH_{c2}/dT). \qquad \text{(Eq. 5.1)}$$

Using this field in the dirty limit Ginsburg-Landau (GL) expression,

$$H_{c2}(0) = \Phi_0/2\pi\xi^2, \qquad \text{(Eq. 5.2)}$$

we deduce a coherence length of 46Å. Upon comparison with past studies,[9,10,11,12,13,14] all these values are in reasonable agreement with results obtained from low field magnetization measurements in bulk composites[15] and single crystals[16,17] of BKBO.

Subsequent pulsed field measurements > 30T have cast doubt on the validity of WHH approximation for BKBO. Thin film measurements have measured H_{c2} at 17T (film $T_c = 22°K$) and 24T ($T_c = 20°K$), while single crystals ($T_c = 32°K$) have obtained 32T.[18,19] Fig. 5.4 illustrates the H_{c2} vs. T phase diagrams. Seen in the first film and especially notable in the crystal is an upwards curvature of H_{c2} with decreasing temperature. Thus, it appears that H_{c2} can exceed the WHH relation.

First, let us discuss the films. Notice that the film that had the higher resistivity and lower transition sample had a higher critical field. This is understandable in the context of GL as more scattering occurs with increased resistivity which reduces the coherence length.[20] A smaller coherence length will produce higher H_{c2}, shown in Eq. 5.2, and a lower T_c. The film with $T_c(0) = 22°K$ had a small

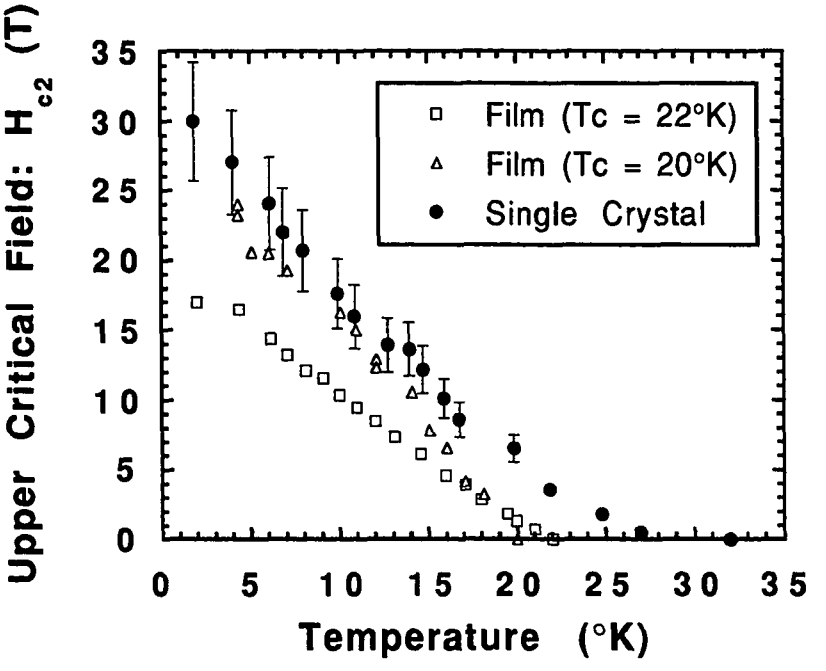

Figure 5.4 Temperature dependence of H_{c2} for sputtered $Ba_{0.55}K_{0.45}BiO_3$ thin films and $Ba_{1-x}K_xBiO_3$ single crystal at optimal doping. Resistivity of T_c =20°K and 22°K films near the zero field transition are 2.8 and 0.4 mΩ, respectively. Figure adapted from data in Sato and Escribe-Filippini.[21]

upwards curvature of the H_{c2} curve, similar to our PLD film. Measured from Fig. 5.4, $(dH_{c2}/dT)_{Tc}$ is -0.8 and -1.6 T/°K. The first value is similar to our observed value of -0.78 T/°K while the second is significantly higher. The sputtered film data suggests that a better low field approximation to $H_{c2}(0)$ for the measured PLD film would be a GL linear extrapolation from $(dH_{c2}/dT)_{Tc}$. From this, we obtain $H_{c2}(0) = 22T$, with $\xi = 38Å$ for our film.

The single crystal data shows extremely high T_c (32°K) and H_{c2} (32T) as well as large upwards curvature in the H_{c2} phase diagram. H_{c2} doesn't significantly saturate at lower temperatures, compared to WHH, which suggests that paramagnetic scattering is minimal with BKBO. This is in agreement with the μSR measurements that show no magnetism[22] and also that $H_{c2} < H_{p0} = 1.84T_c = 59T$, where H_{p0} is the paramagnetic field limit. An interesting question concerns the positive curvature of the H_{c2} phase diagram, also seen in the cuprates. Some positive curvature is seen in all upper field data, including ours (see Fig. 5.3). Film data seems to have less curvature than single crystal or polycrystalline samples. The first question is whether this is intrinsic or extrinsic, i.e. whether the samples are of high enough quality. The difference between films and other samples are likely due to material issues. It is an open question whether single crystals or thin films BKBO have superior material quality. Films have strain and defects which may tend to aid in vortex pinning, but single crystals tend to be less homogeneous. Deviations from WHH are observed from anisotropy, strong coupling

and spin-orbit (magnetic impurity) scattering.[23,24] Anisotropy and spin-orbit scattering don't apply in BKBO as it is cubic and non-magnetic. Upwards curvature can be produced by very strong coupling, but this is difficult to reconcile with numerous measurements showing the electron-phonon coupling constant, λ_c, is about 1,[25,26,27] where upward curvature requires $\lambda_c \geq 4$ (dirty limit). One speculation is that H_{c2} may be attributed to micro-domains with lower K content which superconduct as the field is increased.[28,29] Rather, I suggest that CDW fluctuations may play a scattering role in upper critical field behavior, similar to magnetic impurities in other materials. Karlow, et. al.[30] have observed effects in the dielectric function that suggest the persistence of CDW fluctuations into the metallic state. CDW fluctuations should change significantly with doping near the M-I transition, like superconducting fluctuations change with temperature near T_c. In order to understand the upper critical field in BKBO, we need to understand the effects of doping, defects, and sample quality on H_{c2}.

Let us now move to the transition width which we plot the field-broadening as a function of field in Figure 5.3(c). Although some field-broadening is observed in all Type II superconductors, the effect in BKBO is significant. At 6T, the width of the transition (10%-90%) is about 15% of the zero field T_c; the fractional broadening at the same field in the cuprates (in the c-axis direction) is comparable. However, the transition width in our BKBO films is roughly linear in the applied field, in contrast to the $H^{2/3}$ dependence

reported in the cuprates.[31] A likely source of broadening is caused from the reduction of J_c with field. At the higher fields, J_c near the transition approaches the measurement current density of $65A/cm^2$. For comparison to other quality samples, small but finite broadening was observed for the studies shown in Fig. 5.4.

The rapid suppression of the critical current density with field suggest that flux creep may be important in these materials. We find evidence for thermally-activated behavior in the resistivity in finite field at low temperatures, with a field-dependent activation energy ranging from 0.67eV at 1T to 0.04eV at 6T. Vortex barrier energies of comparable magnitude (0.26eV) have been deduced from magnetic flux relaxation measurements in BKBO single crystals.[32] For comparison, cuprates have a characteristic flux energy barrier of 0.06eV.[33]

In summary, we have studied the field dependence of superconducting transition and critical current of high quality BKBO thin films, with transitions greater than 28°K and current densities above $10^6A/cm^2$. The field dependence of the films behave generally like conventional BCS superconductors in their transport properties. However, the linear resistivity, the upwards curvature of H_{c2}, and strong suppression of the critical current with field show similarities with the cuprates. We have estimated $H_{c2}(0)$ and ξ_{GL} to be 22T and 38Å, respectively for our films. In order to further understand the upper critical field, new studies should be performed

concerning the effects of doping, defects, and sample quality on H_{c2}, preferably in fields approaching $H_{c2}(0)$.

References

[1] R.A. Schweinfurth, C.E. Platt, M.R. Teepe, and D.J. Van Harlingen, "Electrical and magnetic transport properties of laser-deposited Bal-xKxBiO3 thin films," Appl. Phys. Lett., vol. 61 (4), pp. 480-2, July 1992.

[2] E.S. Hellman and E.H. Hartford Jr., "Normal-state resistivity and Hall effect in $Ba_{1-x}K_xBiO_3$ epitaxial films," Phys. Rev. B, vol. 47 (17), pp. 11346-11352, May 1993.

[3] P.D. Han, L. Chang, and D.A. Payne, "Top-seeded growth of superconducting $(Ba_{1-x}K_x)BiO_3$ crystals by an electrochemical method," Journal of Crystal Growth, vol. 128(1-4), pp. 798-803, Mar. 1993.

[4] G.T. Seidler, T.F. Rosenbaum, P.D. Han, D.A. Payne, and B.W. Veal, "Critical fields and flux pinning in single crystal $Ba_{1-x}K_xBiO_3$," Physica C, vol. 195, p. 373, 1992.

[5] R.A. Schweinfurth, C.E. Platt, M.R. Teepe, and D.J. Van Harlingen, "Electrical and magnetic transport properties of laser-deposited Bal-xKxBiO3 thin films," Appl. Phys. Lett., vol. 61 (4), pp. 480-2, July 1992.

[6] R.A. Schweinfurth, ibid.

[7] R.A. Schweinfurth, ibid.

[8] N.R. Werthamer, E. Helfand, and P.C. Hohenberg, "Temperature and purity dependence of the superconducting critical field, H_{c2}. III. Electron spin and spin-orbit effects," Phys. Rev., vol. 147(1), pp. 295-302, Jul. 1966.

[9] H.C. Yang, et. al., Phys. Rev. B., vol. 42, p. 2551, 1990.

[10] N. Savvides, S.J. Collocott, C. Andrikidis, and K.-H. Muller, "AC susceptibility, resistivity, and specific heat of the cubic superconductor $Ba_{0.6}K_{0.4}BiO_3$," Physica C, vol. 171, pp. 181-186, 1990.

[11] N.V. Anshukova, V.B. Ginodman, A.I. Golovashkin, L.N. Zherikhina, L.I. Ivanova, A.P. Rusakov, and A.M. Tskhovrebov, "Anomalies in the temperature dependences, resistance, critical current, and critical magnetic fieldin $Ba_{1-x}K_xBiO_3$," Sov. Phys. JETP, vol. 70(5), pp. 923-27, May 1990.

[12] J.E. Graebner, L.I. Schneemeyer, and J.K. Thomas, Phys. Rev. B., vol. 39, p. 9682, 1989.

[13] B. Batlogg, R.J. Cava, L.W. Rupp Jr., A.M. Mujsce, J.J. Krajewski, J.P. Remeika, W.F. Peck Jr., A.S. Cooper, and G.P. Espinosa, "Density of states and isotope effect in BiO superconductors: Evidence for nonphonon mechanism," Phys. Rev. Lett., vol. 61(14), pp. 1670-3, Oct. 1988.

[14] U. Welp et. al., Physica C, vol. 156, p. 27, 1988.

[15] W.K. Kwok, U. Welp, G.W. Crabtree, K.G. Vanderwoort, R. Hulsher, Y. Zheng, B. Drabowski, and D.G. Hinks, "Magnetic and resistive measurements of the superconducting critical fields of melt-cast $Ba_{0.65}K_{0.35}BiO_3$," Phys. Rev. B, vol. 40(13), p. 9400-3, Nov. 1989.

[16] P.D. Han, ibid.

[17]G.T. Seidler, ibid.

[18]K. Tatsuhara, N. Miura, H. Sato, and S. Uchida, "Magnetoresistance and upper critical fields of $Ba_{1-x}K_xBiO_3$ thin films," Physica C, vol. 212, pp.459-464, 1993.

[19]C. Escribe-Filippini, J. Marcus, M. Affronte, H. Rakoto, J.M. Broto, J.C. Ousset, and S. Askenazy, "Upper critical field of $Ba_{1-x}K_xBiO_3$ single crystal," vol. 210, pp. 133-137, 1993.

[20]H. Sato, T. Ido, S. Uchida, S. Tajima, M. Yoshida, K. Tanabe, K. Tatsuhara, and M. Miura, "Superconducting and normal states of $Ba_{1-x}K_xBiO_3$ studied with use of high-quality thin films," Phys. Rev. B, vol. 48 (9), pp. 6617-6625, Sep. 1993.

[21]C. Escribe-Filippini, ibid. and H. Sato, ibid.

[22]Y.J. Uemura, et. al. "Absence of magnetic order in (Ba,K)BiO_3," Nature, vol. 335 (8), pp. 151-2, Sept. 1988.

[23]E.Z. Melilikhov and V.G. Shapiro, "Critical fields of high Tc superconductors (review)," Superconductivity, vol. 4(8), pp. 1353-1402, Aug. 1991.

[24]Ø. Fischer, M. Decroux, R. Roth, R. Chevrels, and M. Sergent, "Compensation of the paramagnetic effect on Hc2 by magnetic moments: 700 kG superconductors," J. Phys. C, vol. 8, pp. L474-77, 1975.

[25]Q. Huang, J.F. Zasadzinski, N. Tralshawala, K.E. Gray, D.G. Hinks, J.L. Peng, and R.L. Greene, "Tunnelling evidence for predominately electron-phonon coupling in superconducting $Ba_{1-x}K_xBiO_3$ and $Nd_{2-x}Ce_xCuO_{4-y}$," Nature, vol. 347, pp. 369-372, Sept. 1990.

[26]D.G. Hinks, B. Dabrowski, D.R. Richards, J.D. Jorgensen, S. Pei, and J.F. Zasadzinski, "Evidence for phonon-mediated coupling in superconducting $Ba_{1-x}K_xBiO_3$," Physica C, vol. 162-164, pp. 1405-1408, 1989.

[27]H. Sato, ibid.

[28]C. Escribe-Filippini, ibid.

[29]E.S. Hellman and E.H. Hartford Jr., "Normal-state resistivity and Hall effect in $Ba_{1-x}K_xBiO_3$ epitaxial films," Phys. Rev. B, vol. 47 (17), pp. 11346-11352, May 1993.

[30]M.A. Karlow, S.L. Cooper, A.L. Kotz, M.V. Klein, P.D. Han, and D.A. Payne, "Optical conductivity of $Ba_{1-x}K_xBiO_3$ through the metal-insulator transition," Phys. Rev. B, vol. 48(9), pp. 6499-6505, Sept. 1993.

[31]M. Tinkham, Phys. Rev. Lett., vol. 61, p. 1658, 1988.

[32]G.T. Seidler, ibid.

[33]C.W. Hagen and R. Griessen, Phys. Rev. Lett. vol. 62, p. 2857, 1989.

Chapter 6

TUNNELING

This chapter discusses tunneling in BKBO thin films; including, superconductor-insulator-superconductor (SIS) tunneling, superconductor-insulator-normal metal (SIN) tunneling, and SIS Josephson tunneling. Tunneling theory will be discussed first. Then the various types of tunneling will be sequentially described. From the tunneling measurements, we determine both the coupling strength and the gap of our BKBO films.

6.1 Tunneling Theory

Let us now look at some basic tunneling theory required to understand the study. I will discuss quasiparticle tunneling, and then Josephson tunneling. At the end of this section, I will discuss some qualities of good Josephson and quasiparticle tunnel junctions.

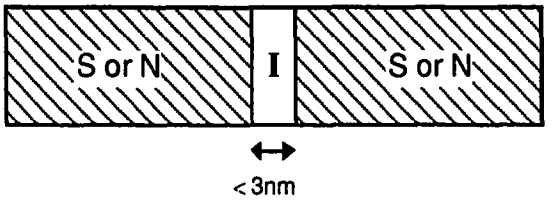

Figure 6.1 A representation of a tunnel junction. S stands for superconductor, N stands for a normal metal, and I is an insulator.

6.1.1 Single Electron Tunneling

Quasiparticles are the excitations above the BCS ground state of Cooper pairs. Quasiparticle excitations behave in a similar manner to electron or hole excitations. Like electrons and holes, quasiparticles

are fermions, and may recombine to form photons or phonons, although they have different density of states (DOS) and dispersion curves. Fortuitously, one may usually use the Semiconductor tunneling model for both, and can even obtain quantitative results.[1] Consider the model of a tunnel junction in Fig. 6.1. The tunneling current between two metals is represented by the following equation:[2]

$$I = \frac{1}{h}\int |T_{RL}|^2 N_L(E-eV)N_R(E)[f(E-eV)-f(E)]dE \quad \text{(Eq. 6.1)}$$

where h is Planck's constant, e is the charge on an electron, $|T_{RL}|^2$ is the transmission probability through the barrier, N_L and N_R are the DOS of the left and the right electrodes, respectively, f(E) is the Fermi function, V is a voltage applied across the barrier, and E is the energy of the excitation, measured from the Fermi energy. If we consider a normal metal-insulator-normal metal junction (NIN), we can simplify Eq. 6.1 to the following near T=0 °K:

$$I = \left[\frac{e}{h}|T_{RL}|^2 N_L(0)N_R(0)\right]V \quad \text{(Eq. 6.2)}$$

One can see at this point that we have simply obtained Ohm's Law, I = [1/R]V, as the DOS and transmission probability are insensitive to small changes in voltage. Next, let us look at the tunneling current in a SIN tunnel junction also near T= 0 °K:

$$I = \frac{1}{h}|T_{NS}|^2 N_N(0)\int_0^{eV} N_S(E)dE \quad \text{(Eq. 6.3)}$$

$$\frac{dI}{dV} = \frac{e}{h}|T_{NS}|^2 N_N(0)N_S(eV) \quad \text{(Eq. 6.4)}$$

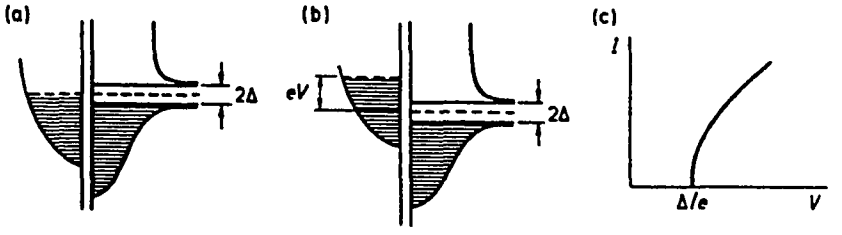

Figure 6.2 The energy diagram of an NIS junction in the semiconductor representation; (a) V = 0, (b) V > Δ/e, (c) the I-V characteristic at finite temperature. Adapted from Solymar.[3]

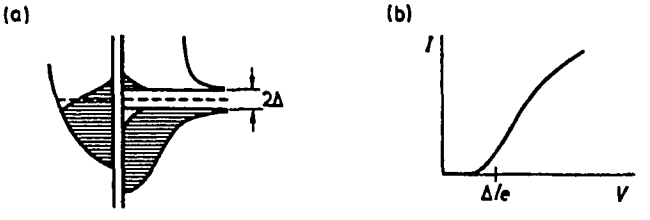

Figure 6.3 (a) The energy diagram of an NIS junction at finite temperature in thermal equilibrium, (b) the I-V characteristic at finite temperature. Adapted from Solymar.[4]

N and S subscripts represent the normal and superconducting sides of the junction in the transmission coefficients and the DOS. The differential conductance (dI/dV), is directly proportional to the DOS of the superconductor, as the other factors are constant. This is why tunneling is a good spectral probe of the superconducting state. Above the gap, the BCS conductance is roughly constant in this model,[5] although this is not seen in the cuprates and rarely in BKBO.

The Semiconductor model can be represented in a pictorial fashion that presents a qualitative understanding of tunneling behavior. Let us first look at an SIN junction current-voltage characteristic (IV) at T=0 shown Fig. 6.2, then at finite temperature shown in Fig. 6.3. The junction is biased by a voltage V, which offsets the Fermi energies (E_F) by V. Current will flow when there are occupied states on the left and open states on the right, and visa-versa.

SIS' junctions are similar in behavior to the SIN junctions at T=0 in Fig. 6.2, but the conductance jumps at $\Delta_1+\Delta_2$ instead of Δ. At finite temperatures, however, a feature at $|\Delta_1-\Delta_2|$ can appear, as shown in Fig. 6.4. These models give good predictions of what real IV characteristics look like, except that there is often a larger subgap current, due to pinholes or material limitations.

6.1.2 Josephson Tunneling

If one reduces the thickness of the insulating barrier to less than 2 nm, then Josephson tunneling may be seen between two

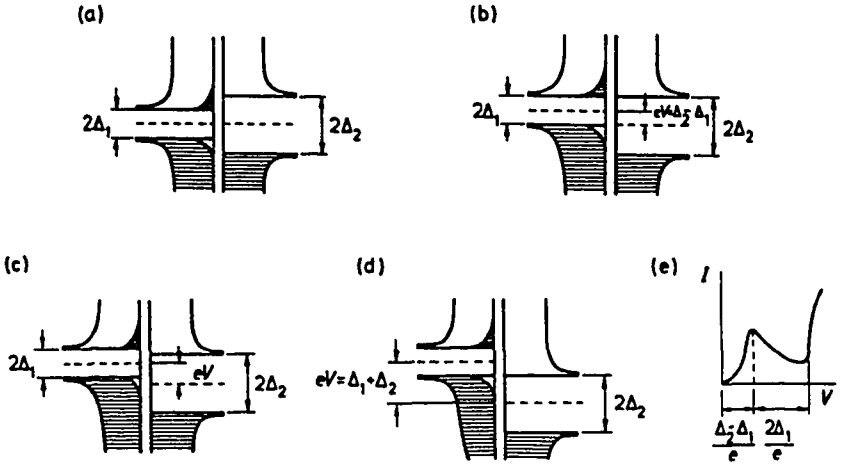

Figure 6.4 The energy diagram and I-V characteristic of an SIS junction at finite temperature: (a) V = 0, (b) V = $(\Delta_2 - \Delta_1)/e$, (c) $(\Delta_2 - \Delta_1)/e < V < (\Delta_2 + \Delta_1)/e$, (d) V = $(\Delta_2 + \Delta_1)/e$, (e) the I-V characteristic. Adapted from Solymar.[6]

superconductors. In zero magnetic field, the Josephson equations are as follows:[7]

$$I = I_o \sin(\phi), \qquad \text{(Eq. 6.5)}$$

$$\frac{d\phi}{dt} = \frac{2e}{\hbar} V, \qquad \text{(Eq. 6.6)}$$

where ϕ is the quantum mechanical phase difference between the two superconductors. Eq. 6.5 represents the dc Josephson effect where one can have current passing through the junction without a voltage, up to a maximum of I_0 (the critical current). In the weak coupling limit, $I_0(T)$ has the following form:[8]

$$I_o(T) = \frac{\pi \Delta(T)}{2eR_n} \tanh \frac{\Delta(T)}{k_B T}, \qquad \text{(Eq. 6.7)}$$

where R_n is the normal state resistance and k_B is Boltzmann's constant. The limit as T=0 yields $I_0 = \pi\Delta(0)/2eR_n$, which represents the theoretical upper value of the critical current. Magnetic impurities, stray magnetic fields, thermal effects (discussed below), electron traps, and strong coupling effects will reduce I_0. Eq. 6.6 represents the ac Josephson effect in which a voltage-biased junction will oscillate the current through the junction at a frequency of 483 MHz/μV. A method of determining whether a device is a JJ is to observe microwave-induced current steps (Shapiro steps) in the current-voltage characteristic. These steps are caused by the microwaves resonating with the ac Josephson oscillations. They are characteristically spaced at voltages of

$$V_n = \frac{nh}{2e} f_o, \qquad \text{(Eq. 6.8)}$$

where n is an integer and f_o is the driving microwave frequency.[9]

Thermal effects must be considered, especially in high temperature superconductivity, as they can eliminate the Josephson effect. A qualitative understanding of this can be seen in the ratio of the two competing energies; the thermal energy and the Josephson coupling energy E_J, shown below:

$$\frac{k_B T}{|E_J|} = \frac{2\pi k_B T}{I_o \Phi_o} \approx \frac{2e k_B T R_n}{\pi \Delta \Phi_o} \propto \frac{T}{T_c} R_n, \qquad \text{(Eq. 6.9)}$$

where k_B is Boltzmann's constant. In order to see the Josephson effect, this ratio should be << 1. Eq. 6.9 shows that it is important to have a low resistance junction and I_o rounding is less at lower temperatures. Experimentally, one can see $I_o \approx 1\ \mu A$ at 4 °K.

The Resistively Shunted Junction (RSJ) model is commonly used to model JJ's. For thin film junctions, the RSJ equivalent circuit used is in Fig. 6.5, where the Josephson element has current $I_o \sin\phi$, the resistor has current V/R_n, and the capacitor has a current of $C(dV/dt)$. This leads to the following relation:

$$I = I_o \sin\phi + \frac{V}{R_n} + C\frac{dV}{dt}, \qquad \text{(Eq. 6.10)}$$

This equation can be solved numerically to give the results pictured in Fig. 6.6, where $\kappa = I/I_o$, $\eta = V/I_o R_n$, and $\beta_c = 4\pi e I_o R_n^2 C/h$. βc is a hysteresis parameter, where the amount of hysteresis in the IV curve increases with β_c. The hysteresis manifests itself as a difference between the maximum zero voltage current as the current

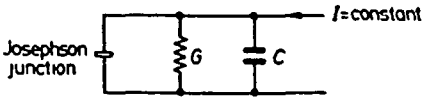

Figure 6.5 Circuit representation of a RSJ model junction made up of an "ideal" junction satisfying the dc Josephson effect, an ohmic conductor, and a capacitance. After Solymar.[10]

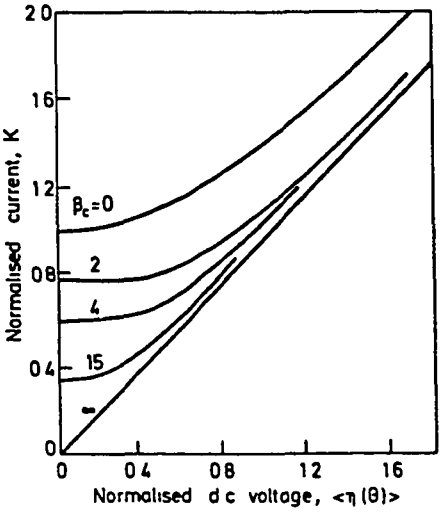

Figure 6.6 Normalized I-V characteristics of a junction represented by the circuit shown in Fig. 6.5, analyzed with constant current. After McCumber.[11]

is increased and decreased. Since R_n is used, this specific model is useful for shunted tunnel junctions, such as those used in SQUID's. In order to model our (unshunted) tunnel junctions, the nonlinear tunneling resistance must replace R_n.

To include magnetic fields in the Josephson relations, we need only to make the following substitution into equations 6.5 and 6.6:[12]

$$\phi \rightarrow \phi - \frac{2\pi}{\Phi_o}\oint \vec{A}\cdot\vec{ds} \quad , \qquad \text{(Eq. 6.11)}$$

where A is the vector potential, and Φ_o = hc/2e, the unit flux quantum. Since Φ_o is so small (2.07 x 10^{-7} gauss-cm^2), we see the JJ is very sensitive to magnetic fields. By applying a small magnetic field, one may see an oscillation of the critical current, similar to a single-slit diffraction pattern. The relation is shown below for a small SIS Josephson junction:[13]

$$I_o(H) = I_o(0)\left|\frac{\sin(\pi\Phi/\Phi_o)}{\pi\Phi/\Phi_o}\right|, \qquad \text{(Eq. 6.12)}$$

where $\Phi = 2\lambda HL$. H is the field parallel to the plane of the junction interface. L is the junction length perpendicular to H and parallel to the junction plane. λ is the magnetic penetration depth for the superconductors. This pattern is very sensitive to the uniformity of the critical current density of the barrier, and to the geometry of the junction.

One final point concerns the behavior of a SN interface and the associated proximity effect. The amplitude of the superconducting wavefunction is decreased near the boundary, and a psuedo-

superconducting wavefunction extends into the normal metal. The coherence length inside the normal metal ξ_N (dirty limit) is the following:

$$\xi_N = \sqrt{\frac{\hbar v_F \ell}{6\pi k_B T}} \qquad \text{(Eq. 6.13)}$$

where v_F is the fermi velocity, and ℓ is the electron mean free path. ξ_N for clean copper has been measured to be 470 Å at 3 °K.[14] The proximity effect allows Josephson coupling between superconductors at longer lengths in SNS junctions (microns) than in SIS junctions (< 2 nm).

From the various relations and ideas above, we have many ways to test and determine the quality of a junction. For tunnel junctions, the main criterion for quality is to have well-developed gap structure. This consists of low conductance in the gap (no pinholes in the barrier) and a sharp conductance increase at the gap which levels off to the normal state resistance. Josephson tunnel junctions should also have a well defined gap. The dc Josephson effect must be observed, preferably near the Ambegaokar limit of I_0. If I_0 is small, one can confirm the Josephson effect by observing microwave steps in the IV, as in Eq. 6.8. The most stringent JJ test is the dependence of I_0 with field. Only a uniform tunnel barrier will yield equation 6.12. An example of a $Sn/Sn_xO_y/Sn$ Josephson tunnel junction is demonstrated in Fig. 6.7.

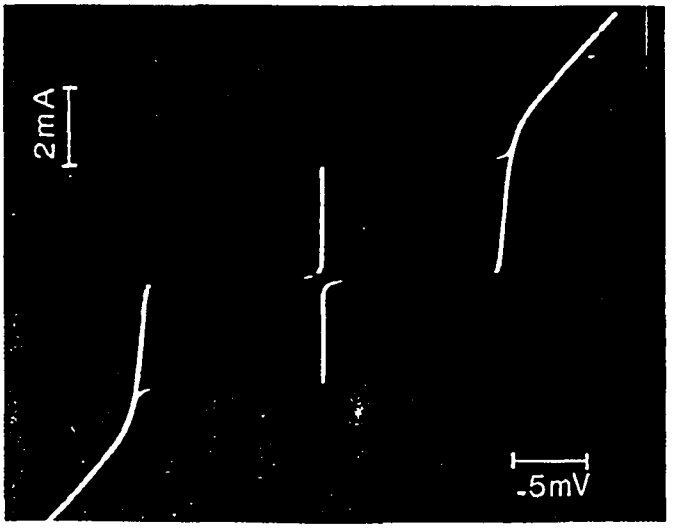

Figure 6.7 I-V characteristic for a $Sn/Sn_xO_y/Sn$, Josephson junction at T= 1.52 °K. Horizontal scale: 0.5 mV/div; vertical scale; 2 mA/div. After Barone.[15]

6.2 Measurement

We measure our samples by mounting them on an insert weakly linked to a He^4 bath, on which the temperature can be both monitored and regulated between 2 °K-100 °K. The IV is taken in a 4-probe configuration, using a current source to drive the junction, and a preamplifier to monitor the voltage. The conductance (dI/dV) may be directly measured by superimposing a small ac modulating signal on the dc bias current. The conductance is then obtained using a lock-in amplifier to measure the ac voltage as the dc current is slowly stepped through the entire IV curve. For the data shown in section 6.4; however, the dI/dV was obtained by numerically differentiating the IV curve and subsequently filtering the result. Data acquisition was accomplished with a computer by slowly sweeping the junction current via a voltage controlled current source driven by a DAC computer output. The amplified voltage and differential conductance were acquired by the computer from ADC inputs as the current was ramped.

6.3 Junction Fabrication

All junctions hereafter discussed were made with at least one electrode of BKBO film grown with PLD. The tunneling barriers were made either by exposure to air or with ion milling. With ion milling, the thickness of the tunneling barrier decreases by lowering beam energy, rotating the sample normal away from the impinging angle of the ions, and adding oxygen (20%) to the mill gas. For more details on ion milling, see Chapter 3.

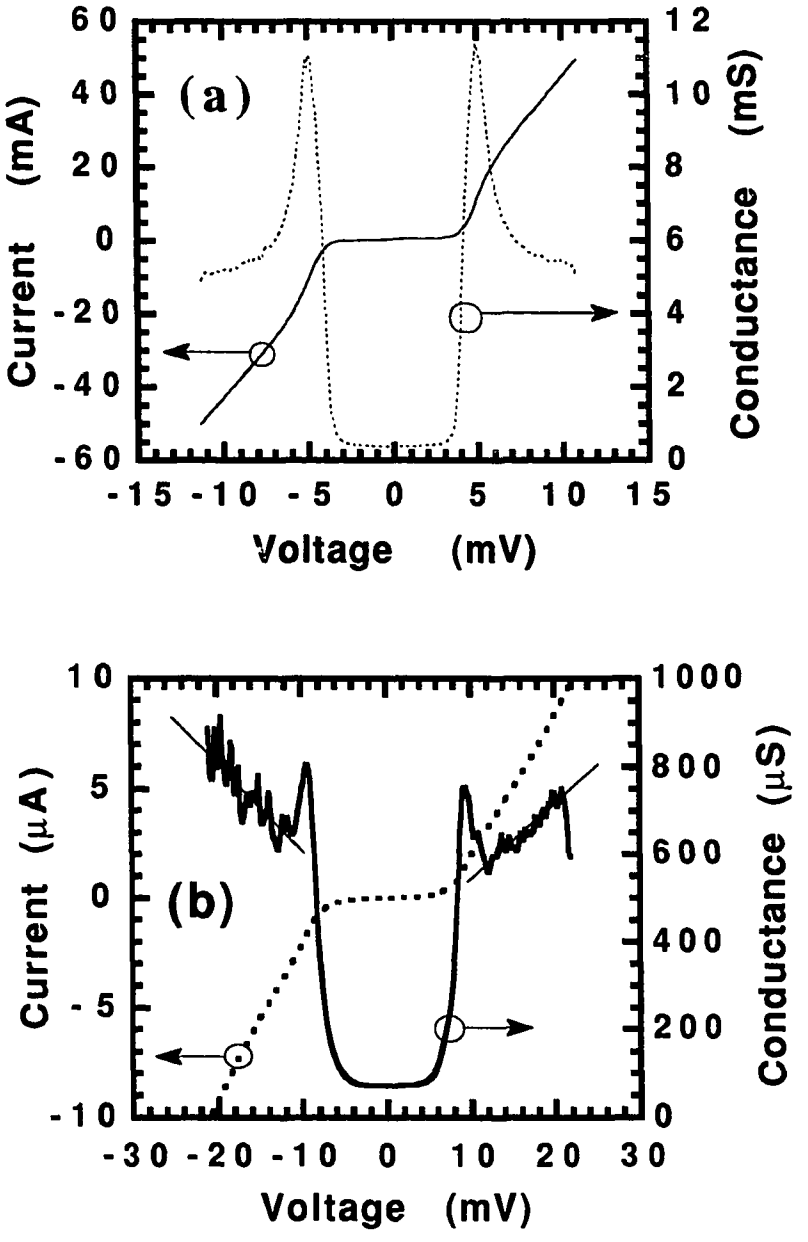

Figure 6.8 (a) BKBO/I/Ag tunnel junction at 2 °K with ion mill formed barrier. Film T_c was 27.5 °K and Δ = 4.5 meV, therefore $2\Delta/k_BT_c$ = 3.8. (b) Two junctions in series, BKBO/I/Ag/I/BKBO, at 4 °K, showing linear conductance background. Film T_c was 25 °K.

After ion milling, the counter-electrode was deposited *in-situ*. In the case of metals that react with the BKBO like Pb and Nb, we have also used a different method. Before the counter-electrode is deposited, a thin layer (<100 Å) of Ag is deposited to act as a diffusion barrier for the BKBO.

We used a natural barrier to make film/film and film/crystal junctions. The junctions were made by pressing the counter-electrode film or crystal into the film electrode; sometimes even using an alligator clip. By varying how strongly the two electrodes were held together, the tunneling barrier was changed.

6.4 Results

In Fig. 6.8 are tunneling IV and conductance characteristics of two different SIN tunneling junctions. Fig. 6.8a is a clean BKBO/I/Ag tunnel junction of area 1 mm^2, where the barrier was formed by ion milling at 500 eV in Ar. The conductance can be fit phenomenologically to a lifetime broadened density of states.[16] The normalized conductivity can be represented by,

$$\frac{\sigma_s}{\sigma_n} = \mathrm{Re}\left\{\frac{E - i\Gamma}{\sqrt{(E - i\Gamma)^2 - \Delta^2}}\right\} \qquad \text{(Eq. 6.14)}$$

where σ_S and σ_n are the superconducting and normal conductivities, E is the energy measured from the fermi surface, and Γ is the broadening. Fitting Fig. 6.8a gives Δ = 4.5 meV and Γ = 0.5 meV. Using the film transition of 27.5 °K, the coupling, $2\Delta/k_BT_c$, is 3.8. As this low leakage junction can be fit with the least ambiguity, this gap and coupling values are our best. In Fig. 6.8b is a

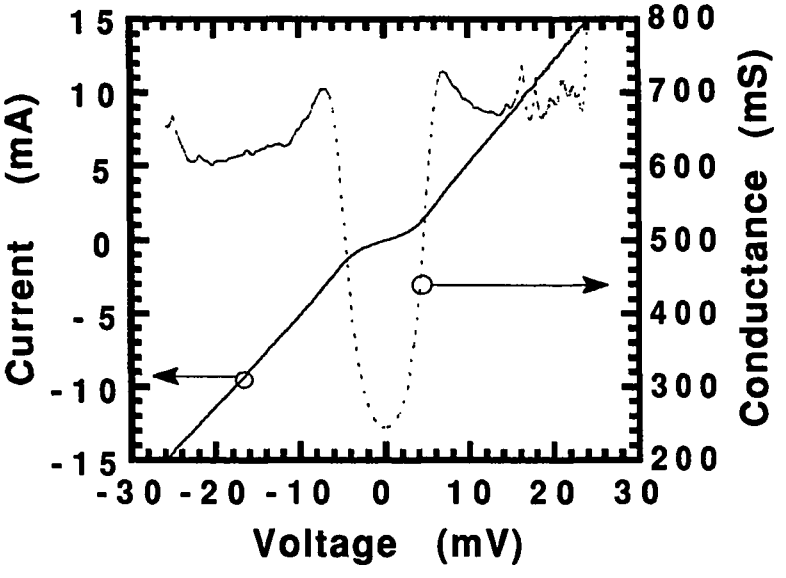

Figure 6.9 IV and dI/dV BKBO/I/Ag/Nb tunnel junction characteristics. The tunneling gap, $\Delta_{Nb}+\Delta_{BKBO}$, is 6.0 meV.

BKBO/I/Ag/I/BKBO series tunneling circuit composed of two tunnel junctions formed from exposure to air. Fig. 6.8b illustrates the linear conductance background typical of the cuprates and bismuthate compounds.[17,18,19] At low voltages (energies) seen in Fig. 6.8a, we do not always see the linear background in our tunneling curves, as the effect of the gap extends to beyond this range.

As discussed above, we have made junctions with and without a Ag diffusion barrier with Nb and Pb counter-electrodes. We have been able to make tunnel junctions (BKBO/I/Nb) using this method, but the tunneling resistance was too high to observe the Josephson effect. Therefore, we tried to lower the contact resistance by using a Ag buffer layer, making a BKBO/I/Ag/Nb junction. An example of a tunnel junction using this method is shown in Fig. 6.9. We see a leaky gap between 5-6 meV, the width being what we would expect from $\Delta_{Nb}+\Delta_{BKBO}$, as the gap of our Nb junctions is $\Delta \approx 1.3$ meV.

We have also made all BKBO tunnel junctions and Josephson tunnel junctions. A BKBO junction made by pressing two films together is shown in Fig. 6.10a, where $2\Delta/k_BT_c$ is 3.8-4. We have also made a Josephson tunnel junction with a BKBO crystal pressed into a film, as demonstrated in Fig. 6.10b.

The ultimate goal, however, is making a single substrate thin film BKBO/I/BKBO Josephson tunnel junction. While some all-thin film junctions made been made, no low leakage Josephson junctions with significant critical currents have been produced.[20,21,22] It appears that these junctions are formed by pinholes or grain

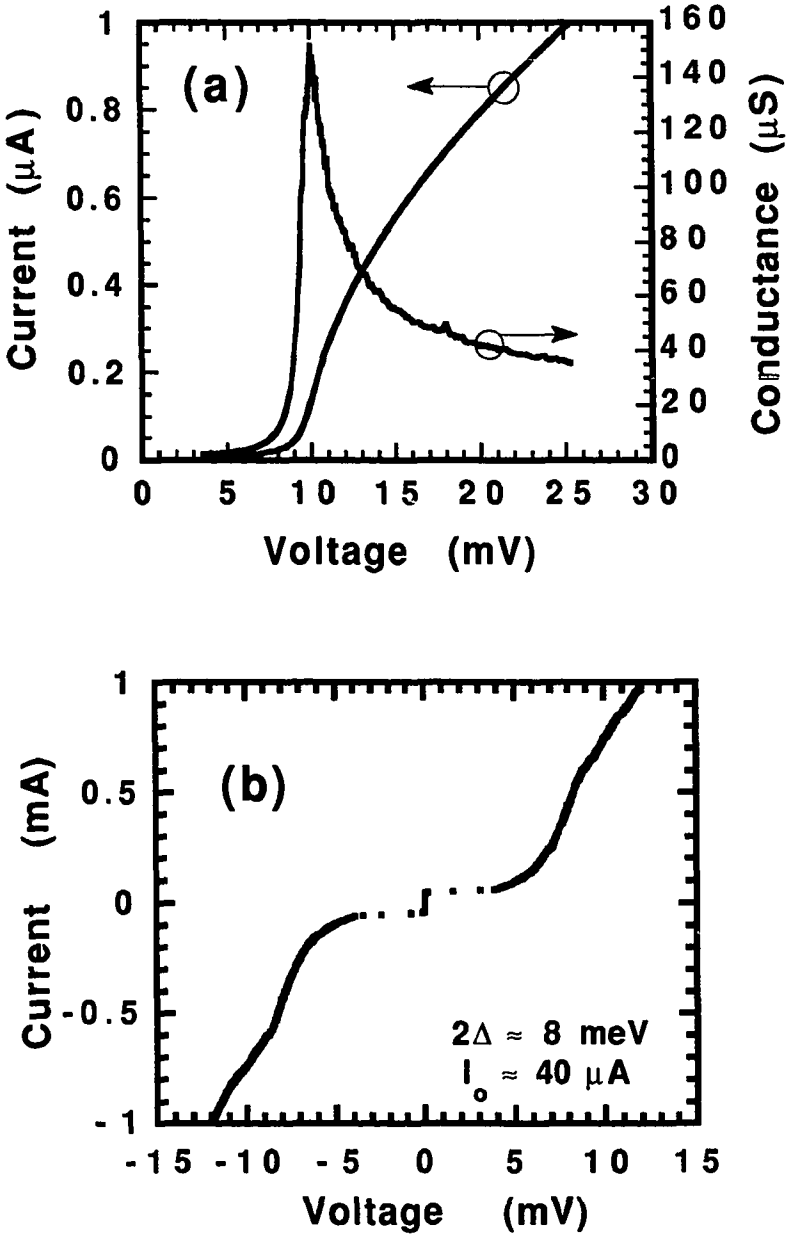

Figure 6.10 (a) Current-voltage and differential conductance characteristics of a BKBO/I/BKBO tunnel junction made by pressing two films together with a natural (air exposed) barrier. $\Delta \approx 9$ meV.[23] (b) Current-voltage characteristic of a BKBO/I/BKBO Josephson tunnel junction made from a crystal pressed into a film, with a natural barrier at 2 °K.

boundaries,[24] as the current modulations (Eq. 6.12) are poor, and in the case of sandwich junctions, don't correspond to the area of the junction.

There are many things for further study and improvement. The ultimate goal of a quality thin film Josephson tunnel junction is largely undone and faces many materials difficulties. To make a sandwich-type junction, a major obstacle is the ability to grow multilayers sequentially, breaking vacuum between layers. This ability is necessary for any multilayer BKBO technology. Reduction of stress in the film is also important to multilayer development and improves the coupling.[25] An inherent difficulty that exists in making traditional junctions is formation of an abrupt barrier. One needs a pinhole free insulator, with crystalline and uniformly K doped superconductor on either side. Some insulators that have been explored include $KNbO_3$, $KTaO_3$, $SrTiO_3$, and MgO.[26,27,28] The challenge is best illustrated by comparison to $Nb/Al/Al_2O_3/Nb$ technology, where the barrier degrades near 200 °C, compared to our growth temperatures near 600 °C. Thus low temperature growth techniques may be important for at least the top counterelectrode layer.

We have made BKBO tunnel and Josephson tunnel junctions and have measured the BKBO gap at 4.5 meV and coupling strength $2\Delta/k_BT_c = 3.8$. These values are in agreement with other studies, and the gaps are among the highest published results for BKBO.[29,30,31,32,33,34,35,36] For a weak coupled superconductor,

$2\Delta/k_BT_c$ =3.53 compared to the measured coupling of 3.8. This shows that BKBO is a weak-to-moderately coupled superconductor. Further progress towards high quality Josephson junctions is a prerequisite for practical application of thin film BKBO superconducting devices.

References

[1] L. Solymar, Superconductive Tunnelling and Applications, John Wiley and Sons, New York, 1972, p41.

[2] A. Barone and G. Paterno, Physics and Applications of the Josephson Effect, John Wiley and Sons, New York, 1982, p. 6.

[3] L. Solymar, ibid, p. 32.

[4] L. Solymar, ibid, p. 33.

[5] L. Solymar, ibid, pp. 38-40.

[6] L. Solymar, ibid, p. 36.

[7] A. Barone and G. Paterno, ibid, p. 11.

[8] V. Ambegaokar and A. Baratoff, Phys. Rev. Lett., vol. 10, p. 486, 1963; erratum, vol. 11,p. 104, 1963.

[9] A. Barone and G. Paterno, ibid, p13.

[10] L. Solymar, ibid, p170.

[11] L. Solymar, ibid, p170.

[12] A. Barone and G. Paterno, ibid, p. 16.

[13] A. Barone and G. Paterno, ibid, p. 17.

[14] J. Clarke, Proc. Roy. Soc. A., vol. 308, p. 447, 1969.

[15] A. Barone and G. Paterno, ibid, p13

[16] R.C. Dynes, V. Narayanamurti, and J.P. Garno, "Direct measurement of quasiparticle-lifetime broadening in a strong-coupled superconductor," Phys. Rev. Lett., vol. 41(21), pp. 1509-12, Nov. 1978.

[17] F. Sharifi, A. Pargellis, and R.C. Dynes, "Tunneling density of states in the lead-bismuth-oxide superconductors," Phys. Rev. Lett., vol. 67(4), pp. 509-511, Jul. 1991.

[18] J.R. Kirtley, S. Washburn, D.J. Scalapino, "Origin of the linear tunneling conductance background," vol. 45(1), pp. 336-46, Jan. 1992.

[19] R.C. Dynes, F. Sharifi, A. Pargellis, E.S. Hellman, B. Miller, E. Hartford Jr., and J. Rosamilia, "Tunneling spectroscopy in Ba1-xKxBiO3," Physica C, vol. 185-189, pp. 234-240, 1991.

[20] R.L. Fink, M. Thompson, C. Hilbert, and H. Kroger, "Hysteretic Josephson junctions from high T_c superconducting thin films," IEEE Trans. Appl. Superconductivity, vol. 3(1), pp. 2219-2221, Mar. 1993.

R.L. Fink, C. Hilbert, and H. Kroger, "$Ba_{1-x}K_xBiO_3$ thin film Josephson tunnel junctions," Appl. Phys. Lett., vol. 62(25), pp. 3360-3, Jun. 1993.

[21]J. Amano, H. Ko, M. Narbutovskih, J. Sheats, and K. Tibbs, "Superconducting $Ba_{1-x}K_xBiO_3$ thin films and junctions," J. Appl. Phys., vol. 74(7), pp. 4620-4626, Oct. 1993.

[22]A. Kussmaul, E.S. Hellman, E.H. Hartford Jr., and P.M. Tedrow, "Superconductor-insulator-superconductor tunneling in $Ba_{1-x}K_xBiO_3$ grain boundaries," Appl. Phys. Lett., vol. 63(20), pp. 2824-2826, Nov. 1993.

[23]B.M. Moon, C.E. Platt, R.A. Schweinfurth, and D.J. Van Harlingen, "In situ pulsed laser deposition of superconducting $Ba_{1-x}K_xBiO_3$ thin films," Appl. Phys. Lett., vol. 59(15), pp. 1905-7, Oct. 1991.

[24]S. Martin, E.S. Hellman, A. Kussmaul, and E.H. Hartford, "Quasiparticle-tunneling properties of $Ba_{1-x}K_xBiO_3/BaBi_2O_y/Ba_{1-x}K_xBiO_3$," Phys. Rev. B, vol. 47(21), pp. 14510-14513, Jun. 1993.

[25]K. Char, L. Antognazza, T.H. Geballe, "Study of interface resistances in epitaxial $YBa_2Cu_3O_{7-x}$/barrier/$YBa_2Cu_3O_{7-x}$ junctions," Appl. Phys. Lett., vol. 63(17), pp. 2420-2, Oct. 1993.

[26]R.L. Fink, C. Hilbert, and H. Kroger, "$Ba_{1-x}K_xBiO_3$ thin film Josephson tunnel junctions," Appl. Phys. Lett., vol. 62(25), pp. 3360-3, Jun. 1993.

[27]J. Amano, ibid.

[28]B.A. Baumert, J. Talvacchio, and M.G. Forrester, "SrTiO3 buffer layer and tunnel barriers for Ba-K-Bi-O junctions," Appl. Phys. Lett., vol. 62(17), pp. 2137-9, Apr. 1993.

[29]Y. Enomoto, K. Moriwaki, and K. Tanabe, "Electrical properties of grain boundaries in Ba1-xKxBiO3 polycrystalline thin films," J. Appl. Phys., vol. 68(11), pp. 5735-5740, Dec. 1990.

[30]Q. Huang, J.F. Zasadzinski, N. Tralshawala, K.E. Gray, D.G. Hinks, J.L. Peng, and R.L. Greene, "Tunnelling evidence for predominantly electron-phonon coupling in superconducting $Ba_{1-x}K_xBiO_3$ and $Nd_{2-x}Ce_xCuO_{4-\delta}$," Nature, vol. 347, pp. 369-72, Sept. 1990.

[31]A.N. Pargellis, F. Sharifi, R.C. Dynes, B. Miller, E.S. Hellman, J.M. Rosamilia, and E.H. Hartford Jr., "All-high Tc Josephson tunnel junction: $Ba_{1-x}K_xBiO_3/Ba_{1-x}K_xBiO_3$ junctions," Appl. Phys. Lett., vol. 58(1), pp. 95-7, Jan. 1991.

[32]H. Sato, H. Takagi, and S. Uchida, "Gap observation by tunneling measurement on superconducting $Ba_{1-x}K_xBiO_3$ thin film: A finite energy gap in $Ba_{1-x}K_xBiO_3$," Physica C, vol. 169, pp. 391-395, 1990.

[33]C.J. Hou, R.L. Fink, C. Hilbert, and H. Kroger, "Low-leakage thin-film S-I-N tunnel junctions on co-evaporated $Ba_{1-x}Rb_xBiO_3$ and RF sputtered $Ba_{1-x}K_xBiO_3$," Appl. Phys. Lett., vol. 60(10), pp. 1262-4, Mar. 1992.

[34]A. Kussmaul, E.S. Hellman, E.H. Hartford Jr., and P.M. Tedrow, "Superconductor-insulator-superconductor tunneling in $Ba_{1-x}K_xBiO_3$ grain boundaries," Appl. Phys. Lett., vol. 63(20), pp. 2824-2826, Nov. 1993.

[35]J. Amano, ibid.

[36]B.A. Baumert, J. Talvacchio, and M.G. Forrester, "SrTiO3 buffer layer and tunnel barriers for Ba-K-Bi-O junctions," Appl. Phys. Lett., vol. 62(17), pp. 2137-9, Apr. 1993.

Chapter 7

MICROWAVE CHARACTERIZATION

BKBO has potential applications in microwave electronic devices due to low attenuation and dispersion intrinsic to superconductivity.[1] There is also scientific interest as BKBO may have lower losses than the cuprates because of its low subgap conductance seen in tunneling (Chapter 6). We have measured both patterned and unpatterned thin film structures to determine the microwave losses of our BKBO thin films. Unpatterned films were measured to determine intrinsic surface losses and for comparison to patterned devices. Micro-fabricated structures were measured to determine feasibility and practical surface losses. BKBO fabricated devices measured were a coplanar waveguide (CPW) transmission line, an effective microstrip resonator, and a CPW resonator. Parts of this chapter are adapted from Schweinfurth, et. al.[2]

There are three main figures of merit that describe a thin film superconductor-- the transition temperature (T_c), the critical current density (J_c), and the surface resistance (R_s). R_s is the most important parameter for microwave applications. Surface resistance is usually determined from studying the response of a microwave resonator made out of the material in question.[3] The resonator quality factor, Q, is inversely proportional to the surface resistance, as shown below:

$$Q = \omega/\Delta\omega \sim 1/R_s. \qquad \text{(Eq. 7.1)}$$

7.1 Film Measurement

There have been few reported measurements of BKBO surface resistance. From bulk values, low field surface resistance has been measured to be 640 μΩ at 0.82 GHz and 4 °K.[4] MBE unpatterned thin films ($T_c \approx 17$ °K) have reported $R_s = 400$ μΩ at 6.5 GHz and 2 °K in a parallel plate resonator.[5] We have measured our films ($T_c \approx 26$ °K) in a end-wall replacement cavity resonator[6,7] to be 1.2 mΩ at 9.6 GHz and 4 °K.[8] In order to compare these values, we need to scale the results to the same frequency. Surface resistance can be represented as shown in the superconducting representation in the two fluid model:

$$R_s = \omega^2 \mu_o^2 \lambda^3 \sigma_1 / 2, \qquad \text{(Eq. 7.2)}$$

where ω is the rf frequency, μ_o is the permeability constant, λ is the superconducting penetration depth, and σ_1 is the real part of the conductivity ($\sigma = \sigma_1 + j\sigma_2$) below T_c. From Eq. 2, we can scale the superconducting surface resistance proportionally to ω^2, as shown in Table 7.1. For comparison, BKBO films are about 1 mΩ at 10 GHz and 4 °K, while YBCO is 1-2 orders of magnitude lower at the same conditions. Using Eq. 7.1, one can calculate the theoretical losses. According to the two fluid Gorter-Casimir theory,[9] $\sigma_1 = \sigma_n\{1 - (T/T_c)^4\}$, where the normal state resistivity $\rho_n = 1/\sigma_n$. Using a value of 3400 Å for the penetration depth,[10] $\rho_n = 250$ μΩ-cm, T = 4 °K, and $T_c = 30$ °K, the theoretical loss is $R_s = 1.2$ μΩ at 10 GHz. While this calculation may be simplistic for this material, it suggests as does the

Sample	Scaled R_S @ 10 GHz
Bulk (Melt Quenched)	95 mΩ @ 4°K
MBE	0.95 mΩ @ 2°K
PLD	1.3 mΩ @ 4°K

Table 7.1 Scaled surface impedance measurements of BKBO film and bulk samples.

results from the cuprates, that R_S can be further reduced. From a materials viewpoint, there is large potential for improvement as the growth techniques of BKBO films have yet to be optimized for surface resistance.

7.2 MIC Background

In order to make microwave integrated circuits (MICs), standard circuit design must be changed. Failure of Kirchhoff's laws occur when as the electrical wavelength approaches circuit dimensions. In MICs, signals are propagated via transmission lines. Some transmission lines relevant to this thesis are the coplanar waveguide (CPW), microstrip, and stripline designs shown in Fig. 7.1.

Most microwave devices are connected by two-port junctions. These are characterized with scattering parameters (S-parameters), also common to high energy physics. The incident (V^+) and scattered (V^-) wave amplitudes from ports 1 and 2 are related by,

$$\begin{bmatrix} V_1^- \\ V_2^- \end{bmatrix} = \begin{bmatrix} S_{11} S_{12} \\ S_{21} S_{22} \end{bmatrix} \begin{bmatrix} V_1^+ \\ V_2^+ \end{bmatrix} \qquad \text{(Eq. 7.3)}$$

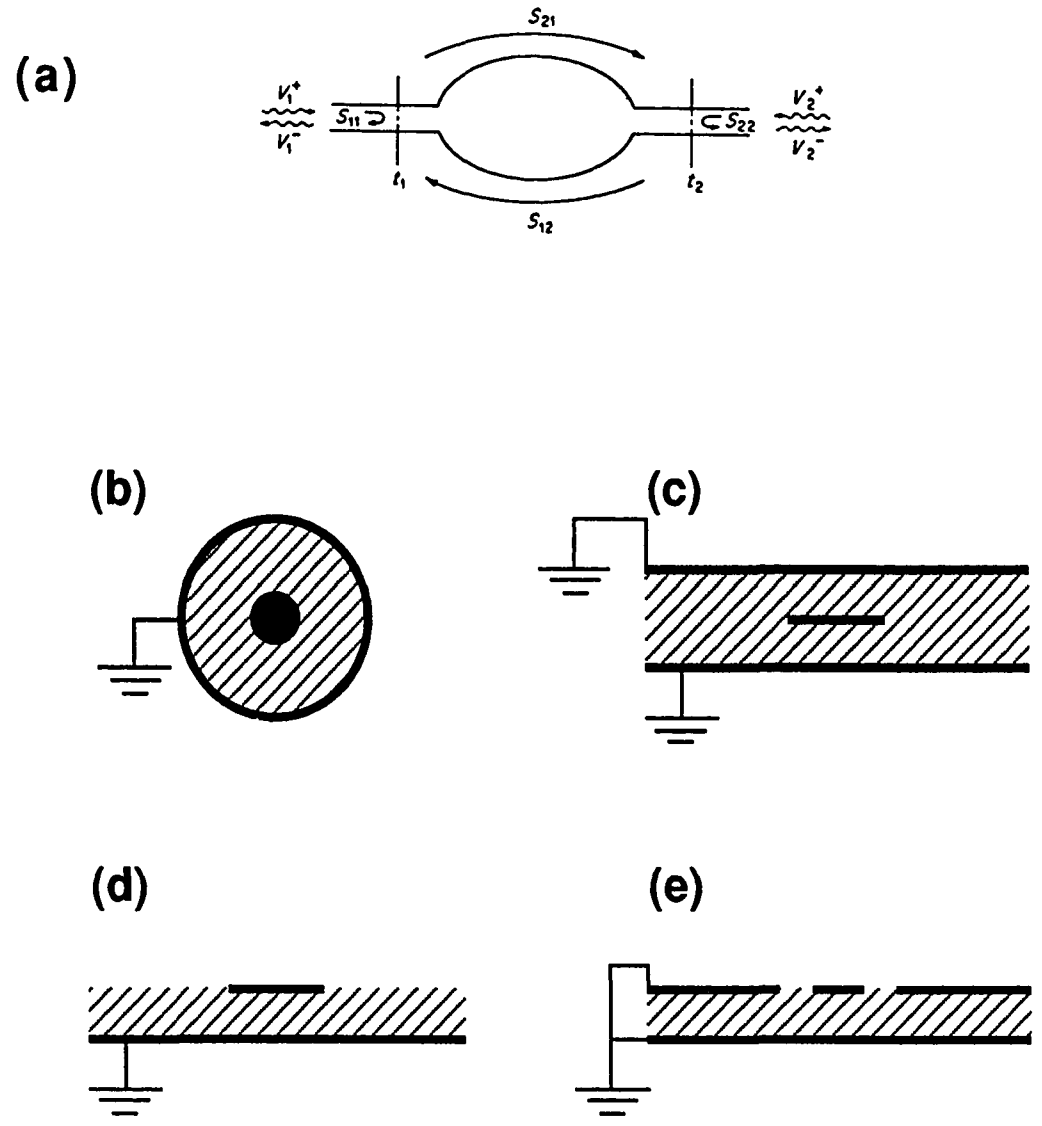

Figure 7.1 (a) Illustration of a two port network adapted from Collins.[11] Cross sections of various transmission line structures: (b) Coaxial ,(c) stripline, (d) microstrip, and (e) coplanar waveguide. The shaded areas contain dielectrics with relative dielectric constant ε_r.

where [S] is the scattering matrix.[12] For our resonator measurements, we used a one port measurement which determined only S_{11}. For the transmission lines, we needed a two port measurement, and the transmission (S_{21}) was the relative measure. Further details of microwave MICs, theory and measurement can be found elsewhere.[13,14,15,16]

7.3 Device Measurement

Microfabricated devices consisting of a CPW transmission line, a microstrip resonator, and a CPW resonator were measured to determine feasibility and practical surface losses of BKBO structures. These devices were fabricated from PLD BKBO films deposited on 5 mm x 5 mm x 0.5 mm (100) MgO substrates using Ar ion milling techniques as described in Chapters 2 and 3.

The devices were measured utilizing a novel on-wafer cryogenic measurement system shown in Figure 7.2.[17] The samples were mounted on a flow-through liquid He cold stage located inside a vacuum chamber. Network scattering parameters (S-parameters) were measured with a HP 8510B network analyzer. Cascade Microtech on-wafer probes were used and a full two-port calibration was made at the sample using a Cascade impedance standard. This method is very accurate for measuring the performance of microwave devices as it compensates for loading associated with the measurement probes, cables, and connectors. In order to measure the temperature of the film, a Si diode was placed on the cold stage.[18] Since the probes acted as a heat source to the film, we were

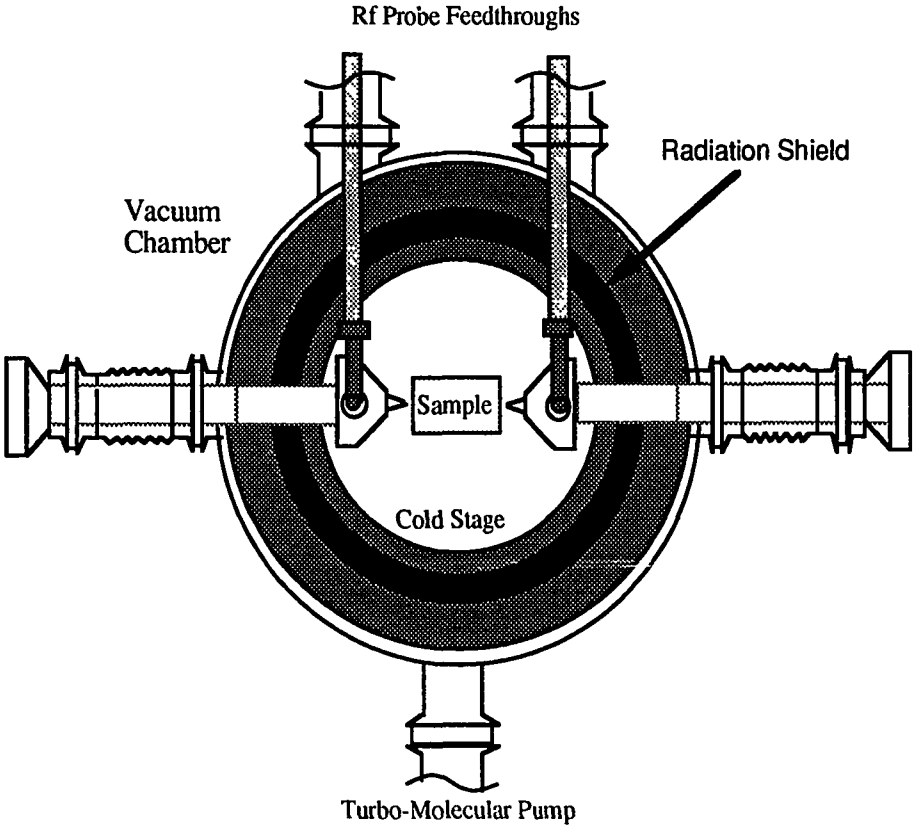

Figure 7.2 Schematic representation of a cryogenic microwave on-wafer measurement system (top view). Probes are heat sunk to the cold stage to test wafers down to 15 °K, at frequencies up to 40 GHz. Adapted from Kruse.[19]

careful to heat sink the probes with copper braid to the cold chuck, allowing the system to measure wafer S-parameters down to 15 °K. We calibrated the system's thermometer to the film's temperature by offsetting the observed microwave superconducting transition to the inductive T_c of the film.

7.4 Coplanar Transmission Line

The transmission line, the first resonator, and a four probe resistance structure were fabricated without T_c degradation from a 0.18 μm thick BKBO thin film with the following superconducting properties: $T_{c(0)}$ = 28.5 °K, $\Delta T \leq 0.5$ °K, and 1.3 MA/cm^2 (at 4.2 °K). We designed our own devices as our PLD films could only cover 5 mm x 5 mm substrate; established designs required 1cm^2 substrates. The lateral dimensions of the transmission line (T-line) were selected to give the coplanar waveguide a 50 Ω impedance[20] and 150 μm probe pitch on a MgO substrate using ε_r = 9.6.[21] As previously described, the transmission line was measured in a two-port configuration. The probes directly contacted the BKBO surface, as the Ag contact pads had degraded. In Fig. 7.4, the insertion loss of the BKBO is shown. The two-port insertion loss (S_{21}) at 21 °K was -4.2 dB (10 GHz) and -2.1 dB (20 GHz) along the length of the 2.5 mm transmission line. While the loss of -2.1 dB at 20 GHz and 21 °K is somewhat high, it proves feasibility and can be improved with design, film quality, and contact resistance.

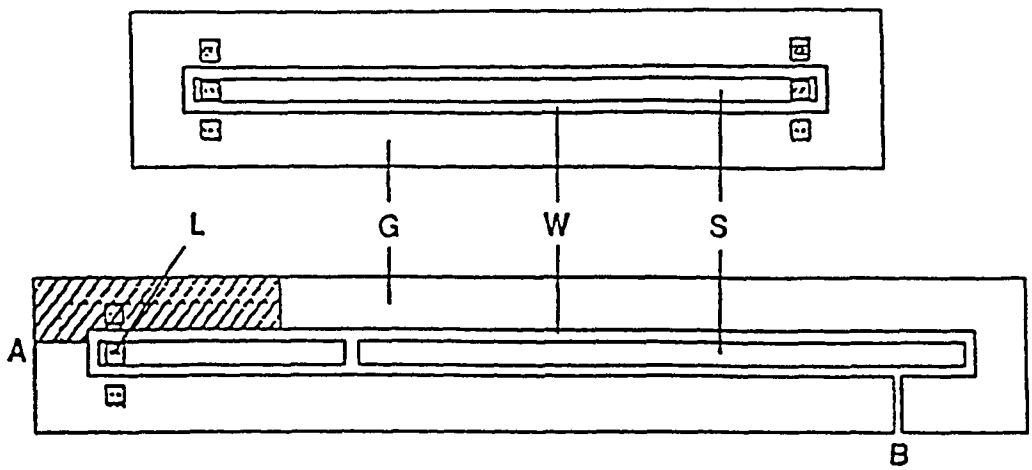

Figure 7.3 The top figure is the coplanar transmission line and the bottom is the resonator. The lateral dimensions W (center conductor), S (trench), and G (ground plane) are 86 μm, 43 μm, and 210 μm, respectively. L is where the resonator was probed. The marked areas on the resonator ground plane are Ag, as are the small square contact pads.[22]

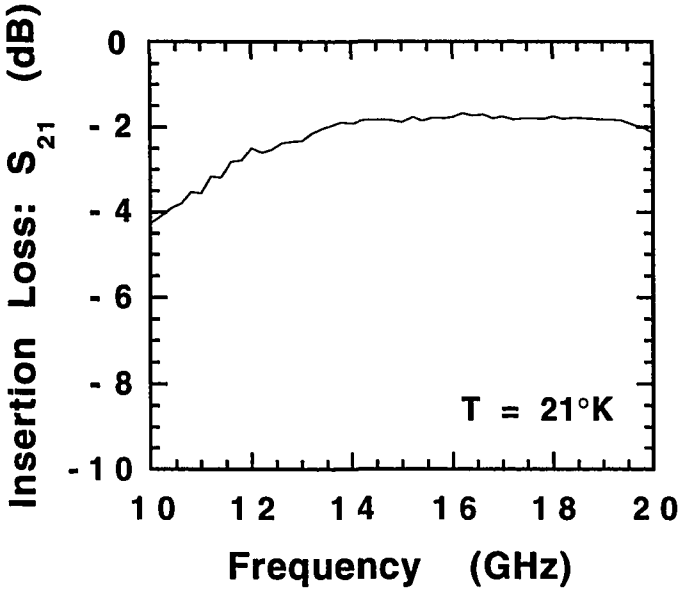

Figure 7.4 Two-port transmission through a 2.5mm BKBO coplanar transmission line.[23]

7.5 Microstrip Resonator

The resonator was fabricated from the same film as the T-line and was measured using a single probe, located as shown in Fig. 7.3. S_{11} data are shown in Fig. 7.5a, demonstrating sharp resonant behavior near 16 GHz and no resonance above T_c. The temperature dependence of the loaded Q (Q_L), unloaded Q, and resonant frequency are illustrated in Fig. 7.5b. Fig. 7.6 is a larger frequency scan, showing the second harmonic peak at 31.5 GHz, and a comparison with a Touchstone model of the resonator described below.

Although the original resonator design was coplanar with the fundamental frequency at 27 GHz, the observed signal was at 16 GHz. In order to explain the observed resonance, I propose that a part of the outer ground plane (G in Fig. 7.3) was acting as a microstrip resonator. The signal was launched from point L (in Fig. 7.3) to the effective resonator between lines A and B. Line A was the edge of degraded BKBO under Ag, and line B was a break in the ground plane. The centerline distance of the resonator is 3.66 mm, between lines A and B. The OFHC copper cold chuck acted as the back ground plane to the structure. The probes probably did not effectively ground the ground plane, due to degraded Ag contact pads, as seen in the transmission line. We used the CAD program Touchstone by EEsof to model a straight, gold microstrip line (3.66 mm long and 210 μm wide) on a 0.5 mm MgO ($\varepsilon_r \approx 9.6$) substrate. As seen in Fig. 7.6, this simple structure has the same fundamental frequency (16 GHz) as the resonator. One should note, however, that this

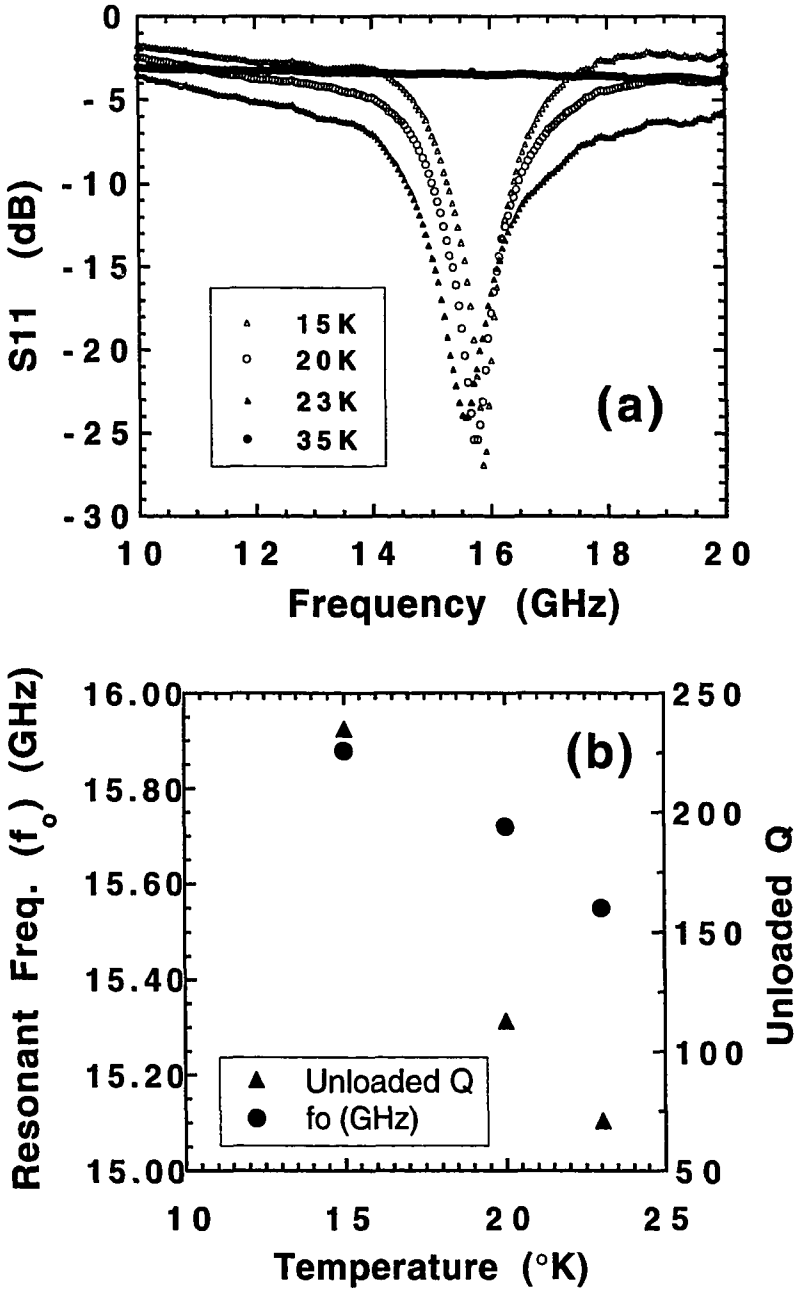

Figure 7.5 (a) S_{11} vs. Frequency for a BKBO resonator at different temperatures. (b) Unloaded Q and Resonant Frequency vs. Temperature for a BKBO resonator. Loaded Q values are 122, 60, and 38 at 15°K, 20°K, and 23°K, respectively.[24]

model is used to demonstrate the basic mechanism of the resonance, not to describe the entire behavior of the structure.

We can make an estimate of the surface impedance of the superconductor by assuming the microstrip behavior. The relationship between R_S and Q_C is shown below:

$$R_S = \Gamma f_o / Q_C, \qquad \text{(Eq. 7.3)}$$

where f_o is the resonant frequency, Γ is a calculated geometric factor, and Q_C is the quality factor contributed by the superconductor. The microstrip has a geometry which gives Γ=0.5 Ω/GHz.[25] One obtains Q_C from the measured loaded Q (Q_L) in the following relation:

$$\frac{1}{Q_L} = \frac{1}{Q_{EX}} + \frac{1}{Q_C} + \frac{1}{Q_D} + \frac{1}{Q_R}, \qquad \text{(Eq. 7.4)}$$

where Q_{EX} is the loading of the circuit, Q_D is from the substrate, and Q_R is from signal radiation. Surface wave losses were determined to be small in this case, and were ignored. We obtain the unloaded Q (subtracting the Q_{EX} contribution) by the procedure described in Rohrer.[26] $1/Q_D = \tan\delta$, which for MgO (at 9 GHz and 4.2 °K) is 1.6×10^{-4}.[27] A rough estimate of Q_R is given by

$$Q_R \approx 3\varepsilon_r Z_o \lambda_o^2 / (32\eta_o h^2), \qquad \text{(Eq. 7.5)}$$

where ε_r is the relative dielectric constant, Z_o is the microstrip characteristic impedance, λ_o is the free space wavelength, η_o is the free space impedance (377 Ω), and h is the substrate thickness in mm. Z_o was evaluated to be 72 Ω, using both Touchstone[28] and standard microstrip relations.[29] Using Eq. 7.5, we find that $Q_R \approx 247$. Since this is nearly the unloaded Q at 15 °K, we see that the

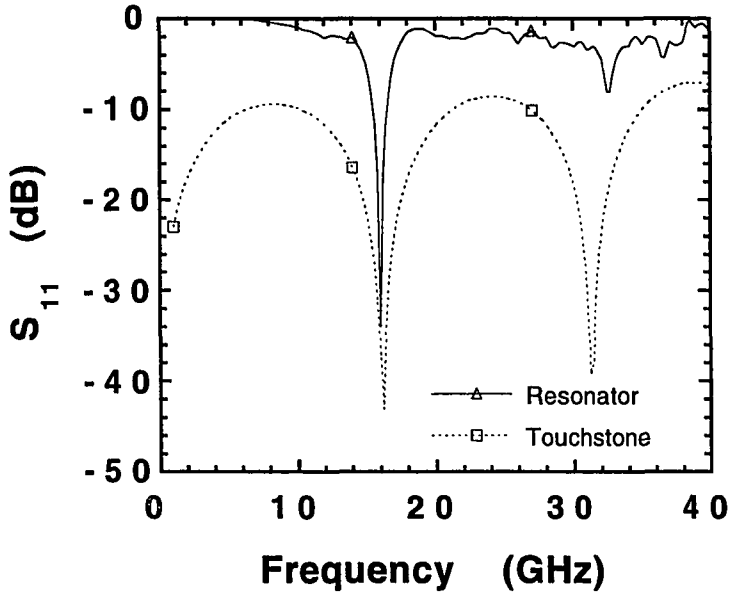

Figure 7.6 Comparison of BKBO resonator S_{11} data vs. Frequency and Touchstone model for S_{11} data. Both have the same fundamental frequency.[30]

microstrip is limited by radiation losses. We can still obtain an upper bound on the R_S, albeit too large, by setting the unloaded $Q = Q_C$. This neglects the effects of both radiation and the dielectric substrate. Evaluating Eq. 7.3 yields that the resonator has $R_S \leq 34$ mΩ.

7.6 CPW Resonator

The next generation of masks produced a proper CPW resonator. We used Touchstone version 4.0 to simulate the CPW structure and discovered that attenuation decreased as the separation of the center conductor and ground plane increased.[31] The new geometry changed the impedance of the CPW to 67 Ω, so a taper was used to match the 50 Ω probe to the CPW impedance. The gap between the input stub and the resonator were experimentally varied, trying to achieve weak coupling where $Q_L \approx Q_C$; we found Touchstone was unable to model the coupling accurately.

We achieved a near critically coupled ($Q_C \sim Q_{EX}$) CPW resonator pictured in Fig. 7.7a. The film was grown with off-center ablation with a K rich ablation target and had the following properties: T_c of 28 °K, $\Delta T \approx 0.5$ °K, and a thickness of 500 Å. We found that the metal chuck was loading the resonator, so we measured the device on top of another MgO substrate; making the effective MgO thickness 1mm. Otherwise, the fabrication and the measurement of the device were standard.

The S_{11} resonance of the CPW resonator is shown in Fig. 7.7b. We see that resonant frequency, f_0, is 23 GHz with $Q_L = 115$ at 15 °K. To determine the geometric factor Γ in Eq. 7.3, a 1 μm evaporated

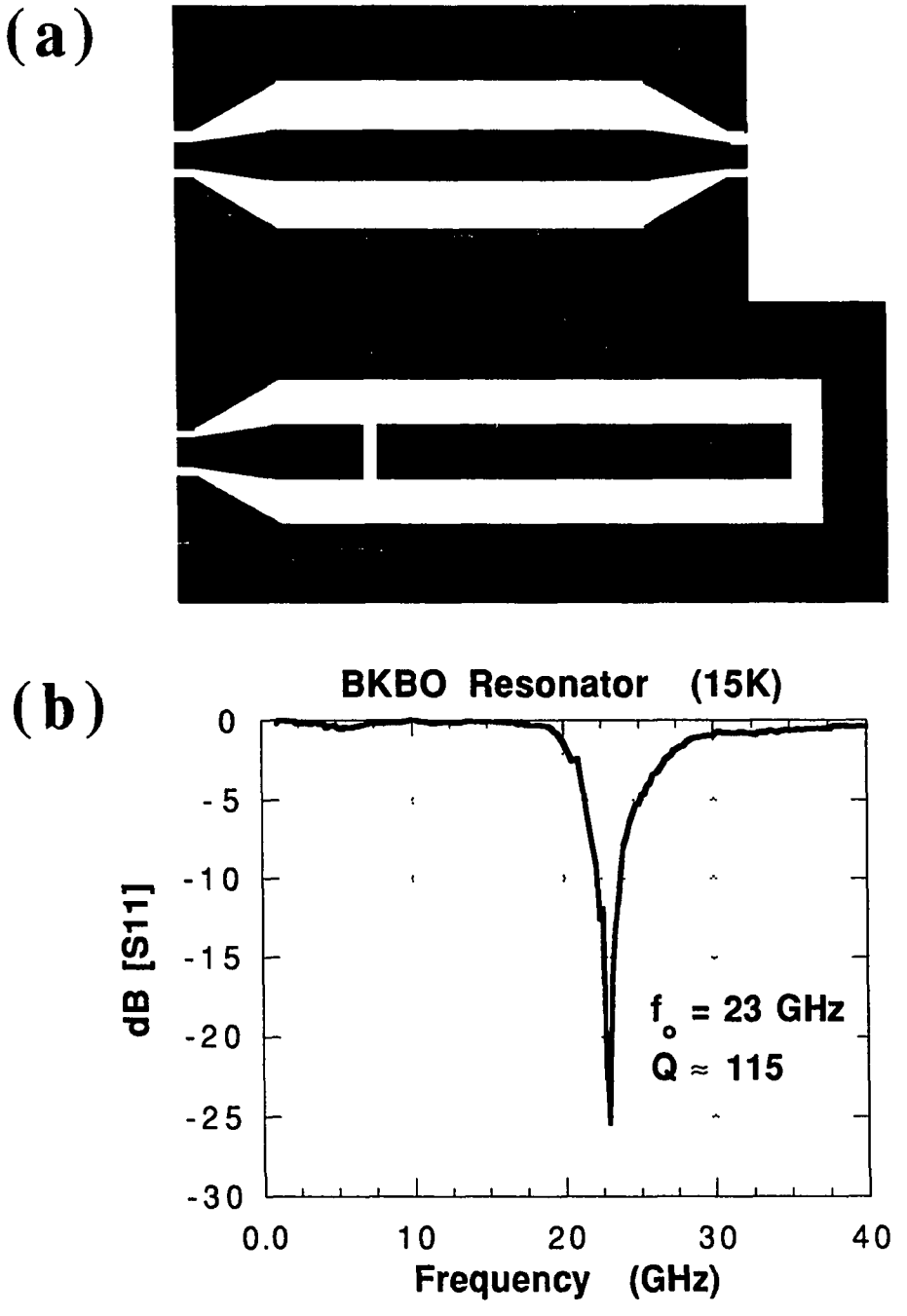

Figure 7.7 (a) Micrograph of fabricated CPW resonator. The length of the resonator is 2.45mm. The lateral dimensions W (trench), S (center conductor), and coupling gap are 200μm, 200μm, and 100μm, respectively. (b) Reflected power measurement (S_{11}) of the CPW resonator at 15°K.

aluminum resonator was made out of the same pattern on MgO. The room temperature resonance was measured at f_0 = 23.6 GHz and Q_L(Al) = 160. The theoretical surface resistance can be calculated from,

$$R_s = \frac{1}{\sigma\delta} = \sqrt{\frac{\pi f \mu_0}{\sigma}}, \qquad \text{(Eq. 7.6)}$$

where σ is the conductivity, δ is the metallic skin depth, f is the frequency, and μ_0 is the permeability constant. The conductivity of Al is 3.5 x 10^7 S/m at room temperature.[32] This gives R_s(Al) = 52 mΩ at 23.6 GHz. Lumping various losses together, we can use Al surface impedance to approximate Γ_L(CPW) = 0.35 Ω/GHz, substituting Q_L for Q_C in Eq. 7.3. This yields a BKBO surface resistance of 70 mΩ at 23 GHz, and scaled to 10 GHz is 13 mΩ.

We have also estimated these losses by calculating the attenuation in a low loss CPW transmission line.[33,34] The losses are assumed to occur on the surface of the structure. We assume $Q_C \approx \beta/2\alpha$, valid in the low loss limit, where α is the attenuation of the coplanar line and β is the wave number Collins's relations yield $R_s \approx$ 33 mΩ at 23 GHz, scaled to 6 mΩ at 10 GHz, for $Q_C \approx 2Q_L$ = 230.

The calculated values of 13 mΩ and 6 mΩ are up to an order of magnitude larger than the 1 mΩ surface resistance measured for the unpatterned film. However, both calculations neglect corrections for the thickness less than the penetration depth, and thus overestimate the resistance. These corrections are significant as the thickness is much smaller than the penetration depth. Thickness corrections are

difficult to estimate. Intrinsic losses should vary predictably with thickness, but some extrinsic losses like surface roughness, etc. may not scale. In lieu of a full wave electromagnetic simulation incorporating finite thickness and superconductivity, I will make a lower bound estimate by approximating $R_S \approx R_S(eff)t/\lambda$, where t is the thickness. This is in analogy to finite thickness metals, where $R_S \approx 1/\sigma t$ for $t \ll \delta$. This yields values of 2 mΩ and 1 mΩ for the two calculations. We can conclude the surface resistance of the CPW is within an order of magnitude of the unpatterned film. Although unclear of the absolute amount, additional loss on this scale can be attributed to degradation from fabrication. These difficulties illuminate the need for developing better CPW simulations, a current research topic in the field, and thick BKBO films.

7.7 Summary

We have shown the feasibility of BKBO microwave devices, including transmission lines and resonators. Unpatterned thin films have demonstrated surface resistances ~1 mΩ at 10 GHz, while patterned films are within an order of magnitude. Fundamental studies of BKBO surface losses require lower defect material. Better films are also needed for improved BKBO device results. Film homogeneity, stress and surface roughness are likely causes of these losses. Reduction of stress will also allow fabrication of thicker films, leading to better microwave performance. Fabrication processes also impact R_S, and need to be improved to prevent degradation. Thus far, BKBO microwave properties and devices are reminiscent of

beginning work in other HTS compounds. If BKBO follows the trend, films will improve their microwave performance dramatically.

References

[1] T. Van Duzer and C.W. Turner, Principles of Superconductive Devices and Circuits, New York: Elsevier, 1981, pp. 124-138.

[2] R.A. Schweinfurth, D.J. Van Harlingen, J. Kruse, J. Laskar, M. Feng, C.E. Platt and M.R. Teepe, "Thin film $Ba_{0.6}K_{0.4}BiO_3$ microwave devices," IEEE Trans. Appl. Superconductivity, vol. 3(1), pp. 1559-62, Mar. 1993.

[3] S.M. Anlage, B.W. Langley, H.J. Snortland, C.B. Eom, T.H. Geballe, and M.R. Beasley, "Magnetic penetration depth measurements with the microstrip resonator technique," Journal of Superconductivity, vol. 3, pp. 311-316, 1990.

[4] J.R. Delayen, C.L. Bohn, and C.T. Roche, "Measurements of RF Surface Resistance of High-Tc Superconductors," IEEE Trans. Magn., vol. 27, pp. 1532-35, Mar. 1991.

[5] M.S. Pambianchi, S.M. Anlage, E.S. Hellman, E.H. Hartford Jr., M. Bruns, and S.Y. Lee, "Penetration depth, microwave surface resistance, and gap ratio in NbN and $Ba_{1-x}K_xBiO_3$ thin films," Appl. Phys. Lett., vol. 64, pp. 244-6, Jan. 1994.

[6] L.D. Chang, M.J. Moskowitz, R.B. Hammond, M.M. Eddy, W.L. Olson, D.D. Casavant, E.J. Smith, M. Robinson, L. Drabeck, and G. Gruner, Appl. Phys. Lett., vol. 55 (13), pp. 1357-9, 1989.

[7] R.B. Hammond, G.V. Negrete, L.C. Bourne, D.D. Strother, A.H. Cardona, and M.M. Eddy, Appl. Phys. Lett., vol. 57 (8), pp. 825-7, 1990.

[8] C.E. Platt, M.R. Teepe, C. Ciofi, H. Zhang, V.P. Dravid, R.A. Schweinfurth, D.J. Van Harlingen, J.A. Eades, C.H. Lin, D. Strothers, and R. Hammond, "Pulsed laser deposition and characterization of superconducting $Ba_{1-x}K_xBiO_3$ thin films," in *Layered Superconductors Symposium of MRS*, Boston, MA, Oct. 1992.

[9] T. Van Duzer and C.W. Turner, Principles of Superconductive Devices and Circuits, New York: Elsevier, 1981, p. 124.

[10] E.J. Ansaldo, Z.R. Wang, J.H. Cho, D.C. Johnston, and T.M. Riseman, "Magnetic penetration depth of $Ba_{0.625}K_{0.375}BiO_3$," Physica C, vol. 185-189, pp. 1889-90, 1991.

[11] R.E. Collins, Foundations for Microwave Engineering, McGraw-Hill, New York, 1966, p. 176.

[12] R.E. Collins, Foundations for Microwave Engineering, 2nd Ed., McGraw-Hill, New York, 1992.

[13] I. Bahl and P. Bhartia, Microwave Solid State Circuit Design, John Wiley & Sons, New York, 1988.

[14] R.E. Matick, Transmission Lines for Digital and Communication Networks, New York, McGraw-Hill, 1969.

[15] D.M. Pozar, Microwave Engineering, Addison-Wesley, Reading, MA, 1990.

[16]K.C. Gupta, R. Garg, and I.J. Bahl, Microstrip Lines and Slotlines, Artech House, Inc., Dedham, MA, 1979.

[17]J. Laskar, J. Kalodzey, "Cryogenic vacuum high frequency probe station," J. Vac. Sci. Tech., vol. B5 (5), pp. 1161-5, Sep./Oct. 1990.
J. Laskar, J. Kruse, M. Feng, and J. Kolodzey, "Cryogenic Vacuum On-Wafer Probe System, " in *38th IEEE-ARFTG Conference Digest*, San Diego, CA, Dec. 1991, pp. 44-52.

[18]Si diode temperature sensor, part #DT-470, Lakeshore Cryotronics, Inc., Westerville, OH.

[19]J. Kruse, R.A. Schweinfurth, F. Gao, D. Scherrer, D. Barlage, C.E. Platt, D.J. Van Harlingen, and M. Feng, "Cryogenic on-wafer microwave character-ization of GaAs MESFETs and superconducting coplanar resonance and transmission line structures," to be published in *SPIE Proceedings of High-Tc Microwave Superconductivity and Applications*, Los Angeles, CA, January 1994.

[20]G. Ghione, C. Naldi, and R. Zich, "Q-factor evaluation for coplanar resonators," Alta Frequenza, vol. 52, pp. 191-193, June 1983.
G. Ghione and C. Naldi, "Analytic formulas for coplanar lines in hybrid and monolithic MICs," Electronics Letters, vol. 20 (4), pp. 179-181, Feb. 1984.

[21]D.R. Lide, Handbook of Chemistry and Physics, Ann Arbor: CRC Press, 1992, p. 12-43.

[22]Schweinfurth, ibid.

[23]Schweinfurth, ibid.

[24]Schweinfurth, ibid.

[25]I. Bahl and P. Bhartia, Microwave Solid State Circuit Design, John Wiley & Sons, New York, 1988, pp. 7-64.

[26]N.J. Rohrer, H.Y. To, G.J. Valco, K.B. Bhasin, C. Chorey, and J.D. Warner, "Sequentially evaporated thin film $YBa_2Cu_3O_{7-x}$ superconducting microwave ring resonator," in *NASA Technical Memorandum 103180*, Denver, CO, Apr. 1990, pp. 1-10.

[27]A.A. Valenzuela and P. Russer, "High Q coplanar transmission line resonator of $YBa_2Cu_3O_{7-x}$ on MgO," Appl. Phys. Lett., vol. 55, pp. 1029-1031, September 1989.

[28]Touchstone 4.0 microwave CAE program by EEsof.

[29]I. Bahl and P. Bhartia, ibid.

[30]Schweinfurth, ibid.

[31]K.C. Gupta, R. Garg, and I.J. Bahl, Microstrip Lines and Slotlines, Artech House, Inc., Dedham, MA, 1979, Chapter 7.

[32]R.E. Collins, Foundations for Microwave Engineering, McGraw-Hill, New York, p. 176, 1966, Appendix III.

[33]R.E. Collins, Foundations for Microwave Engineering, 2nd Ed., McGraw-Hill, New York, 1992, Chapter 3.

[34]J. Kruse, R.A. Schweinfurth, F. Gao, D. Scherrer, D. Barlage, C.E. Platt, D.J. Van Harlingen, and M. Feng, "Cryogenic on-wafer microwave character-ization of GaAs MESFETs and superconducting coplanar resonance and transmission

line structures," to be published in *SPIE Proceedings of High-Tc Microwave Superconductivity and Applications*, Los Angeles, CA, January 1994.

Chapter 8
SUMMARY

8.1 Status

We have developed the foundation for a BKBO thin film technology and have characterized the superconducting properties of these films. Pulsed laser deposition has proven to produce excellent quality BKBO thin films. Fabrication techniques have also been developed to successfully pattern single layer films into working structures and devices. Thin films, transport structures, resonators, and tunneling studies have yielded the data below in Table 8.1.

T_{c0}	≤ 29 K
J_c (4K)	≤ 3 MA/cm^2
H_{c2} (T=0)	22 T
ξ_{GL}	4 nm
R_s (4K, 10GHz, film)	1 mΩ
Δ	4.5 meV
$2\Delta/kT_c$	3.8

Table 8.1 Superconducting characteristics of BKBO thin films

8.2 Future Directions

Scientifically, there are many future directions this research could take. First, it would be important to determine the above properties as a function of K doping. This is important for comparison to theory, as the band structure changes with K content. Additional properties to be measured include electromigration and

photoelectric effects with BKBO, as well as penetration depth and Hall effect on PLD BKBO films.

There are also many different future applied directions these studies could take. First, there are still materials difficulties with BKBO thin films. Stress, homogeneity, reproducibility, clean abrupt superconducting interfaces, and multilayers with sequential layer fabrication still need to be either developed or improved. Specific to PLD, the kinetics of the BKBO growth process needs to be understood; especially the role of oxygen and argon. Concerning fabrication of devices, the normal metal contact resistance needs to improved, especially for small circuit applications. Also, the development of a selective etch for BKBO, analogous to the CF_4 RIE etch for Nb device technology, would greatly facilitate mulilayer processing. The most important device development would be a quality thin film Josephson tunnel junction; how far away is unknown. It may well depend on further developments such as reducing film stress, new barrier materials, or new growth methods.

I believe this thesis demonstrates the complexity and depth of the $Ba_{1-x}K_xBiO_3$ material. Interest in this material encompasses material, engineering, and physics issues. I believe the knowledge gained from understanding the BKBO system are thus widely applicable and well worth the effort.

Vita

Ralph Alan Schweinfurth was born in San Francisco, California on January 27, 1965. He graduated in 1983 from Northgate H.S., located in Walnut Creek, California. He then attended Harvey Mudd College in Claremont, California and graduated with Distinction in May 1987 with a B.S. degree in Physics and a minor in Economics. Moving to Urbana, Illinois, he enrolled as a graduate student at the University of Illinois at Urbana-Champaign; whereupon graduating with a M.S. and Ph.D. in Solid State Physics during May of 1989 and 1994, respectively.